
Alterations of neuronal activity and
protein homeostasis in a mouse model
of Huntington's disease

Elena Katharina Schulz-Trieglaff



München 2017

Alterations of neuronal activity and
protein homeostasis in a mouse model
of Huntington's disease

Elena Katharina Schulz-Trieglaff

Dissertation

zur Erlangung des Doktorgrades der Naturwissenschaften

an der Fakultät für Biologie der Ludwig–Maximilians–Universität
München

vorgelegt von

Elena Katharina Schulz-Trieglaff

München, Oktober 2017

1. Gutachter: Prof. Dr. Rüdiger Klein

2. Gutachter: Prof. Dr. Hans Straka

Tag der Abgabe: 12. Oktober 2017

Tag der mündlichen Prüfung: 01. Februar 2018

Die wissenschaftliche Arbeit, die dieser Dissertation zugrunde liegt, wurde im Labor von Prof. Dr. Rüdiger Klein, Department Moleküle – Signale – Entwicklung, am Max-Planck-Institut für Neurobiologie, Martinsried, Deutschland durchgeführt.

Für Svenja und für meine Eltern

Table of contents

<i>Abbreviations</i>	4
<i>List of figures</i>	8
<i>List of tables</i>	10
<i>Abstract</i>	11
1. Introduction	13
1.1. Huntington's disease	13
1.1.1. Neurodegeneration	13
1.1.2. Huntington's disease	16
1.1.3. Huntingtin	19
1.1.4. Mouse models of Huntington's disease	22
1.1.5. Two approaches	24
1.2. Cortical activity project	25
1.2.1. Interneurons	25
1.2.2. Alterations of cortical functionality in mouse models of HD	26
1.2.3. Open questions	27
1.2.4. Aims	28
1.2.5. Method	28
1.3. Protein homeostasis project	29
1.3.1. Protein homeostasis	29
1.3.2. Proteostasis in neurodegeneration	34
1.3.3. Open questions	35
1.3.4. Aims	37
1.3.5. Method	37
2. Results	41

2.1. Cortical activity in R6/2 mice	41
2.1.1. Data generation	41
2.1.2. More cells are active in R6/2 mice at disease onset	45
2.1.3. Synaptic proteins are downregulated at disease onset in proteome of R6/2 mice	45
2.1.4. PV-positive terminals on pyramidal cells are reduced in R6/2 mice at disease onset	50
2.1.5. Aggregate load and neuronal pathology correlate	53
2.2. Protein homeostasis in R6/2 mice	55
2.2.1. Data generation	55
2.2.2. Fluc functions in primary neurons	55
2.2.3. Fluc senses the presence of an aggregation-prone protein in primary neurons	62
2.2.4. Measurements of protein folding in mice	64
2.2.5. Fluc is better folded in R6/2 than in wt mice in specific brain regions at 1 week of age	69
2.2.6. Mass-spectrometry analyses reveal transient upregulation of specific ubiquitin-related proteins in R6/2 mice at young ages	72
3. Discussion	79
3.1. Functional and molecular alterations in motor cortex of R6/2 mice	79
3.1.1. Summary	79
3.1.2. What does the increase in neuronal activity in R6/2 mice encode?	79
3.1.3. Decrease in synaptic proteins	81
3.1.4. Link between aggregate load and neuronal pathology	84
3.1.5. Hyperactivity in HD	85
3.1.6. Outlook	86
3.2. Alterations of protein homeostasis in R6/2 mice	87
3.2.1. Summary	87
3.2.2. Fluc as a proteostasis sensor in primary neurons	88
3.2.3. No decrease in proteostasis capacities in R6/2 mice at advanced disease stage	89

3.2.4. Region-specific improvement of proteostasis in young R6/2 mice	90
3.2.5. Aspects to consider	92
3.2.6. Outlook	93
4. Materials and Methods	97
4.1. Materials	97
4.1.1. Chemicals, reagents and kits	97
4.1.2. Solutions and buffers	97
4.1.3. Media	101
4.1.4. Oligonucleotides and plasmids	103
4.1.5. Antibodies	106
4.1.6. Mouse lines	107
4.2. Methods	108
4.2.1. Molecular biology and immortalized cell culture	108
4.2.2. Mouse work	110
4.2.3. Primary neuronal culture and biochemistry	113
4.2.4. Histology and Immunofluorescence	116
4.2.5. Data analysis	118
4.2.6. Calcium imaging	118
Bibliography	121
Appendix	133
Appendix I: Supplementary tables	133
Appendix II: Curriculum Vitae	141
Appendix III: List of publications	142
Appendix IV: Contributions and Affidavit	143
Appendix V: Acknowledgements	144

Abbreviations

A	ampere
AD	Alzheimer's disease
ALS	Amyotrophic lateral sclerosis
APS	ammonium persulfate
ATP	adenosine triphosphate
BSA	bovine serum albumin
CR	calretinin
CNS	central nervous system
CA	cornu ammonis region
Dapi	4',6-diamidino-2-phenylindole
DIV	days <i>in vitro</i>
dm	double mutant
DMEM	Dulbecco's modified Eagle's medium
DMSO	dimethyl sulfoxide
DNA	deoxyribonucleic acid
dNTP	deoxyribonucleotide
DREADDs	designer receptors exclusively activated by designer drugs
DS	normal donkey serum
DTT	dithiothreitol
E	embryonic day
ECL	enhanced chemiluminescence
EDTA	ethylenediaminetetraacetic acid
eGFP	enhanced green fluorescent protein
FBS	fetal bovine serum

Fluc	firefly luciferase
FOV	field of view
FTLD	Frontotemporal dementias
GABA	γ -aminobutyric acid
GFP	green fluorescent protein
GO	gene ontology
h	hour
HA	hemagglutinin
HBSS	Hanks balanced salt solution
HD	Huntington's disease
HEK	human embryonic kidney
HEPES	4-(2-hydroxyethyl)-1-piperazineethanesulfonic acid
HRP	horseradish peroxidase
HS	heat shock
HSD	honest significance difference
Hsps	heat shock proteins
<i>HTT</i>	huntingtin (human gene)
HTT	huntingtin (human protein)
IB	inclusion body
iPSC	induced pluripotent stem cells
IPSC	inhibitory postsynaptic currents
IT	intratelencephalic
IUE	<i>in utero</i> electroporation
kDa	kilo Dalton
LB	Luria-Bertani
m	milli
mCh	mCherry
mHTT	mutant Huntingtin

Abbreviations

mRNA	messenger RNA
MSN	medium spiny neurons
MTOC	microtubule organizing centre
n	nano
N-terminal	amino-terminal
NeuN	neuronal nuclei
NMDA	N-methyl-D-aspartic acid
p	pico
P	postnatal day
PAGE	polyacrylamide gel electrophoresis
PBS	phosphate buffered saline
PCR	polymerase chain reaction
PD	Parkinson's disease
PFA	paraformaldehyde
polyQ	poly-glutamine
proteostasis	protein homeostasis
PrP	prion protein
PSD	postsynaptic density
PT	pyramidal tract
PV	parvalbumin
PVDF	polyvinylidene difluoride
RNA	ribonucleic acid
ROI	region of interest
rpm	rounds per minute
RT	room temperature
s	second
SA	sodium azide
SDS	sodium dodecyl sulfate

SEM	standard error of the mean
sm	single mutant
SST	somatostatin
TAE	TRIS-acetate buffer
TEMED	tetramethylethylenediamine
Tris	tris(hydroxymethyl)aminomethane
UPS	ubiquitin-proteasome system
VIP	vasoactive intestinal peptide
wt	wildtype
μ	micro
°C	degree celsius
5HT3aR	ionotropic serotonin receptor 5HT3a

List of figures

- Figure 1-1 Cortical connectivity
- Figure 1-2 Time course of pathological alterations in the R6/2 mouse model
- Figure 1-3 The Protein quality control system
- Figure 1-4 The ubiquitin-proteasome system
- Figure 1-5 Readouts of the Fluc sensor
- Figure 2-1 Experimental set-up
- Figure 2-2 Experiment design and time frames
- Figure 2-3 Re-finding of the same cells over all imaging time points
- Figure 2-4 Increased neuronal activity in R6/2 mice at 8.5 weeks of age
- Figure 2-5 Synaptic proteins are main drivers of sample separation in PCA
- Figure 2-6 Synaptic proteins are downregulated in R6/2 cortex at 8 weeks of age
- Figure 2-7 The excitatory postsynaptic marker PSD-95 is reduced in motor cortex of 8-week old R6/2 mice
- Figure 2-8 Neither excitatory nor inhibitory synapses are reduced in 8-week old R6/2 mice
- Figure 2-9 PV-positive terminals on pyramidal neurons are reduced in layer 2/3 of 8-week old R6/2 mice
- Figure 2-10 SST-positive neurons are reduced by 50 % in 8-week old R6/2 mice
- Figure 2-11 mHTT inclusion load correlates with neuronal pathology
- Figure 2-12 The HA-tag does not influence the reaction of Fluc to proteotoxic stress
- Figure 2-13 Fluc expression in primary neurons is not toxic
- Figure 2-14 Fluc reacts to proteasome and Hsp90 inhibition in primary neurons
- Figure 2-15 Retrograde transport and fusion of Fluc inclusions in neurons
- Figure 2-16 FlucSM-HA reacts differently to heat shock as compared to proteasome and Hsp90 inhibition

-
- Figure 2-17 Fluc can measure decreased and increased capacities of the PQCS
- Figure 2-18 Fluc reacts to presence of mHTT inclusion bodies and the presence of soluble aggregation-prone mHTT
- Figure 2-19 Fluc reacts to heat shock in the intact brain but shows no reaction in the R6/2 background
- Figure 2-20 Generation of a transgenic mouse expressing Fluc
- Figure 2-21 Linearity of the bioluminescence assay and normalization
- Figure 2-22 Increased folding capacities in specific brain regions of young R6/2 mice
- Figure 2-23 Slight increase of folding capacities in hippocampal tissue of HD94 mice
- Figure 2-24 Differential folding capacities in cortical and hippocampal R6/2 cultures
- Figure 2-25 PCA of soluble proteome from young mice shows no difference between R6/2 and controls
- Figure 2-26 Ubiquitin-related proteins are enriched in cerebellar and hippocampal tissue of young R6/2 mice
- Figure 2-27 Upregulation of candidates is transient
- Figure 2-28 Chymotrypsin-like proteasome activity is not altered in tissue of young R6/2 mice
- Figure 2-29 Degradation of CPY*-mCh is faster in hippocampal than in cortical cultures
- Figure 3-1 Proposed model explaining increased cellular activity
- Figure 3-2 Proposed model explaining how increased folding capacities could influence vulnerability of different brain regions to the HD phenotype in R6/2 mice

List of tables

Table 2-1	Imaged mice
Table 2-2	Proteostasis-related candidates upregulated in the soluble proteome of young R6/2 mice
Table 4-1	Oligonucleotides for cloning
Table 4-2	Oligonucleotides for genotyping
Table 4-3	Oligonucleotides for sequencing
Table 4-4	Plasmids
Table 4-5	Primary antibodies
Table 4-6	Secondary antibodies
Table 4-7	PCR protocols
Table A-1	PCA drivers, downregulated in old R6/2 mice
Table A-2	PCA drivers, upregulated in old R6/2 mice
Table A-3	Synaptic proteins most significantly regulated in the soluble proteome of R6/2 mice
Table A-4	Synaptic proteins significantly upregulated in the insoluble proteome of R6/2 mice
Table A-5	Synaptic proteins significantly downregulated in the insoluble proteome of R6/2 mice

Abstract

Huntington's disease (HD) is a genetically-caused disorder characterized by aggregation of polyQ-expanded mutant Huntingtin (mHTT) protein and progressive neurodegeneration in the striatum and cortex. HD is associated with motor, cognitive and psychiatric symptoms. In this thesis, pathology in R6/2 mice, a mouse model of HD, was assessed using two different approaches, *in vivo* calcium imaging and protein homeostasis (proteostasis) measurements. Both approaches center on monitoring cellular states of neurons in specific brain regions throughout the course of the disease.

Studies in mouse models and human patients suggest that disturbance of neuronal function in cortex plays an important role in HD. However, longitudinal changes in neuronal activity have not been investigated *in vivo* in an intact animal during the course of the disease. Therefore, in the first part of this thesis, cellular activity was assessed in layer 2/3 of the primary motor cortex via chronic two-photon calcium imaging using a genetically encoded calcium indicator. We observed an increase in neuronal activity that coincided with disease onset. To understand the mechanisms behind this, I analysed mass-spectrometry data from cortex of R6/2 mice of three different ages and found a reduction in synaptic proteins at disease onset. To further investigate this decrease in synaptic proteins, I performed histology on tissue of R6/2 mice and littermates in primary motor cortex. I observed that parvalbumin-positive terminals on pyramidal neurons were reduced in number and also found a 50 % decrease in the density of somatostatin-positive interneurons. This reduction in cell density correlated with a higher aggregate load in these cells compared to other interneuron subtypes. Therefore, lack of inhibition could explain the increase in aberrant neuronal activity measured.

Protein folding capacities in a cell are dictated by the cellular proteostasis system. A decline in proteostasis and thereby protein folding capacities is believed to occur in neurodegenerative disorders, including HD. Nevertheless, functional studies in HD mouse models, measuring

folding capacities at different disease stages, are still lacking. Therefore, in the second part of this thesis I monitored proteostasis in the R6/2 model. For this I used a proteostasis sensor based on the conformationally unstable GFP-tagged firefly luciferase. In primary neurons transfected with mHTT the sensor measured a disturbance of proteostasis. I then developed a transgenic mouse line expressing the sensor and crossed it to R6/2 mice to measure proteostasis in four brain regions at different ages. Contrary to our expectations, I did not see a decline in proteostasis in symptomatic mice. Instead, I observed an increase in protein folding capacities at a very young age in brain regions less affected by the disease. A proteomic screen revealed a transient upregulation of several protein degradation components in these regions. This data suggest that these early proteome changes might provide protection against mHTT toxicity in disease-resistant brain regions, whereas a failure to upregulate these protein quality control mechanisms might contribute to the selective vulnerability of the striatum in HD.

1. Introduction

1.1. Huntington's disease

1.1.1. Neurodegeneration

1.1.1.1. The central nervous system

The human brain consists of roughly 90 billion neurons. Neurons can be divided into projection neurons that innervate other brain regions or other regions of the same brain structure over long distances, and interneurons that innervate neurons in close proximity. The brain is primarily divided into the cerebrum, the cerebellum, and the brain stem [1].

The cerebellum is strongest related to fine-tuned motor control but is also known for cognitive functions such as attention and language. It is highly gyrified and consists of three cellular layers: the granule cell layer, the Purkinje cell layer and the molecular cell layer.

The cerebrum develops out of the telencephalon, with the dorsal telencephalon becoming the cerebral cortex and the ventral telencephalon becoming the basal ganglia. One main structure of the basal ganglia is the striatum, which will be discussed below. The cerebral cortex contains the hippocampus, which is functionally mostly studied in the context of memory. The hippocampus is highly interconnected with other brain regions via the entorhinal cortex (EC) and consists of the dentate gyrus and the cornu ammonis regions 1 and 3 (CA1 and CA3).

For simplicity I will refer to the neocortex as cortex for the rest of this thesis. About 80 % of cortical neurons are pyramidal excitatory (glutamatergic) projection neurons [2], [3]. The remaining fraction are inhibitory interneurons, which serve to inhibit other cells of the cortex through short distance projections. The cortex of mammals is divided into 6 different layers. The first layer harbors no pyramidal and only few interneuron cell bodies. Pyramidal cells are present in all other layers of the cortex. The cortex is highly interconnected, with most input onto layers 5 and 6 arising from layer 2/3. Neuronal populations that project to either cortical or subcortical

regions are mutually exclusive (reviewed by Shipp [4]). Most subcortically projecting neurons are harbored by layers 2/3, 5 and 6. Motor cortex, the main focus of the first part of the thesis, does not contain a cortical layer 4. Most projections onto striatum arise from layer 5. In the motor cortex, contrary to sensory cortex, some projections also arise from layer 2/3 [5] (Fig. 1-1).

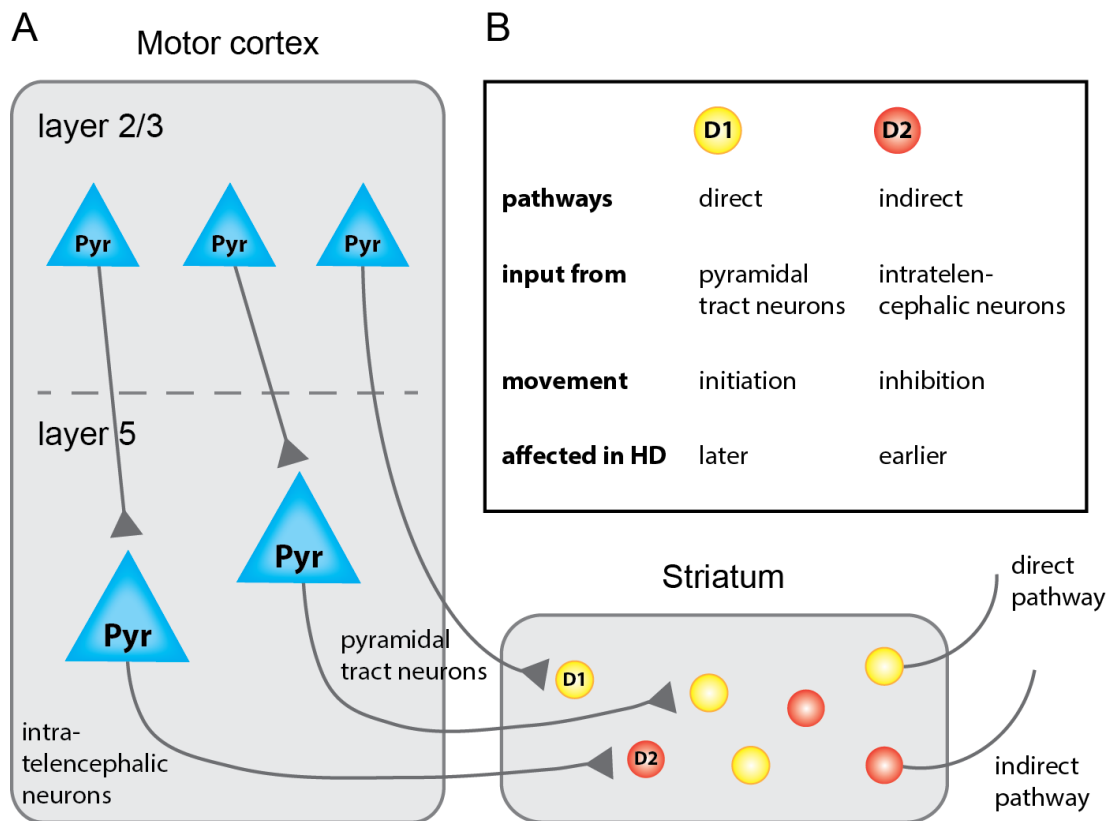


Figure 1-1: Cortical connectivity.

A: In primary motor cortex, pyramidal neurons of layer 5 are the main output from this brain region onto striatum. From lower layer 5 intratelencephalic (IT) neurons project onto dopamine receptor 2 (D2)-expressing medium spiny neurons (MSN) in the striatum (orange), belonging to the indirect pathway. Pyramidal tract (PT) pyramidal neurons reside in upper layer 5 and in layer 2/3 and project onto dopamine receptor 1 (D1)-expressing MSNs (yellow), belonging to the direct pathway. Layer 2/3 pyramidal neurons mainly innervate pyramidal neurons of layer 5. B: The direct pathway is affected later in HD than the indirect pathway, leading to the phenomenon of involuntary movement early in disease and lack of voluntary movement later in disease.

The cortex connects to the striatum monosynaptically, whereas the striatum connects to the cortex in an indirect way via more than one synapse. For this thesis I will focus on the connections from cortex to striatum. Cortical projection neurons can be divided into pyramidal tract type (PT)

and intratelencephalically (IT) projecting neurons. As part of the pyramidal tract, PT neurons target axons down to the brain stem or spinal cord. PT axon collaterals however project, among other regions, to the striatum [6]. The IT neurons project within the telencephalon (cortex and basal ganglia) [7].

Striatum, globus pallidus, the ventral pallidum, substantia nigra and the subthalamic nucleus all belong to the basal ganglia. The basal ganglia are involved in motivation, reward and working memory, but also movement. The striatum consists of the caudate nucleus and putamen (dorsal striatum), and the nucleus accumbens (ventral striatum). 95 % of the striatal neurons are GABAergic projection neurons, so-called medium spiny neurons (MSNs) [8]. The rest are interneurons. The striatum receives two forms of main input, glutamatergic input arising from the cortex and dopaminergic input from the substantia nigra. Motor control can be divided into the elicitation of movement that is the initiation and execution of movement, which is controlled by the direct pathway of movement, and the inhibition of unwanted muscle movement, controlled by the indirect pathway. The indirect pathway contains MSNs that express enkephalin and dopamine receptor 2 (D2) and project mainly to the external segment of the globus pallidus. The direct pathway contains MSNs that express substance P and dopamine receptor 1 (D1) and project to the internal segment of the globus pallidus and the substantia nigra [9], [10]. Indirect pathway neurons (D2 MSNs) preferentially receive input from IT neurons and direct pathways neurons (D1 MSNs) from PT projection neurons ([10], Fig. 1-1).

1.1.1.2. Degeneration of the nervous system

Neurodegeneration is the pathological age-dependent degeneration of cells of the central nervous system. Prominent examples of neurodegenerative diseases are Alzheimer's disease (AD), Parkinson's disease (PD), Frontotemporal dementias (FTDs), Amyotrophic lateral sclerosis (ALS) and Huntington's disease (HD). All of these diseases have several features in common [11]: Disease onset usually occurs in the second half of life, with the exception of rare juvenile cases. One of the typical symptoms is dementia. All of these disorders are currently incurable. And interestingly, in all of these, disease-specific proteins misfold and aggregate.

These proteins differ between the different diseases, as does the intracellular aggregate location and the affected brain regions. For example, in AD, amyloid- β and tau proteins misfold and form extracellular and cytoplasmic aggregates, respectively [12, 13]. The most and firstly affected regions are the cerebral cortex and the hippocampus. In PD, the protein α -synuclein forms cytoplasmic aggregates and the most affected regions are the substantia nigra of the basal ganglia and the hypothalamus [14]. The vast majority of cases of all major neurodegenerative disease, with the exception of HD, are sporadic. This of course makes modelling of the disease in cellular systems or animals very difficult, again with the exception of HD.

1.1.2. Huntington's disease

HD is an autosomal-dominant neurodegenerative disease with a typical onset during the fourth decade of life [15]. One of the first detailed descriptions of this disorder was made by George Huntington in the year 1872 [16], who referred to it as “chorea”, because of the stereotypical dance-like muscle twitchings observed in the disease. HD is caused by an expansion of a CAG-repeat in exon 1 of the huntingtin (*HTT*) gene on chromosome 4, which encodes a polyglutamine (polyQ) stretch [17], [18]. Subjects with 36 or less CAG repeats are not affected by the disease, whereas 41 or more repeats lead to a full penetrance of the disorder; and subjects with a CAG-expansion between 37 and 40 can develop the disease [19], [20]. Symptoms include motor deficits [16], cognitive impairments [21], [22], and neuropsychiatric dysfunctions [23], [24]. Death typically occurs around 15 – 20 years after diagnosis [24]. The prevalence of HD lies at 5 – 10 per 100 000 worldwide with highest prevalence seen in people of western European origin [15], [25].

Motor symptoms in HD can be roughly divided into added involuntary motor symptoms, such as chorea and dystonia (repetitive muscle contractions), appearing earlier in disease progression, and impaired initiation of voluntary movements, such as bradykinesia (deceleration of movement) and rigidity, appearing later in disease progression [24]. Motor impairment scoring during disease, but not chorea, seems to be a good correlate to post-mortem neuropathology [26]. Cognitive decline and dementia are also major symptoms of HD [21], [22] and have been reported

to appear earlier than motor symptoms in some cases. Psychiatric symptoms include anxiety, irritability, depression, obsessive-compulsive disorders, apathy, and psychosis [23], [24]. Increased suicidal inclinations have been reported in HD patients [27], [28].

1.1.2.1. CAG-repeat expansion causative for HD

HD is the most common of nine polyQ-related neurodegenerative disorders. PolyQ repeats may also cause dentatorubral-pallidoluysian atrophy (DRPLA), spinal and bulbar muscular atrophy and six types of spinocerebellar ataxias (SCA1, 2, 3, 6, 7, and 17) [29], [30]. All of these disorders present with protein aggregates and selective neurodegeneration. Nevertheless, the CAG-repeat expansions occur in different proteins, and the cells affected most by these disorders differ. In all of these disorders CAG-repeat length correlates inversely with age of onset [20], [19], [29], [31].

CAG repeat numbers in monozygotic twins have been shown to be identical [32]. Because HD is genetically caused and because the genetic mutation has a full penetrance in people with over 40 CAG-repeats, in affected monozygotic twin pairs both individuals develop the disease. However, exact age at disease onset, disease progression and symptomology can differ [33], which suggests that progression and symptomology can be environmentally and epigenetically influenced. CAG-repeats are unstable in germ lines, especially in sperm cells, which can lead to increased CAG-repeat expansions in offspring of mutation carriers [32], [34]. Instability of CAG-repeat lengths has also been described in somatic cells, for example in striatal neurons of an HD mouse model [35] and cortical neurons of HD patients [36], but not in blood cells of HD patients [32].

1.1.2.2. Pathology

Pathologically, HD leads to drastic brain atrophy, especially of the caudate nucleus and putamen. But also other regions, such as the cortex, thalamus and white matter, are affected [37], [38], [39]. In general, vulnerability is highest in striatum, followed by the cortex. The hippocampus is relatively spared [40], as is the cerebellum [41], [42].

The most vulnerable neurons are striatal MSNs [43], [44]. D2 MSNs are more susceptible and die prior to D1 MSNs [45]. This could explain the biphasic symptomology of HD, in which first additive involuntary movements and in later stages a lack of voluntary movement is observed. In line with the loss of striatal GABAergic MSNs, the neurotransmitter GABA is reduced in HD patients in the caudate nucleus and the putamen [46]. A loss of GABAergic interneurons could also play a role in this reduction, nevertheless striatal interneurons have been described to be relatively spared in the disease [43], [44]. Synaptic vesicle fusion proteins, specifically SNARE proteins such as SNAP-25, Synaptobrevin 2 and Complexin II, have been shown to be downregulated in striatum of HD patients [47], hinting at atrophy of the corticostriatal tract. In the caudate nucleus, glucose metabolism is impaired prior to measured atrophy [37] and onset of motor symptoms [48]. This could be due to loss of corticostriatal synapses, which are regions of high activity and therefore glucose metabolism. Such hypometabolism was also observed in the motor cortex [48]. Cortical thinning and cell loss is very pronounced in HD patients [38], [49], [50], [39]. In the cortex mainly pyramidal neurons of layers 5 and 6 are reduced in number [49]. The neuronal loss is stronger in motor cortex than in anterior cingulate cortex in HD patients primarily exhibiting motor symptoms and stronger in the anterior cingulate cortex in HD patients primarily exhibiting mood and cognitive changes, hinting at a causal effect of cortical cell loss on symptomology [50].

1.1.2.3. Synaptic dysregulation

In the striatum of HD patients, synaptophysin, a marker of synaptic terminals is dramatically reduced [51]. Postsynaptic D1 and D2 dopamine receptors as well as dopamine transporter molecules were found to be reduced in the striatum of HD patients in positron emission tomography studies [52]. In the temporal cortex, a reduction of D1 receptors was observed [52]. Many synaptic proteins such as postsynaptic density (PSD) protein PSD-95 and PASCIN have been reported to interact with normal huntingtin (HTT, [53], [54]). In HD post-mortem tissue, glutamate uptake was found to be significantly reduced in prefrontal cortex compared to controls and to correlate inversely with CAG-repeat length [55]. Also, the glutamate transporter EAAT2

and GABA levels were reduced in the mediofrontal cortex [55], suggesting an alteration in synaptic function. Synaptic inhibition is known to be disrupted by mHTT, because mHTT impairs the delivery of GABA receptors to synapses [56].

1.1.2.4. Aggregates

PolyQ expansion renders mHTT aggregation-prone [57]. Aggregation proceeds through multiple stages, resulting in the formation of mature insoluble inclusion bodies. The first time mHTT aggregates were described was in the R6 mouse models for HD [58]. Based on these findings, ubiquitinated nuclear mHTT aggregates and ubiquitinated accumulations of mHTT were found in dystrophic neurites in HD patient cortex [59]. Most of the times a cell harbors one and not more nuclear inclusion bodies (IB) [60], [61], [62]. Nuclear inclusions are mostly seen in the caudate nucleus, putamen, globus pallidus and cortex and less so in the thalamus, subthalamic nucleus, substantia nigra, amygdala and hippocampus [60], [61]. The number of inclusions in the cortex correlates with the CAG-repeat length, whereas this is not true for inclusions in the striatum [60], [61]. Some neurons exhibit granular cytoplasmic mHTT staining, which tends to be perinuclear [61] or located in neurites [62]. Although glial cells have been described to not exhibit nuclear inclusions [61], [62], in a recent report low levels of aggregate burden has been observed in oligodendrocytes and astrocytes of HD patients and several HD mouse models [63].

1.1.3. Huntingtin

1.1.3.1. Huntingtin and its function

The protein HTT is expressed ubiquitously, with highest levels in the testes and the nervous system [64], [65], [66]. HTT is a cytosolic protein that is mostly expressed in neuronal cells of the central nervous system (CNS) [65], where it is localized in the soma and in dendrites [67], [65]. The protein is completely soluble, despite its size of 3144 amino acids or 384 kDa [66], [68]. Other proteins, among them many transcription factors, have been described to contain polyQ-repeats [69]. PolyQ stretches have been proposed to form a polar zipper structure made of beta-strands important for transcriptional activity [70] and HTT is known to interact with several

proteins through its polyQ stretch [71]. HTT has been reported to be important for proper function of several distinct cellular compartments, such as the nucleus, the ER and the Golgi apparatus [72] [71]. It associates with vesicle membranes [67] and microtubules [65], [73]. Among other functions, HTT is known to control vesicle transport [74], cell division [73] and transcription [71].

Increased expression of wild-type (wt) HTT protects striatal cells in culture from apoptotic cell death after starvation and heat stress [75] and from N-methyl-D-aspartic acid (NMDA)-mediated excitotoxicity [76]. HTT null mice are not viable and die around embryonic day 8.5 [77], [78], [79], whereas expression of wt (18Q) or mHTT (46 or 72Q) rescues this lethality [80], indicating that HTT is essential during embryonic development and that even mHTT can exert this function. Male mice expressing mHTT exclusively are not fertile due to decreased sperm production [80], showing that HTT plays a role in male fertility, which mHTT cannot fulfill. Inactivation of HTT in postmitotic neurons using a Cre/loxP strategy leads to neuronal degeneration, motor deficits and increased lethality [81], strikingly demonstrating a role of HTT in neuronal function and survival. However, expression of mHTT does not lead to the loss of transcription of normal HTT [82], which means that patients have at least one copy of wt HTT, contrary to the aforementioned mouse models. Interestingly, homozygosity for the mutation does not change disease onset [83], [84].

1.1.3.2. Formation and cellular localization of HTT aggregates

HTT aggregates purified from human tissue consist of polymers, which are probably associated through covalent bonds, oligomers of full-length HTT and amino (N)-terminal fragments of the protein [59], [85]. HTT aggregates can recruit polyQ-containing proteins, for example wt HTT with a non-extended polyQ stretch [86]. HTT is cleaved by cysteine proteases, leading to N-terminal fragments, and this proteolysis increases with CAG-repeat length [87]. N-terminal fragments of mHTT are found in cultured cells and transgenic mice expressing full-length mHTT as well as in patients [88]. Aggregate formation itself is also dependent on CAG repeat length [89]. HTT exon1 peptides can form aggregates that contain amyloid-like fibrils [57].

In cultured cell lines and primary neurons, truncated N-terminal fragments of HTT are more likely to form aggregates than full-length HTT [90], [89], [91], [92]. In accordance, cells expressing truncated HTT are more susceptible to stress than those expressing full-length HTT [90], [91], suggesting that shorter fragments could be the more toxic forms of HTT. Additionally, truncated N-terminal fragments form nuclear and perinuclear aggregates, whereas full-length HTT tends to form more perinuclear aggregates [91], [92]. Nuclear aggregation seems to be more toxic to cells compared to cytoplasmic aggregation, as shown by directed targeting of mHTT in transiently transfected neuro-2a cells [93]. In line with this, Gu et al. described the pathology of an HD mouse model expressing mHTT excluding the N-terminal 17 amino acids [94]. This region has been reported to function as a nuclear export signal [95]. The mouse model lacking this region exhibited decreased nuclear export of mHTT fragments and more overt symptoms and pathology than the same line expressing intact mHTT [94], suggesting that the presence of mHTT in the nucleus is detrimental. Nevertheless, a recent publication argues against this by reporting that in immortalized cell lines cytosolic mHTT inclusions impair nucleocytoplasmic transport more than nuclear mHTT inclusions [96].

1.1.3.3. Modes of toxicity

Many mechanisms of toxicity have been proposed in HD; first of all, a reduction of huntingtin function. Although HTT can be protective in neurons and cell lines [75], [76], a conditional loss of HTT after embryonic development or heterozygosity for the endogenous protein do not lead to HD phenotypes in mice or humans [81]. A loss-of-function of HTT therefore does not seem to be a primary cause of HD, leaving the possibility of a gain-of-function toxicity, induced by the elongated polyQ stretch. It has been shown that HTT aggregates can induce toxicity. But whether these aggregates are causative of the neuronal pathology remains uncertain. In favour of their toxicity are studies that describe sequestration and therefore inactivation of vital proteins [97], [98], [99], for example impairing the nucleocytoplasmic transport [96], [100], [101]. Also direct interference with cellular organelles, for example through interaction with membranes [102] has been reported. In this case a good therapeutic approach would be to inhibit aggregate formation.

Nevertheless, they could also be a mere byproduct of the toxic events, in which case they would not be the best target of intervention. Aggregates could even be a mechanism of protection employed by the cell against the toxicity of mHTT. The rate of death of primary neurons transfected with mHTT correlates with the length of the mHTT polyQ stretch and the amount of mHTT expressed, but the neurons die independently of IB formation. Indeed, IB formation increases the chances of survival per neuron [103]. This goes in line with findings that in the striatum of HD patients, neuronal populations most afflicted with aggregates are not the cells most susceptible to the disease [104]. Also, aggregate load in motor cortex or superior frontal gyrus does not correlate with symptoms (motor versus mood) [105], whereas region-specific cell loss does correlate with symptoms as described above [50]. If IB were not the toxic agents, aggregation could actually be a desired phenomenon, especially, because then monomers and oligomers of mHTT would be candidates for the toxicity-causing agents. Indeed, in an HD mouse model, proteasome activity was impaired after acute expression of mHTT but reverted to normal function after IB had formed and administration of aggregation inhibitors prolonged the proteasome impairment [106].

1.1.4. Mouse models of Huntington's disease

Genetic mouse models of HD can be divided into three categories. 1) Transgenic mice expressing exon1 of HTT with a expanded polyQ stretch. 2) Full-length transgenic models. 3) Full-length knock-in models. Mice of the first category are the oldest of the genetic models (e.g. R6 models, [107]). Although they are criticized for only expressing a truncated form of HTT and therefore being less physiological, they not only have been widely studied, but also model HD symptomology very well. Also, as reviewed above, N-terminal fragments do occur in HD and could be the most toxic species. Last but not least, it has been shown that transgenic mice expressing exon1 of HTT with a certain polyQ stretch develop similar phenotypes and depict similar molecular alterations as knock-in models [108], [109], [110].

1.1.4.1. The R6/2 model

The R6 models were published by the lab of Gillian Bates [107] and were the first genetic models of HD. The R6/2 model was first published carrying 144 CAG repeats, but due to repeat instability the CAG stretch has expanded. Mice in our colony carry between 160 and 190 CAG repeats. This model exhibits onset of obvious motor symptoms at the age of 8 weeks [107], [111] (Fig. 1-2). Earliest motor alterations were detected at 5 weeks of age [111]. At 8 weeks of age motor and balance coordination was poorer and the gait less regular compared to wt controls.

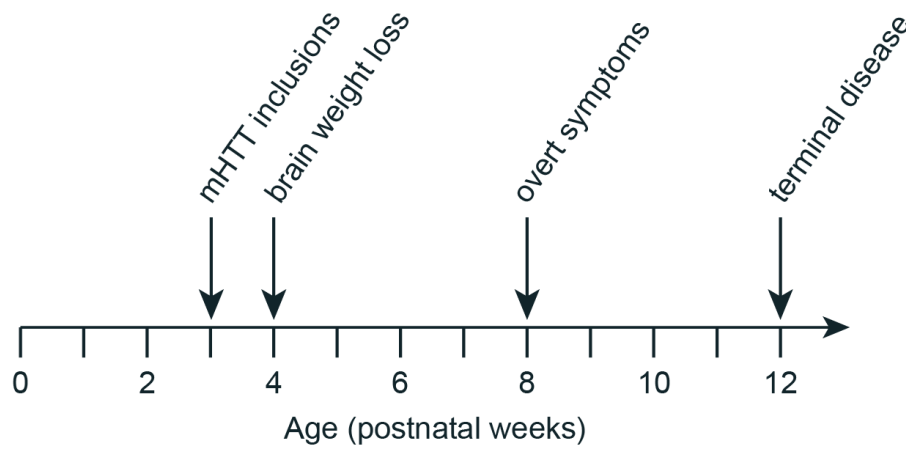


Figure 1-2: Time course of pathological alterations in the R6/2 mouse model

At later disease stages, clear resting tremor, stereotypical grooming, and infrequent epileptic attacks were observed [111]. R6/2 mice gain weight comparably to their wt littermates until 10 weeks of age and then lose weight [111]. R6/2 mice also show decreased cognitive performance based on several behavioural tests before an age of 8 weeks and therefore before onset of obvious motor impairments [112], [113]. Females are infertile and males can breed up to an age of 9 weeks. At 12 to 15 weeks of age the mice are terminally ill and have to be sacrificed [107]. Based on animal well-fare regulations, we always sacrifice animals from our colony at 12 weeks of age. R6/2 mice exhibit HTT inclusions [58], which are reminiscent of HD inclusions and possess a beta-sheet like structure [114]. Aggregate formation is observed at 3.5 weeks of age in the striatum and the cortex [115]. In symptomatic R6/2 mice, striatal MSNs are affected in morphology (spine loss) and electrophysiological properties (increased input resistance) [116].

1.1.5. Two approaches

In the scope of this thesis I wanted to study two aspects of HD using the aforementioned mouse model R6/2. Both aspects are centered on investigating the cellular state in specific brain regions and how the disease context affects this state. Therefore, in both projects, measurements are conducted throughout the course of the disease. The first aspect is based on measuring neuronal activity in the primary motor cortex and observing how the HD context alters this activity. Additionally, I wanted to shed light onto the underlying mechanism of these alterations. The second aspect revolves around intracellular protein homeostasis (proteostasis) that I monitored using a mouse model that expresses a chaperone-dependent proteostasis sensor. Specifically, I wanted to compare cells of different brain regions in models of HD. These two approaches tackle different aspects of the disease investigated. Therefore, in the following pages I will introduce both projects separately (refer to section 1.2 and 1.3, respectively).

1.2. Cortical activity project

For locomotion, muscles in the limbs have to be activated by motoneurons. These reside in the lumbar (lower) and cervical (upper) spinal cord to innervate muscle fibres in the hindlimbs and forelimbs, respectively. Although continuous locomotion is generated by central pattern generators in the spinal cord [117], for initiation of motion, motoneurons receive excitatory input from the brain [118]. The motor cortex is known to be important for elicitation of motor function [119]. Several neurodegenerative diseases affect motor functions, for example HD, SCA, PD and ALS. Although for all of these diseases, different brain regions are primarily affected (e.g. the cerebellum in SCA, substantia nigra in PD), the motor cortex is often disturbed by all of these disorders [120], [121]. In HD, the motor cortex is among the most affected regions. Neuronal cell loss in motor cortex increases with disease progression [50], suggesting causality. Several studies have described impaired cortical inhibition in the motor cortex of HD patients [122], [123], [124] and a concomitant increase in excitability [123].

1.2.1. Interneurons

Cortical activity is highly influenced by inhibition exerted by GABAergic interneurons onto pyramidal cells [125]. Interneurons make up 20 % of all cortical neurons [2] [3]. Interneurons receive excitatory input from pyramidal cells that are then again inhibited by the interneurons. This cycle is called feedback inhibition. Interneurons also receive long-range excitatory input from other cortical or non-cortical areas that also target pyramidal neurons, a mechanism called feedforward inhibition [125]. Thus, inhibition of pyramidal cells by interneurons, shapes cortical activity in several ways.

Interneurons have been divided into distinct subpopulations based on specific innervation patterns and cellular markers expressed. In the mouse somatosensory cortex, one can divide almost all GABAergic interneurons into parvalbumin (PV)-, somatostatin (SST)- and ionotropic serotonin receptor 5HT3a (5HT3aR)-positive neurons [126]. PV-positive GABAergic neurons comprise ~ 40 % of all interneurons in somatosensory, motor cortex and visual cortex [3], [126],

[127]. They can be further divided into basket and chandelier cells, based on the pattern of innervation [128]. SST-positive neurons account for ~ 30 % of all interneurons in somatosensory, motor and visual cortex [3], [126], [127]. 5HT3aR-positive neurons comprise ~ 30 % of all GABAergic neurons in somatosensory cortex [126] and can be further divided into vasoactive intestinal peptide (VIP)-positive and negative cells. In visual cortex, VIP-positive cells make up 17 % of all GABAergic interneurons [127]. calretinin (CR)-positive cells do not seem to make up a distinct subclass of interneurons, as they co-express VIP and SST in somatosensory and visual cortex [129], [130].

PV-positive cells innervate other PV-positive interneurons and pyramidal neurons perisomatically. SST-positive neurons innervate pyramidal cells and VIP-, PV-positive and other smaller subgroups of interneurons (which probably make up the 5HT3aR-positive cell group) on more distal dendrites and are therefore much less specific and less effective in their inhibition than PV-positive cells. VIP-positive cells exclusively innervate SST-positive interneurons in the visual cortex [127]. Among the VIP-, SST- and PV-positive neurons PV-positive neurons most strongly inhibit pyramidal cells [127].

1.2.2. Alterations of cortical functionality in mouse models of HD

Microarray analyses in R6/2 mice and human HD induced pluripotent stem cells (iPSC)-derived neural cells showed the strongest downregulation of genes belonging to the gene ontology (GO) categories of synaptic transmission, neurotransmitter release and calcium ion/calmodulin binding [131] [132]. In symptomatic R6/2 mice, cortical pyramidal neurons exhibit decreased spine density and decreased extent of arborization [116]. In 12-week old R6/2 mice several neurotransmitter receptors are decreased in expression. AMPA-, kainate- and group II metabotropic glutamate receptors as well as muscarinic acetylcholine receptors are reduced in the striatum and cortex. Dopamine receptors 1 and 2 are already affected at 8 weeks of age [133].

Electrophysiological recordings from slice cultures of R6/2 striatum suggested that the corticostriatal tract is impaired in this disease model starting at an age of 5 to 7 weeks [134].

These changes might therefore precede postsynaptic alterations in the MSNs. In R6/2 mice, cortical neurons have been shown to be more responsive to NMDA receptor activation, which could lead to excitotoxicity [135]. GAD67 mRNA is significantly reduced in cortical areas of R6/2 mice [136], hinting at a decrease of inhibition in this brain region. An electrophysiological study reported decreased inhibition, cellular hyperactivity and excitotoxicity in the cortex of R6/2 mice [109].

1.2.3. Open questions

Cortical pathology, including a decrease in inhibition and therefore the threat of excitotoxicity, plays an important role in HD and has been detected in mouse models of the disease. Nevertheless, three features have not been tackled in great depth: Firstly, the increase in cellular activity in R6/2 mice has not been shown in awake mice with cellular resolution. This means that either cellular resolution was obtained in tissue (most often by electrophysiological recordings) or imaging was conducted in awake mice using imaging techniques which do not allow for cellular resolution (e.g. [137]). An additional aspect of this is that mice have not been behaving during measurements, since most non-cellular resolution techniques do not allow for movement. Therefore, coupling cellular activity with behaviour has not been possible. An exception to this is the study by Murphy-Nakhnikian et al., in which single neurons were recorded from awake, behaving mice [138]. Nevertheless, this study was conducted in the substantia nigra and not in the motor cortex. Secondly, single-cell electrophysiological recordings, although providing very detailed information, are always restricted to smaller numbers of cells. Larger sample sets provide stronger results and the opportunity to assess intra-neuronal differences and patterns of activity. Last but not least, monitoring of cellular activity has not been conducted in a chronic fashion. However, this would allow a better understanding of the underlying mechanisms, since one could then tie the alterations in activity to landmarks in disease progression. This would improve our understanding of the underlying mechanism of cortical activity impairments in HD.

1.2.4. Aims

In order to address these open questions, the aim of this project was to measure neuron activity in layer 2/3 of primary motor cortex in R6/2 mice during the course of the disease. The monitoring of cortical activity was to be conducted by chronically measuring calcium transients using a genetically encoded calcium indicator (GCaMP) and two-photon imaging in awake behaving mice. The rationale to image from layer 2/3 instead of from layer 5 was technical. Although cortical layer 5 is the layer most affected by HD, it is much more difficult to assess with two-photon microscopy. Thus, imaging was restricted to layer 2/3. To shed light onto the findings made from the imaging experiments, mass-spectrometry data sets of R6/2 mice were to be analysed and immunostainings in R6/2 mice conducted.

1.2.5. Method

1.2.5.1. Calcium imaging

During neuronal activity levels of calcium rise in the cell. The first influx of calcium occurs due to the opening of voltage-gated and receptor-operated calcium channels on the plasma membrane. Here, calcium enters the cell from the extracellular space. Subsequently, calcium-induced signaling pathways lead to the opening of calcium channels in the ER membrane leading to a second influx of calcium into the cytosol from intracellular calcium stores [139]. In calcium imaging, this change in calcium levels is measured and taken as an approximation of neuronal activity. GCaMPs are sensors that sense these calcium increases and were first published by Nakai et al. [140]. They consist of a fragment of the myosin light chain (the target sequence of calmodulin), enhanced green fluorescent protein (eGFP) and calmodulin. Upon calcium binding to calmodulin, the calmodulin - calcium - myosin composition induces a conformational change in the green fluorescent protein (GFP) which leads to higher fluorescent signals [140]. These signals can be picked up by fluorescence microscopy and used to measure neuronal activity by taking the changes in fluorescence as a proxy for neuronal activity [141], [142]. In this work we used an improved version of GCaMP, called GCaMP6s [143]. Genetically encoded calcium

indicators can be used in mouse brains for imaging of individual neurons through an implanted glass window in the skull [144]. Two-photon imaging, in which two photons are needed to hit the fluorophore at the same time to decrease energy per photon [145], decreases laser-induced excitotoxicity and increases depth of the tissue reached by the laser.

1.2.5.2. Advantages of calcium imaging in awake, behaving mice

In other models of neurodegeneration, cortical alterations have been shown through calcium imaging [146] [147]. For example, cellular activity was shown to be altered depending on the distance of the cell to A β plaques. Electrophysiological studies have provided insights into cortical activity alterations in HD mice [148], [109], [149]. Nevertheless, calcium imaging provides several unique possibilities: 1) To measure cellular activity of many cells (tens to hundreds) at the same time, so that paired firing between two or more cells and in dependence of their distance to one another can be analysed, 2) to measure cellular activity during behaviour, for example running, and relate it to this behaviour and 3) to image from the same cells over several imaging episodes and therefore over a prolonged period of time. Calcium imaging clearly provides a unique tool to analyse cellular dysfunction, which in the end is the best correlate of brain dysfunction during disease.

1.3. Protein homeostasis project

1.3.1. Protein homeostasis

Protein homeostasis (proteostasis) is the equilibrium in which a cell resides with regard to the folding state and functionality of its proteome [150]. On the way to properly folded proteins, difficulties arise due to protein complexity, mutations or external stressors and the cell harbors several mechanisms to deal with unfolded, misfolded, degradation-targeted and aggregated proteins. These mechanisms as a whole are called the protein quality control system (PQCS, Fig. 1-3). The PQCS consists of three main components: 1) Chaperones, proteins that help fold refolded and help unfold misfolded proteins. 2) Degradation machinery, such as the ubiquitin-

proteasome system (UPS) and the autophagy system. 3) Compartment-specific quality systems, found for example in mitochondria and the endoplasmic reticulum (ER).

1.3.1.1. Chaperones

Many chaperones are termed heat shock proteins (Hsps), because they are upregulated by the cell upon stress-inducing conditions such as heat shock (HS) [151], [152], [153]. Nevertheless, there are also many constitutively active Hsps (for example Hsc70, constitutively active, versus Hsp70, heat induced). Folding of a protein is based on its primary structure and its surrounding [151]. Molecular chaperones facilitate proper folding for example by binding to certain peptide stretches and therefore masking them to prevent incidental interactions with the rest of the peptide chain [151].

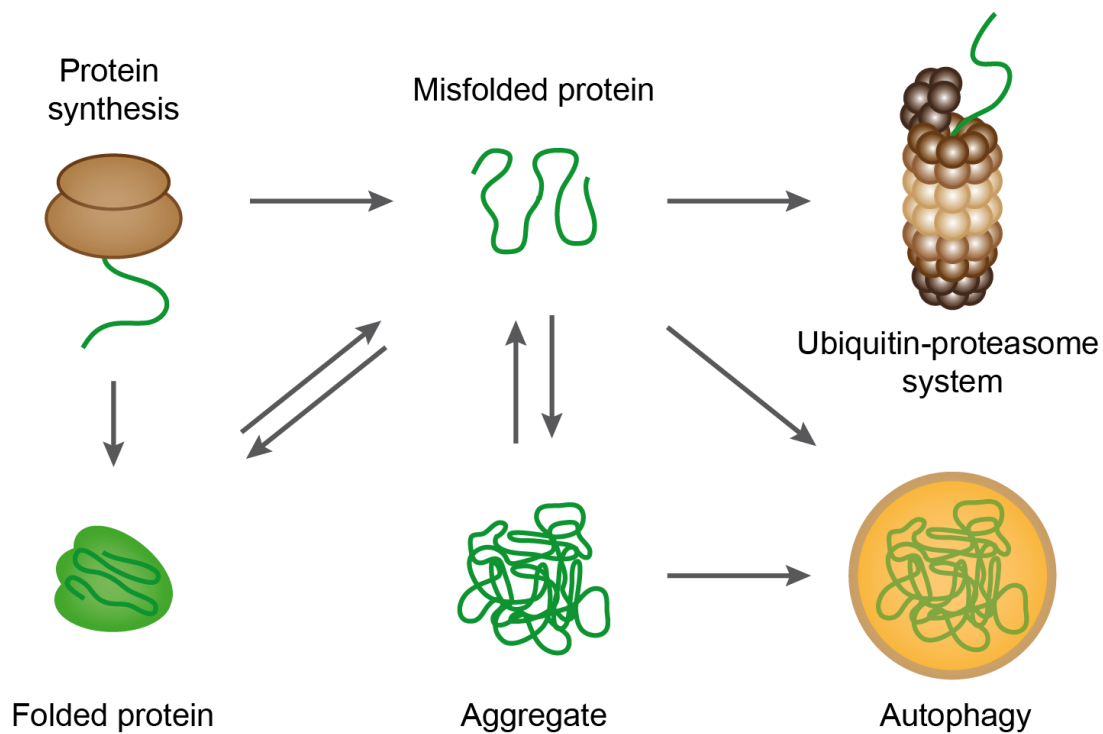


Figure 1-3: The Protein quality control system

After synthesis proteins have to be correctly folded. Nevertheless, due to amino acid composition, mutations or proteotoxic stress proteins can become misfolded and ultimately aggregate. Therefore, chaperones help fold and disaggregate proteins. However, misfolded proteins can also be degraded by the ubiquitin-proteasome system. Aggregated proteins can be degraded by autophagy.

Adenosine triphosphate (ATP)-dependent chaperones can be divided into four classes: Hsp60s, Hsp70s, Hsp90s and Hsp100s [152], [153]. The numbers indicate the molecular weight of the subunits. Hsp70s and Hsp90s interact with many co-factors and regulators, whereas Hsp60s and Hsp100s work together with very few co-factors. Hsp60s work at early stages of folding after protein synthesis, whereas Hsp90s help at late stages of the folding process, thereby, for example, regulating signaling pathways [153].

Hsp100 proteins mainly disaggregate and unfold misfolded and aggregated proteins or protein complexes. They form ring structures and can use mechanical processes to unfold proteins. Hsp60s are barrels that fold proteins by encapsulating them and thereby providing a different folding environment. The Hsp60 class (also-called chaperonins) is divided into two groups. The first one is found in bacteria (as GroEL) and in bacteria-originating organelles, namely mitochondria and chloroplasts (as Hsp60s). The second group is found in archaea and eukaryotes, as the thermosome and TriC, respectively. The Hsp70 family is the most abundant chaperone class in the cell. Its most important co-factors are the proteins of the Hsp40 family (also termed J proteins). Hsp70s are important for inter-compartmental transport. They provide support during folding and re-folding, presumably by stabilizing the intermediate folding state [154] and, together with Hsp100s, they can disaggregate aggregated proteins. As for most chaperones, there are many different Hsp70s, some cytosolic and some compartment-specific. Hsp90s are also highly abundant chaperones that work together with several co-factors, making them tunable. They are an important node of several signaling pathways. Hsp90s are for example critical for the induction of the heat shock response (HSR) [155], [156].

The heat shock response is induced by activation of heat shock factors (HSF) (reviewed by Voellmy [157]). There are four HSFs, 1 to 4, of which HSF1 and HSF3 are necessary and sufficient for induction of the heat shock response in mammalian and avian cells, respectively [157]. In its silenced state HSF1 is bound by Hsp90. For activation it is released from Hsp90, trimerises and translocates to the nucleus, where it binds to the heat shock response element (HSE). This leads to the expression of heat-induced proteins such as Hsps. [156], [158]. This mechanism, termed chaperone titration, implies that proteotoxic stress leads to increased load of

unfolded proteins and therefore high demand for chaperones. This in turn leads to Hsp90 releasing HSF1, which then mounts the HSR and thereby causes an upregulation of chaperones.

1.3.1.2. The ubiquitin-proteasome-system

Degradation of single proteins via the UPS is divided into two steps (Fig. 1-4). First, the target is poly-ubiquitinated. During this process ubiquitin (Ub) peptides are conjugated one by one to the target protein forming a poly-Ub chain. Then, the target protein is sent to the proteasome and degraded by its protease activities. The conjugation of Ub to the target protein is carried out by three classes of proteins. First, an E1 ubiquitin-activating enzyme binds an Ub peptide, this Ub is then transferred to an E2 ubiquitin-conjugating enzyme to finally be conjugated to the target protein by an E3 ubiquitin ligase. In human, more than 1000 different E3 ligases exist, suggesting that their specificity is of great importance for correct functioning of the UPS. Before the target protein enters the proteasome, the ubiquitin chain is removed by ubiquitin peptidases. In order for the poly-Ub to be a degradation signal, a subsequent Ub has to be conjugated to a lysine 48 of the prior Ub. Poly-Ub chains conjugated via the lysine 63 deliver a different signal [159].

The proteasome consists of two particles, the 20S core and the 19S regulatory particle. The 20S core is made up of 4 heptametrical rings that form a barrel structure. These rings are composed of α - and β -subunits, the latter of which contains chymotrypsin-, trypsin-, and caspase-like protease activities. The 19S regulatory particle can bind the 20S core from both sides and forms a lid to the 20S barrel structure. For degradation, proteins are encapsulated in the barrel structure and the 19S lid binds.

After degradation of the protein, amino acid chains are released through the other opening of the barrel (reviewed by Bedford et al. [160]). That the UPS system is very important to prevent neurodegeneration is appreciable through the fact that specific mutations in E3 ligases can cause neurodegeneration. For example, a mutation in the E3 ligase Parkin causes early-onset Parkinson's disease (PD, [161]). But also misfolded proteins can influence the proteasome. Ortega

et al. reported that non-aggregated mHTT can clog the proteasome and make it non-functional [106].

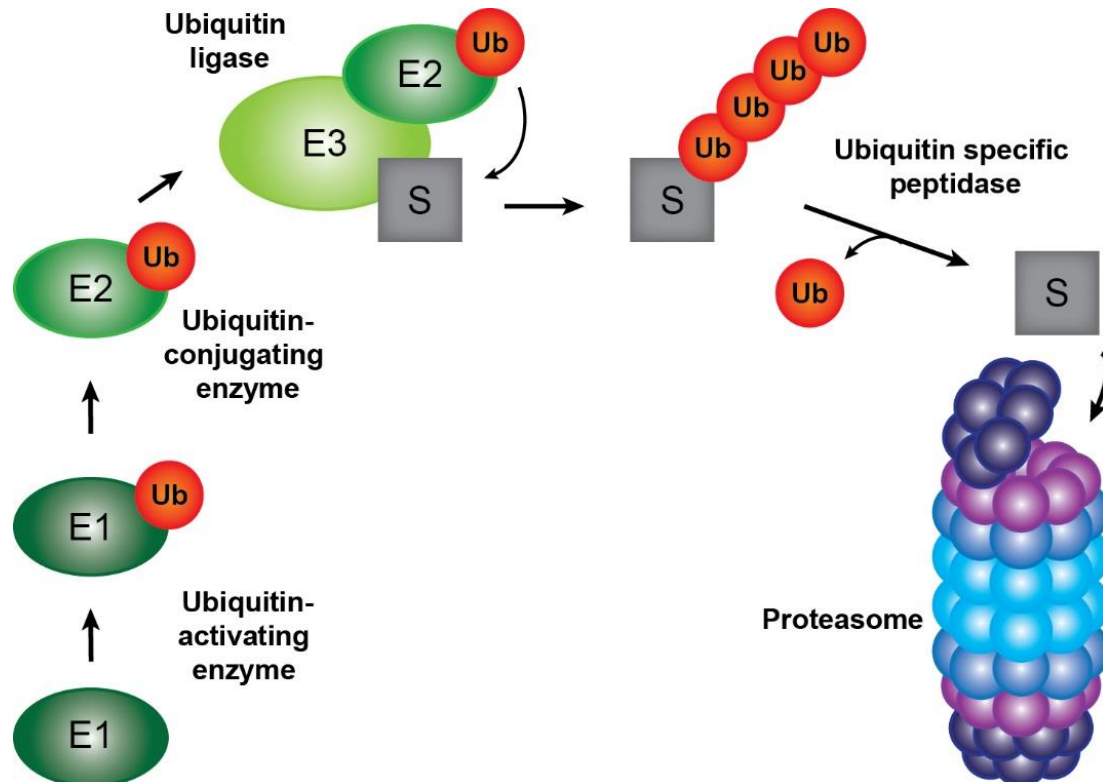


Figure 1-4: The ubiquitin-proteasome system

Ubiquitin (Ub, red circle) conjugates to an E1 ubiquitin-activating enzyme (dark green oval). This Ub is then transferred to an E2 ubiquitin-conjugating enzyme (green oval) to finally be conjugated to the substrate (S, grey square) by an E3 ubiquitin ligase (light green oval). Before the target protein enters the proteasome (purple complex), the ubiquitin chain is removed by ubiquitin peptidases.

1.3.1.3. Autophagy

Autophagy is the second degradation system of a cell. Through autophagy, the cell can degrade masses of proteins, whole protein complexes (or aggregates) or even organelles such as mitochondria (reviewed by Todde et al. [162]). For this, the target to degrade is sent to a lysosome. Autophagy can be divided into micro-autophagy, macro-autophagy and chaperone-mediated autophagy (CMA). The first two forms are not selective and degrade bulks of proteins or organelles and protein complexes, whereas CMA leads to selective degradation of single

proteins. Autophagy seems to be very important in neuronal cells, since suppression of it causes neurodegeneration [163], [164].

1.3.2. Proteostasis in neurodegeneration

It has been reported that cultured neurons mount less of a HSR than glial cells [165]. Nevertheless, a recent report from the lab of Gillian Bates demonstrated that upon Hsp90 inhibition *ex vivo* striatal neurons as well as glia exhibit an upregulation of HSPs [166]. The first time the PQCS was implicated in possibly providing help in neurodegenerative diseases was in 1998 by the lab of Huda Zoghbi. Cummings et al. found inclusions in neurons from patients of spinocerebellar ataxia and in transgenic mice [167].¹ These inclusions were not only ubiquitinated but also stained positive for proteasome subunits and chaperones. Overexpression of chaperones in immortalized cells decreased aggregation of mutant ataxin-1, which is the aggregating protein in SCA1 [167]. Since then many attempts have been made to improve burden of protein aggregation by inducing the heat shock response or overexpressing chaperones in model organisms with modest effects (reviewed by Smith et al.[168]). Manipulation of the PQCS is regarded as a promising therapeutic approach.

1.3.2.1. Protein homeostasis in mouse models of HD

Crossing R6/2 mice to HSF1-null mice increased aggregate load shown by immunofluorescence and filter-trap assay and decreased the life span of the mice suggesting that HSF1 is protective against mHTT expression [169]. Administration of a single strong dose of Hsp90 inhibitor, which elicited a HSR through activation of HSF1, lead to decreased aggregate load and phenotype improvement [170]. HSP upregulation due to Hsp90 inhibitor administration was impaired at 8 weeks of age, whereas this was not the case at 4 weeks of age. This impairment was not due to altered HSF1 activation or its translocation to the nucleus but due to a decreased binding of HSF1 to the DNA [170]. At 12 weeks of age Hsp70 and Hsp40 levels are significantly reduced in brains of R6/2 mice [170], hinting at a decreased HSR at this age and perhaps decreased proteostasis. Nevertheless, crossing R6/2 mice to Hsp27-overexpressing mice did not improve the R6/2 phenotype [171]. Overexpressing Hsp40 by viral delivery led to a decreased

aggregate burden, amelioration of the phenotype and extension of life span in R6/2 mice [172], showing that improving proteostasis can have a positive effect on neurodegenerative models. Overexpression of the DNAJB protein HSJ1a in R6/2 mice reduced aggregation load and increased soluble mHTT levels but had only mild effects on the R6/2 neurological phenotype [173].

Although CAG-length correlates inversely with disease onset in HD, a finding which can be reproduced in mouse models, it has been shown in mice that over a threshold of 150 CAG repeats the phenotype improves and life span increases with increasing CAG-repeat length. A striking difference of several weeks of life span increase appeared after a threshold of 320 CAGs [174], [175]. Tang et al. conducted microarray analyses of R6/2 mice with either 150 or 300 CAG repeats and wt mice as controls to obtain insight into how an increase in CAG repeat length could ameliorate the R6/2 phenotype [131]. Downregulation of transcripts in both transgenic models was largely comparable whereas upregulation showed clear differences based on CAG-repeat length. The R6/2 model with 300 CAG-repeats especially showed an upregulation of genes belonging to the GO categories protein folding and ubiquitin-dependent catabolic process [131]. This suggests that both aspects are very important for improved health under the proteotoxic stress of mHTT expression. So far genetic experiments have given mixed results regarding manipulating the PQCS in HD mouse models, so it seems necessary to first precisely describe what happens to the PQCS in the course of the disease and which components are mostly involved.

1.3.3. Open questions

Because HD is a genetic disease caused by one clearly described mutation the cause of the disease is clear. Nevertheless, three main questions remain to be answered: 1. Why does disease onset occur in the 4th decade of life although the mutation is already present from the beginning of life? 2. Why does HD affect some cells more than others if the mutation is present in all cells? 3. How can the disease be cured or at least treated?

1. Why does disease onset occur in the 4th decade of life although the mutation is already present from beginning of life? There are two possible explanations: Either mHTT toxicity (and/or level) has to accumulate to reach a certain threshold in order to exert its effects or it is because with age, the cellular system loses its capacities to deal with the constant level of stress exerted by mHTT. Both possibilities are not mutually exclusive. It has been reported that in *C. elegans* aging of the worms led to aggregation of metastable proteins [176], suggesting a decrease in cellular defense mechanisms over time. In a beautiful experiment, Yang et al., expressed the protein TBP that causes the disease SCA17 with 105 CAG repeats in mice [177]. They expressed TBP-105Q for the same duration but starting at three different ages. Older mice exhibited a phenotype much earlier than younger mice, showing that age affected how capable the organism was to deal with the expression of the mutant protein. These capacities comprise, among others, the proper folding of mutant misfolded proteins and their degradation. Therefore, it would be useful to measure proteostasis in an HD mouse model throughout its life span.

2. Why does HD affect some cells more than others if the mutation is present in all cells? The answer to this can be divided into two possibilities that are again not mutually exclusive. Either the load of mHTT is higher in certain cells or the capacities to deal with the imposed stress are lower in certain cells. For example, specific cells could express mHTT with longer polyQ stretches due to CAG-repeat instability as proposed by Swami et al. and Kennedy and Shelbourne [36] [35]. Higher load of mHTT could also arise due to increased production or decreased degradation. The second possibility is that certain cells cope less well with the insult that mHTT expression poses onto the system. This could entail better folding of mHTT, but also better shielding of vital systems from mHTT. Therefore, comparisons between different cell types would be beneficial when observing cellular states in response to mHTT toxicity.

3. How can the disease be cured or at least treated? For this there are of course many different approaches, ranging from genetic correction of the mutation to administration of neurotrophic factors that improve the overall health of the cells. Improving the capacities of the PQCS could be a promising therapeutic approach. Nevertheless, for this it is utterly important to see whether and if so, in which areas and at what time there are deficits in this system.

1.3.4. Aims

To address these open questions, I measured protein folding capacities in the HD mouse model R6/2 during the course of the disease in different brain regions for comparison. For this, I used the proteostasis sensor firefly luciferase (Fluc) [178]. Several steps had to be executed. First, the functionality of Fluc had to be tested in transfected primary neurons. This was to be conducted by administration of pharmacological stressors and as a more physiological stress, by expression of an aggregating protein. Secondly, a transgenic mouse expressing the sensor had to be developed which then had to be crossed with R6/2 mice. In these mice proteostasis capacities were to be measured in different brain regions to elucidate whether different cell types deal differently with the burden of mHTT. To investigate how proteostasis changes throughout the disease, measurements were to be conducted at different time points. Any findings made, were to be followed up and potentially explained mechanistically.

1.3.5. Method

1.3.5.1. Proteostasis sensors

Several sensors of the PQCS have been described. There are, for example, redox sensors such as RoGFP [179] that can measure the oxidative state of a cell. A sensor that is more specific to proteostasis is Ub-G76V-GFP [180] that accumulates in the cell if the proteasome is inhibited, which can be visualised by fluorescence microscopy. A mouse expressing Ub-G76V-GFP was published by Lindsten et al. in 2003 [181] and has been used in R6/1 mice [106] and a mutant tau expressing mouse model [182]. Although it is a great tool and widely used, it bears the disadvantage of only measuring the UPS. Sensors, which do not have this disadvantage have been published by the lab of Rick Morimoto. They consist of metastable proteins which are mutated to become more unstable and therefore more sensitive to a decline in proteostasis. An example is paramyosin, which was expressed in *C. elegans*. Upon increased temperature, mutated paramyosin misfolds, aggregates and induces a behavioural phenotype in worms. In the presence of a polyQ peptide paramyosin also aggregates at permissive temperatures, suggesting that polyQ

induces stress onto the proteostasis system, which the sensor detects [183]. This publication nicely demonstrates how the aggregating proteins (here polyQ) can induce stress on the cell that influences other metastable and aggregation-prone proteins (here mutated paramyosin). Nevertheless, this sensor harbors the disadvantage that an endogenous protein is used as a sensor and the lack-of-function of this protein in the overall system induces another stress. A solution for this problem is the use of a metastable exogenous protein. Such a sensor will be described in the next section.

1.3.5.2. The Fluc sensor

The Fluc sensor was published by the lab of Ulrich Hartl in 2011 as a proteostasis sensor [178]. Fluc is comprised of the firefly luciferase and tagged with GFP. It is a metastable protein, which requires chaperones for proper folding [184], [185]. Gupta et al. mutated the protein further to destabilize it and thereby make it more sensitive to stress. From this, a cassette of three different Fluc sensor variants arose: the wt version FlucWT, the more sensitive single mutant (sm) FlucSM and the most destabilized double mutant (dm) FlucDM. The idea underlying its functionality is that proteotoxic stress leads to an abundance of misfolded proteins. More chaperones are needed to deal with this increased amount of misfolded proteins. Therefore, less chaperones are available for proper folding of Fluc, causing Fluc to be more misfolded and to form inclusions. These inclusions can be visualised by fluorescence microscopy based on its GFP tag. Additionally, Fluc catalyses a reaction that transforms luciferin into oxyluciferin. This reaction emits light, which can be measured in a luminometer. Catalytic activity of Fluc is diminished by defects in its folding and can be used to monitor cellular proteostasis. Nevertheless, luciferase activity is not only dependent on Fluc's folding state but of course also on the quantity of Fluc. Therefore, luciferase activity has to be normalized to protein quantity, which is measured through immunodetection after western blotting. Upon proteotoxic stress Fluc therefore forms bright inclusions and exhibits a decrease in its specific activity (Fig. 1-5).

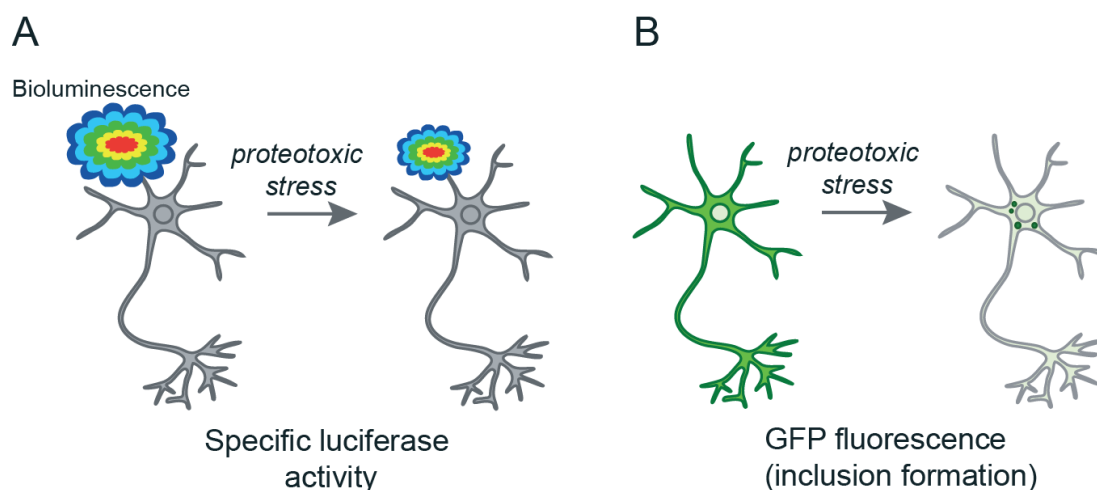


Figure 1-5: Readouts of the Fluc sensor

A: Luciferase catalyzes a reaction involving its substrate luciferin. This catalysis is dependent on the proper folding of Fluc. Under proteotoxic stress Fluc is less well folded. Therefore, it can catalyse the reaction less efficiently, which then emits less light. This difference in emitted light can be measured using luminometers. B: Fluc is GFP tagged, filling the cell, but excluding the nucleus in neurons. Under proteotoxic stress, Fluc re-localises, forming inclusions, which can be visualized by fluorescence microscopy.

One of its advantages over other sensors is that it does not only measure the UPS system but also chaperone availability and therefore gives a more complete readout over proteostasis than the aforementioned Ub-GFP sensors. A second advantage is that using the bioluminescence readout, Fluc can measure positive and negative changes in proteostasis capacities, because at a given time not all Fluc molecules are 100 % correctly folded.

So far, Fluc has been shown to sense proteotoxic stress applied either pharmacologically or by expression of an aggregating protein in immortalized human embryonic kidney (HEK) cells. Additionally, it has been shown to react to the proteotoxic stress that aging causes in *C. elegans* [178]. To what extent Fluc can be used in primary neurons or in the mouse is currently unknown.

2. Results

2.1. Cortical activity in R6/2 mice

2.1.1. Data generation

The two-photon imaging set-up was built by Johanna Neuner. In total, six R6/2 mice and seven wt littermate controls (all female) from three different litters were imaged (Table 2-1). 11 out of 13 mice were imaged by Johanna Neuner.

Table 2-1: Imaged mice

Genotype	Batch	Mouse ID	Genotype	Batch	Mouse ID
wt	1	3985	R6/2	1	3726
wt	1	3974	R6/2	1	3714
wt	1	3978	R6/2	1	3989
wt	1	3732	R6/2	1	3977
wt	2	2	R6/2	2	3
wt	3	5112*	R6/2	2	4
wt	3	5113*			

* imaged by myself

Two animals were imaged by me and Johanna Neuner, who left the project afterwards. Data of all animals was provided to me. First image processing, including motion correction, setting of ROIs and extraction of calcium traces, as well as running analyses was conducted by Johanna Neuner and was continued by me for the remaining animals. I also repeated running analyses of all mice.

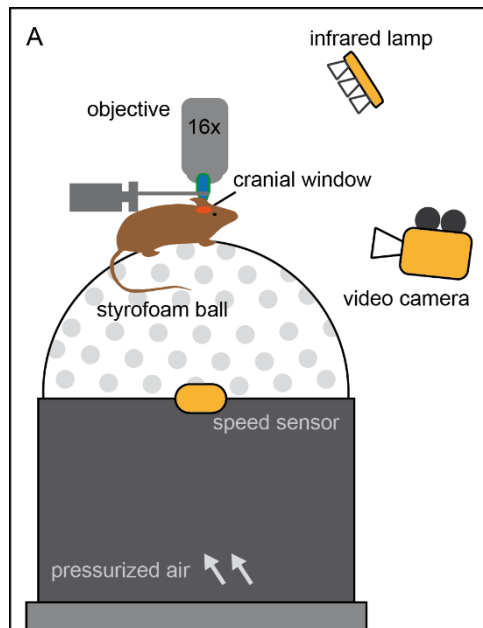


Figure 2-1: Experimental set-up

The mouse was head fixed under a two-photon microscope and free to run on a styrofoam ball, which was lying on a pressurized air bed. Running behavior was detected through a speed sensor and a video camera using an infrared lamp. Imaging was conducted through a 16x objective and a cranial window.

Extensive calcium imaging analyses, including statistical testing of the data, were done by Sabine Liebscher (Institute of Clinical Neuroimmunology, LMU). Mass-spectrometry data was provided by Fabian Hosp (lab of Matthias Mann, MPI of Biochemistry), including the statistical t-test analysis comparing R6/2 and wt mice of different ages. All further analyses of mass-spectrometry data were conducted by me. For histological studies Julia Boshart provided technical assistance. André Wilke and Matthias Fischer helped with processing the tissue and counting of neurons. André Wilke helped with keeping the mouse colony.

2.1.1.1. Chronic two-photon imaging

Mice were weaned at three weeks of age, surgery (virus injection and cranial window implant) was conducted at an age of 3.5 weeks. Subsequently, mice were handled and trained on the ball over several days (Fig. 2-1). Imaging started at 6 weeks of age and was conducted twice a week until an age of 9.5 weeks. The first imaging session (6 weeks) was not used in further analyses, because virus expression and window quality were not yet optimal. Mice were not imaged at the age of 9.0 weeks. After the last awake imaging sessions (9.5 weeks), imaging was additionally conducted in anesthetized animals (Fig. 2-2 A). For detection of calcium transients, GCaMP6s was expressed under the neuron specific synapsin 1 promoter in layer 2/3 of the primary motor cortex (Fig. 2-2 B - C).

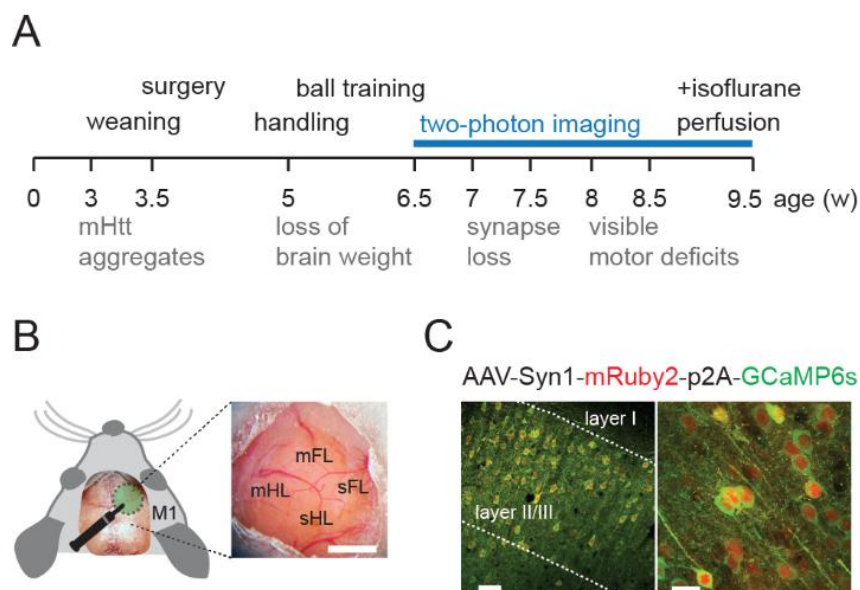


Figure 2-2: Experiment design and time frames

A: Timeline of the experiment. In grey R6/2 phenotype, in black experimental procedures. B: Schematic of a mouse brain, in green area of virus injection. Blowup shows different cortical areas, mHL: motor hindlimb, mFL: motor forelimb, sHL: somatosensory hindlimb, sFL: somatosensory forelimb through a cranial window. C: Expression of the AAV construct. mRuby2 and GCaMP6s are expressed under the neuron-specific synapsin 1 promoter. Expression is targeted to layer 2/3 of the motor cortex (left). Single cells express both mRuby2 and GCaMP6s (right). Scale bars: B) 1 mm, C left) 50 μ m, C right) 20 μ m. Figure by Johanna Neuner.

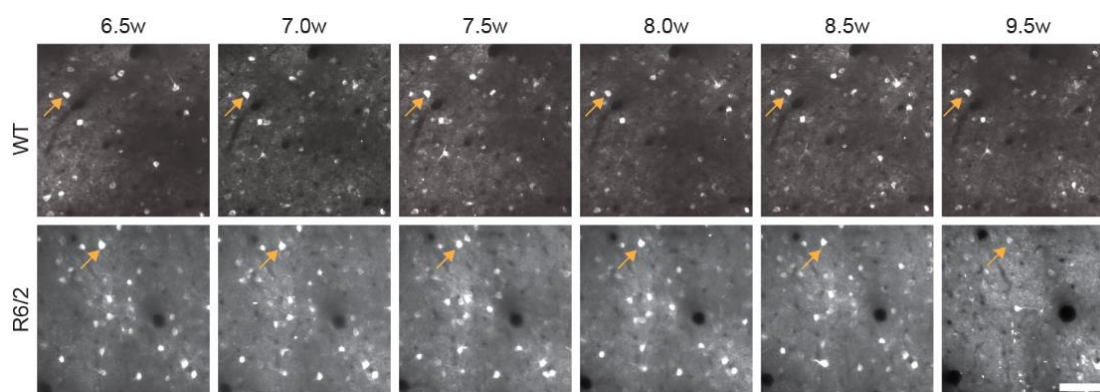


Figure 2-3: Re-finding of the same cells over all imaging time points.

Fields of view (FOV) from a wt and a R6/2 mouse over all six imaging time points. Note that both blood vessel pattern and cellular pattern are re-identified over all time points (arrows). Scale bar: 100 μ m. Figure by Johanna Neuner.

At each time point cortical activity was measured in two regions of interest per mouse for 15 min each. Vasculature patterns and the structural marker mRuby2 were used to re-identify the same regions of interest over the whole imaging period of three weeks (Fig. 2-3).

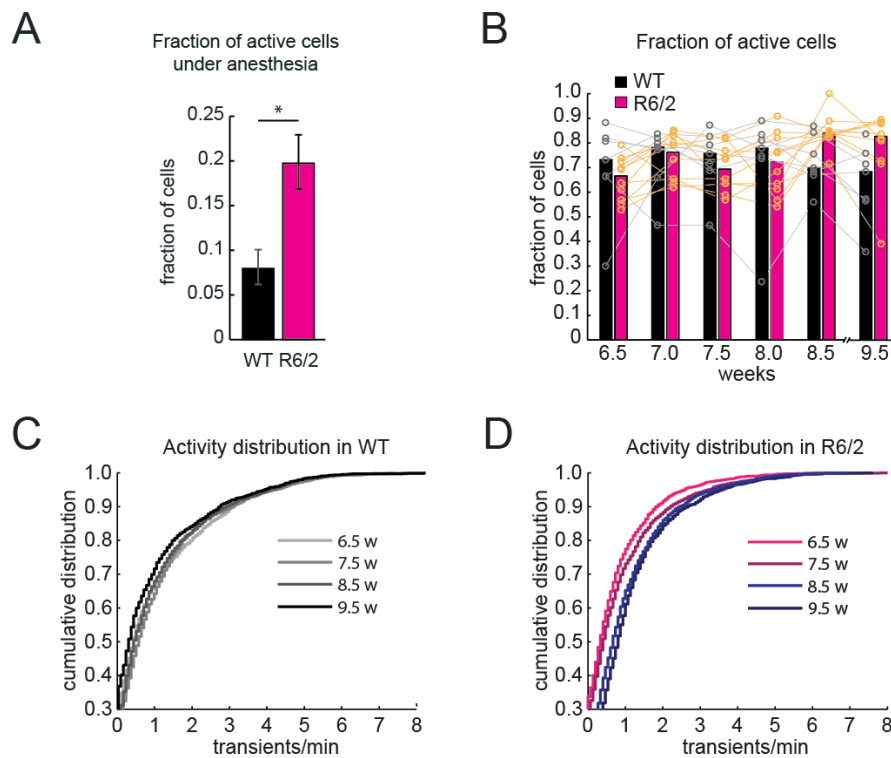


Figure 2-4: Increased neuronal activity in R6/2 mice from 8.5 weeks of age

A: Mice were imaged at 9.5 weeks of age under isoflurane anesthesia using two-photon imaging. The fraction of active cells was more than twice as high in R6/2 mice than in wt controls (wt: 6 experiments (FOV) from 3 mice, R6/2: 4 experiments from 2 mice; Wilcoxon rank-sum test, $p = 0.038$). B - D: Awake, behaving mice were imaged over a period of three weeks using two-photon imaging. B: The fraction of active cells ranged around 70%. For the first four imaging time points the fraction of active cells was similar in R6/2 and wt littermate controls. At time points 8.5 and 9.5 weeks of age the fraction of active cells in R6/2 was higher than in wt controls. 3004 cells from wt and 4156 cells from R6/2 out of 7 and 10 FOV from 6 and 5 mice, respectively. Repeated measures ANOVA, Genotype: $F(1, 75) = 0.37$, $p = 0.55$; Age: $F(5, 75) = 3.32$, $p = 0.009$; Interaction $F(5, 75) = 3.11$, $p = 0.013$. C - D: In R6/2 the cumulative distribution of cell activity plotted as transients/min showed a clear shift towards higher activity for the two time points 8.5 and 9.5 weeks of age, whereas there was no such shift in wt animals. Repeated measures ANOVA, Genotype: $F(1, 20995) = 9.95$, $p = 0.0016$; Age: $F(5, 20995) = 52.17$, $p < 0.001$; Interaction $F(5, 20995) = 57.93$, $p < 0.001$). Figure by Sabine Liebscher.

2.1.2. More cells are active in R6/2 mice at disease onset

At the age of 9.5 weeks the fraction of active cells (over 0 transients / min) in anesthetized R6/2 mice was more than twice as high compared to wt controls (Fig. 2-4 A). In awake animals, between 6.5 and 8 weeks, the fraction of active cells was similar between awake R6/2 and wt mice. At 8.5 weeks of age, and therefore at disease onset, the fraction of active cells in R6/2 mice increased until the end of the imaging period at week 9.5 (Fig 2-4 B). Moreover, neuronal activity (transients / min) plotted as cumulative distribution increased at disease onset (8.5 weeks) (Fig. 2-4 C - D). Increased cellular activity is often due to higher running activity. However, R6/2 mice ran less than wt mice at all time points (2-way ANOVA, p-value = 0.0019) and no augmentation in running at disease onset was observed in R6/2 mice. Thus, this cannot be the reason for the increased cellular activity. At the first imaging time point, fewer neurons were running correlated in R6/2 mice compared to wt controls. Additionally, running correlation over time was less stable in R6/2 mice and the number of cells correlating with running decreased over time more in the transgenic mice than in control animals (data not shown). This suggests that the increased cellular activity observed in R6/2 mice at disease onset is aberrant activity.

2.1.3. Synaptic proteins are downregulated at disease onset in proteome of R6/2 mice

To understand the underlying mechanism of the measured increase in cellular activity, I analysed mass-spectrometry data of R6/2 and wt control mice provided to us by Fabian Hosp. Specifically, I conducted principal component analysis (PCA) on the soluble cortical proteome data of mice aged 5, 8 or 12 weeks of age. Three to four mice per age and genotype were used as replicates. No technical replicates were conducted. This analysis revealed that based on protein expression profile all wt mice and 5-week old R6/2 mice clustered together (Fig. 2-5 A). The first component, which made up 20.6 % of all variance, separated 8- and 12-week old R6/2 mice from the rest of the animals and therefore symptomatic animals from those without disease symptoms. The first component could therefore represent “age + genotype”.

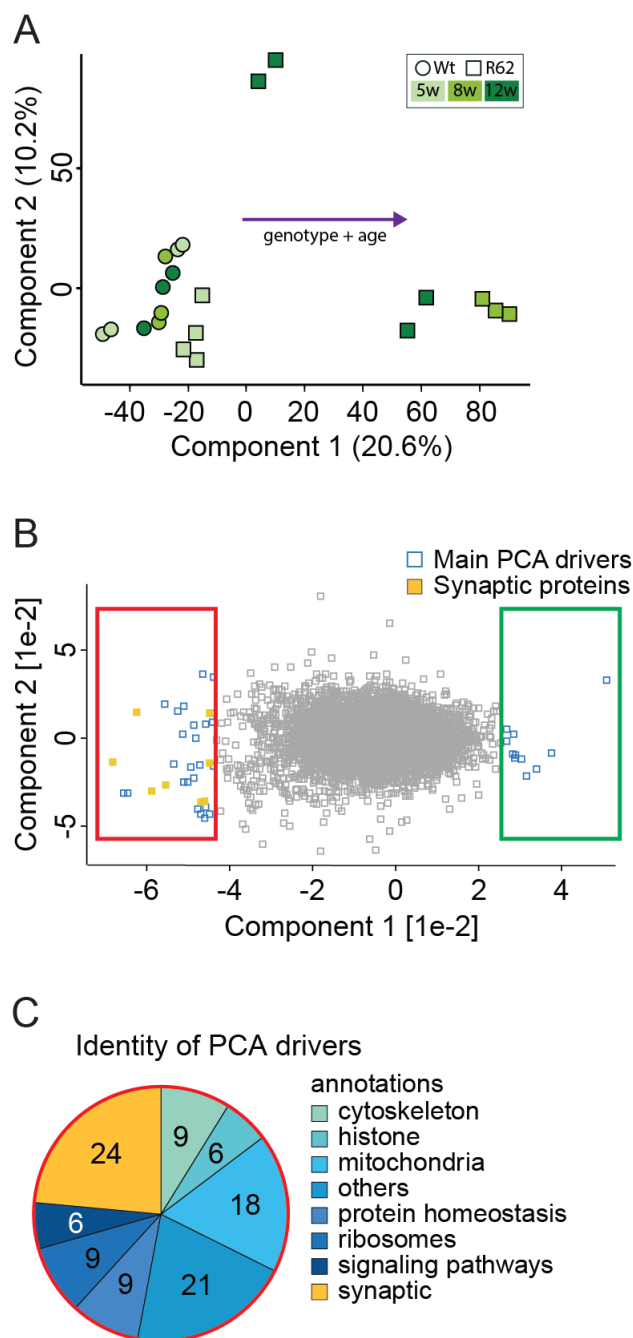


Figure 2-5: Synaptic proteins are main drivers of sample separation in PCA

A: PCA of soluble proteome separates 8-week old and 12-week old R6/2 mice from non-transgenic and 5-week old R6/2 mice. Component 2 separates two of the 12-week old R6/2 mice from all other mice, which were analysed at a different time point and came from our own colony, whereas all the other mice came from Jackson Laboratory. B: Main PCA drivers. Proteins in the green frame are upregulated in symptomatic R6/2 mice whereas the proteins in the red frame are downregulated in symptomatic R6/2 mice. Synaptic proteins are shown in yellow, all other main driver proteins in blue. C: 24% of the main driver proteins downregulated in old R6/2 mice were synaptic, this was also the annotation most represented. Proteins that were the only ones in their annotation were grouped under the label “others”.

The second component, accounting for 10.2 % of all variance, additionally separated two of the four 12-week old R6/2 mice from the rest of the mice. All R6/2 and wt control mice used for these experiments had been purchased at Jackson Laboratory. Two of the four 12-week old R6/2 did not show a R6/2 phenotype and had proteome profiles more similar to the wt than to the other

R6/2 mice. Therefore, these two mice were replaced by two R6/2 mice from our own colony. These two new mice were now separated from the others by the second PCA component. Therefore, this component could account for colony, mouse housing conditions (including hygienic status) or CAG-repeat length.

When analysing at the main drivers of the PCA separation (Fig. 2-5 B, red and green box), I found that the largest group of the proteins downregulated in R6/2 mice (red box) were synaptic proteins (24%, Fig. 2-5 C, Tables A-1 and A-2). For comparison, synaptic proteins made up 7.1% of all measured proteins (703 / 9937) and are therefore over-represented among the proteins most downregulated in symptomatic mice. The next larger group were mitochondria-related proteins (18 %). Proteins, which were the only ones assigned to a given annotation, were grouped under the label 'others' and made up 21 %. Of the proteins that were most strongly upregulated in symptomatic R6/2 mice (green box), none were synaptic proteins.

Next, I plotted all proteins by fold change regulation and p-value (Fig. 2-6). At 5 weeks of age no trend of up- or downregulation of all proteins or specifically synaptic proteins was observed (Fig. 2-6 A). At 8 weeks of age, in R6/2 mice clearly more proteins were downregulated than upregulated. This was also true for synaptic proteins (Fig. 2-6 B). At 12 weeks of age the trend from the 8-weeks old data remained, but was less pronounced (Fig. 2-6 C). To compare whether synaptic proteins were equally, less, or more regulated than all proteins, significantly regulated proteins or significantly regulated synaptic proteins were plotted as percentage of total proteins or of all synaptic proteins (703 and 9937 proteins, respectively) (Fig 2-6 D). While no clear up- or downregulation was observed at 5 weeks of age, at 8 weeks most regulated proteins were down-regulated, and this trend was greater for synaptic proteins (19%) than for all protein (12%), indicating that the synaptic proteins were specifically downregulated and did not just follow the trend of all proteins at this age. The same trend was observed at 12 weeks of age, though less pronounced than at 8 weeks.

I then searched for the significantly downregulated synaptic proteins in the insoluble proteome data set. I found that only 8 synaptic proteins that had been significantly downregulated in the soluble proteome were also significantly regulated in the insoluble proteome (Tables A-4

and A-5). Of these 8 proteins only two were upregulated in the insoluble proteome (one at 8 weeks and one at 12 weeks of age, Fig. 2-6 B – C), and the rest were downregulated. This suggests that sequestration of synaptic proteins by mHTT inclusions is not the main reason for downregulation of these proteins in the soluble proteome.

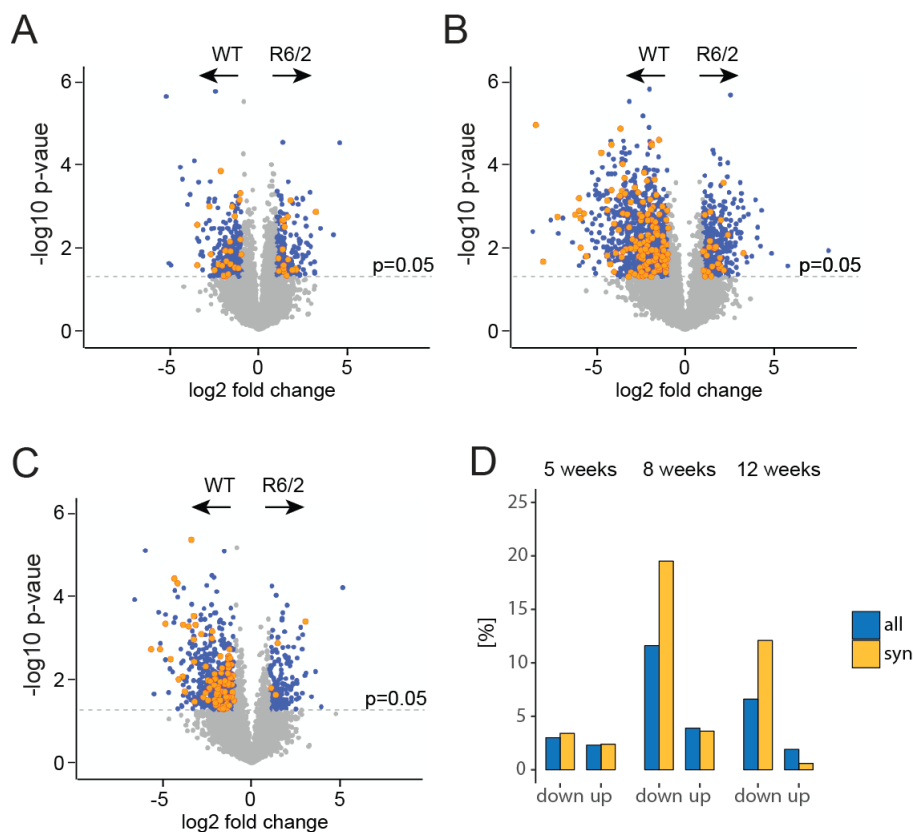


Figure 2-6: Synaptic proteins are downregulated in R6/2 cortex at 8 weeks of age

A-C: Volcano plots show proteins of the soluble cortical proteome of 5-, 8- and 12-week old R6/2 mice and littermate wt controls. On the x-axis fold change is plotted on a log₂ scale. On the y-axis the p-value is plotted on a negative log₁₀ scale. P-values higher than 1.3 on this scale lie under 0.05 and are therefore considered significant. Proteins regulated more than 2-fold (bigger than 1 on the log₂ scale) are considered strongly regulated. All proteins meeting these conditions are plotted in blue, synaptic proteins among these are plotted in yellow. A: At 5 weeks of age, a comparable number of proteins are down- and upregulated. This is also true for synaptic proteins. B: At 8 weeks of age most regulated proteins are downregulated in R6/2. This is also true for synaptic proteins. C: At 12 weeks of age, the same trend as in B) is evident. D: Significantly regulated proteins are plotted as percentage of all measured proteins for the two categories: all proteins (blue, 9937) or synaptic proteins (yellow, 703). At 8 weeks of age approximately 12% of all proteins are downregulated whereas almost 20% of all synaptic proteins are downregulated.

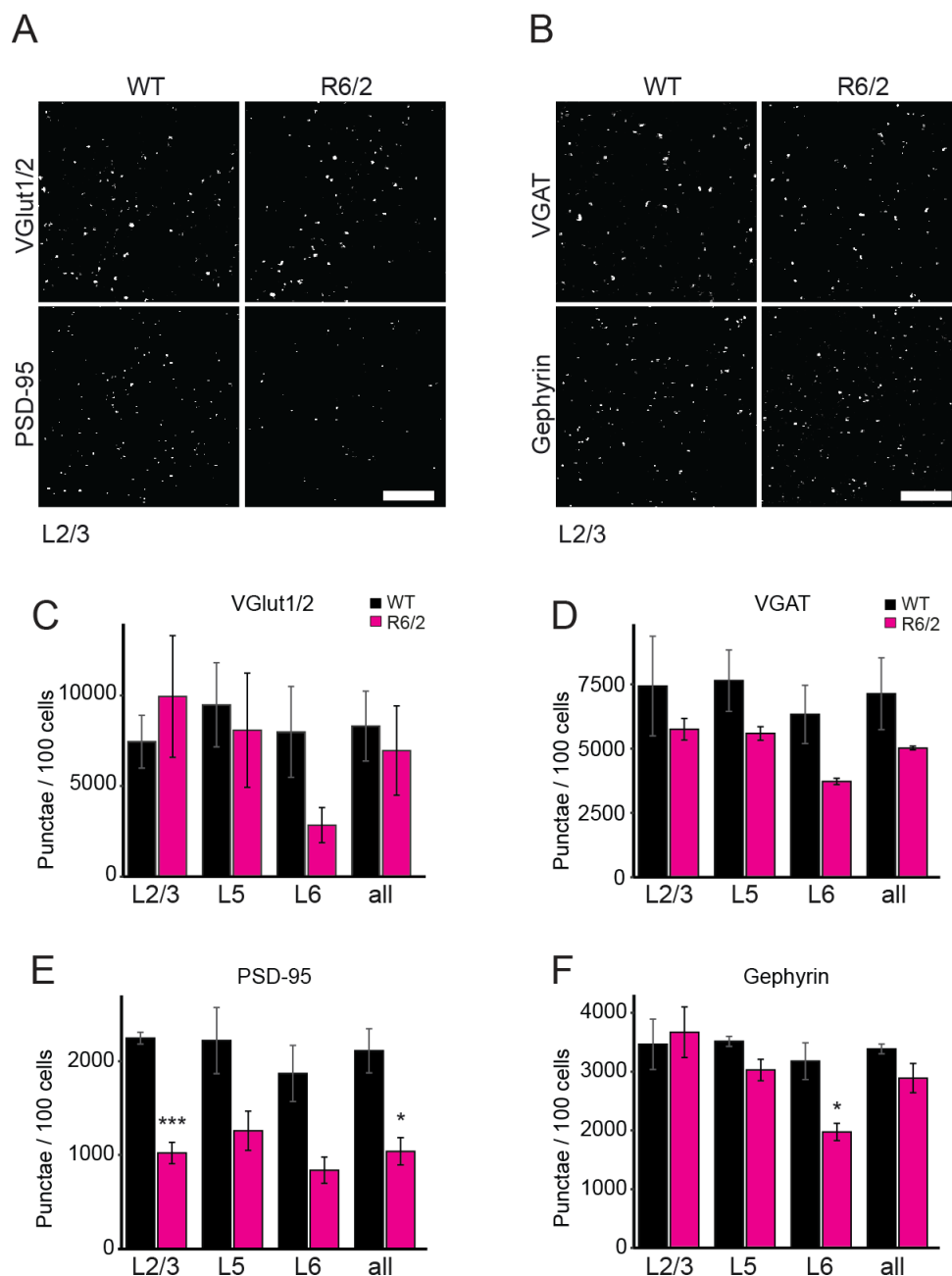


Figure 2-7: The excitatory postsynaptic marker PSD-95 is reduced in motor cortex of 8-week old R6/2 mice

A - B: Example images of excitatory and inhibitory pre-synaptic markers (VGlut1/2 and VGAT, respectively) and excitatory and inhibitory postsynaptic markers (PSD-95 and Gephyrin, respectively) in layer 2/3 of primary motor cortex of 8-week old R6/2 mice compared to wt littermate controls. C - F: Quantification of VGlut1/2-positive punctae (C), VGAT-positive punctae (D), PSD-95-positive punctae (E) and Gephyrin-positive punctae (F) in layers 2/3, 5, 6 and all layers taken together per 100 cells, quantified using DAPI. Data from three mice per genotype, up to three sections per mouse and one FOV per section. Scale bar: A - B) 10 μ m. One-way ANOVA with TukeyHSD posthoc test.

2.1.4. PV-positive terminals on pyramidal cells are reduced in R6/2 mice at disease onset

To test whether the decrease of synaptic proteins in symptomatic R6/2 mice was a consequence of reduced synapse numbers, we performed histology on brain tissue of 8-week old R6/2 mice and wt controls. We stained for pre- and postsynaptic markers of excitatory and inhibitory synapses (VGlut1/2, PSD-95, VGAT, Gephyrin, respectively) and counted the marker-positive punctae in layers 2/3, 5 and 6 of the primary motor cortex (Fig. 2-7).

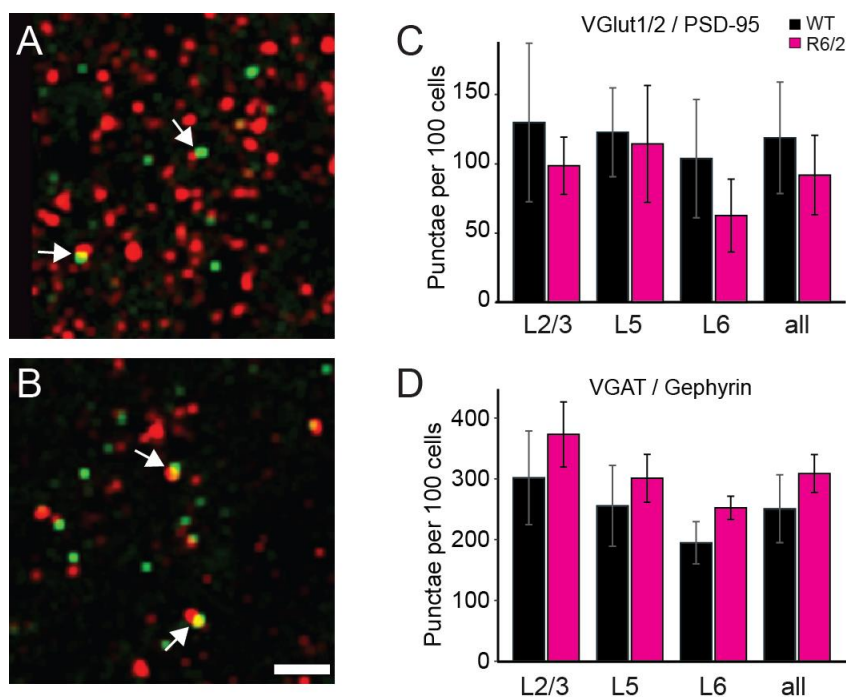


Figure 2-8: Neither excitatory nor inhibitory synapses are reduced in 8-week old R6/2 mice

A – D: Overlay of pre-synaptic and postsynaptic markers of excitatory and inhibitory synapses, in primary motor cortex of 8-week old R6/2 mice. A – B: Example images of synaptic staining. Arrows indicate examples of counted synapses. A: Excitatory synapses. Overlay of VGlut1/2 (red) and PSD-95 (green). B: Inhibitory synapses. Overlay of VGAT (red) and Gephyrin (green). C - D: Quantification of excitatory (C) and inhibitory (D) synapses. Quantification was conducted automatically using self-written macros in ImageJ. Briefly, punctae were dilated to induce overlap of otherwise opposing punctae. Overlapping pixels were extracted and these punctae counted. Data from four mice per genotype, three sections per mouse, one FOV per section. Scale bars: A – B) 3 μ m. One-way ANOVA with Tukey's HSD posthoc test.

Among the four markers only PSD-95 showed a significant decrease in all layers and specifically in layer 2/3 (Fig. 2-7 E). Looking at co-localization of respective pre- and postsynaptic markers, no decrease in excitatory or inhibitory synapse numbers was observed (Fig. 2-8). A decrease in inhibitory input onto pyramidal neurons could have explained the increase in cellular activity measured. I hypothesized that a decrease in a specific synapse type could be masked when counting all (inhibitory) synapses. Therefore, I assessed the PV-positive punctae on pyramidal neuronal nuclei (NeuN)-positive neurons, taken as a proxy of inhibitory synapses from PV-positive interneurons onto excitatory pyramidal neurons. I decided for this marker for three reasons. First, this marker is present in synapses and at the same time identifies an inhibitory cell population, contrary to for example VGlut1, which is not a marker of a specific interneuron cell population, or SST, which is not present in synapses.

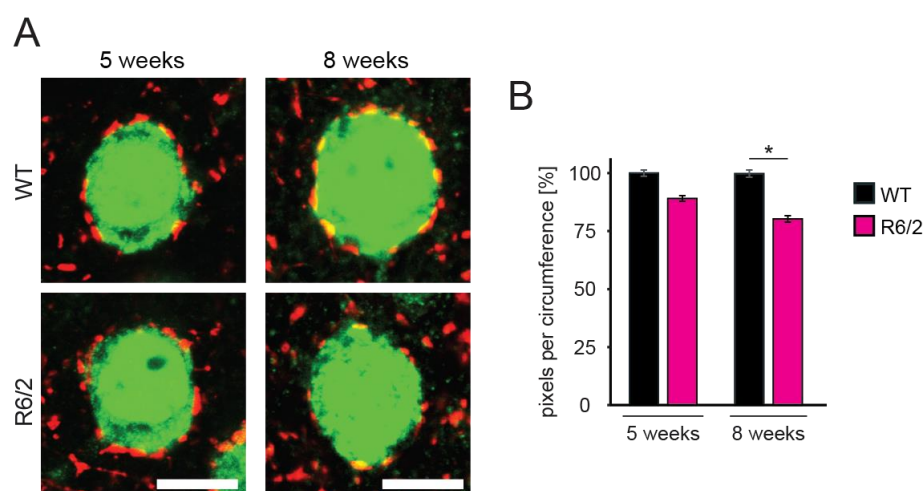


Figure 2-9: PV-positive terminals on pyramidal neurons are reduced in layer 2/3 of 8-week old R6/2 mice

A: Example images of PV-positive terminals (red) on NeuN-positive pyramidal neurons (green) from layer 2/3 of primary motor cortex of 8-week old R6/2 mice compared to wt littermate controls. B: Quantification of PV-positive pixels per circumference of NeuN-positive neurons. Data from four wt and five R6/2 mice, 12-15 cells per mouse. Scale bar: A) 10 μ m. Unpaired, two-tailed Student's t-test.

Secondly, synapses of PV-positive interneurons innervate pyramidal cells perisomatically, therefore applying a strong inhibitory drive on their target. Thirdly, they are easily detectable as they form a ring around NeuN-positive neurons. I observed a decrease in pixels per circumference

of 20 %. This decrease was not evident at 5 weeks of age (Fig. 2-9), which fits to the measured increase of neuronal activity at disease onset.

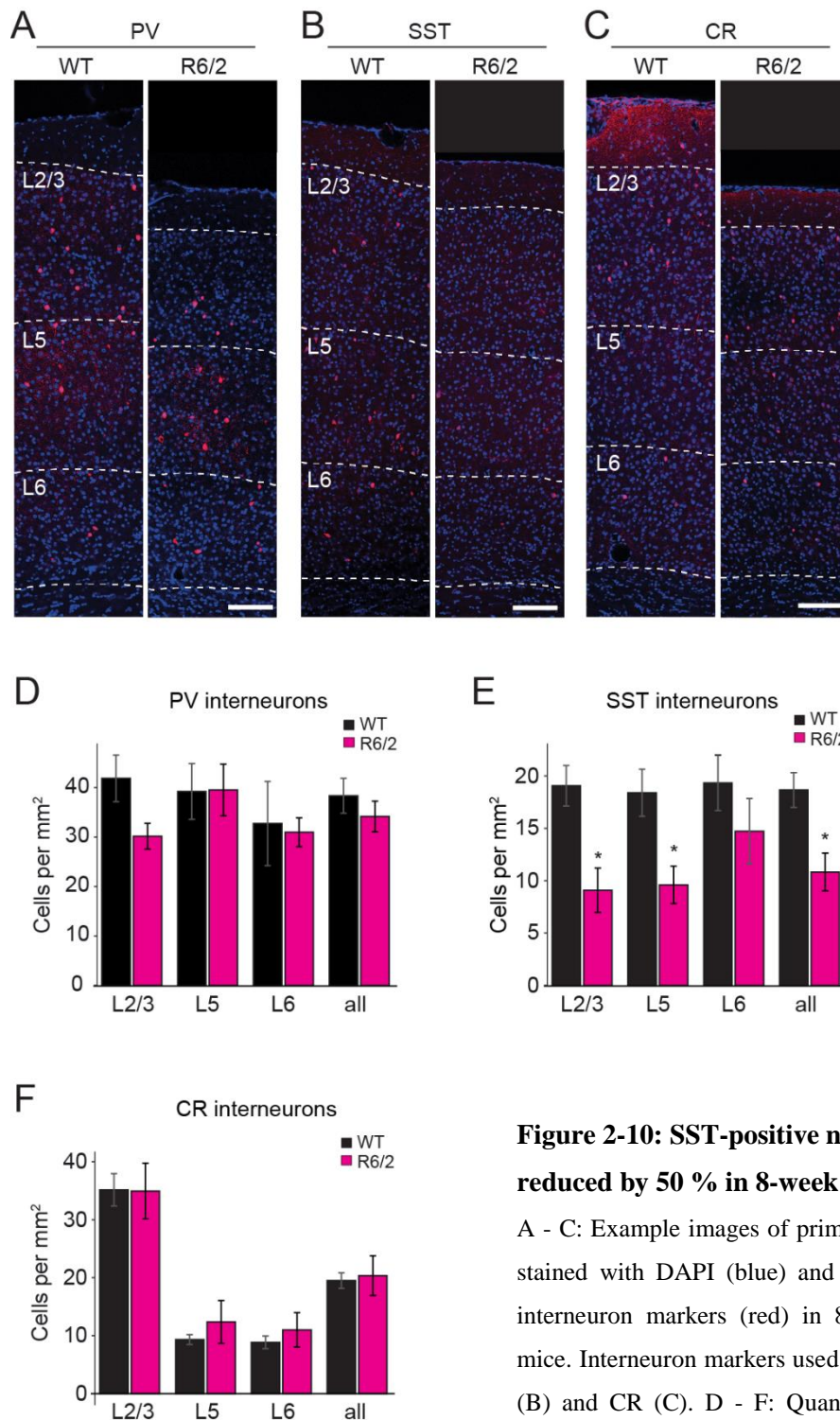


Figure 2-10: SST-positive neurons are reduced by 50 % in 8-week old R6/2 mice

A - C: Example images of primary motor cortex stained with DAPI (blue) and against different interneuron markers (red) in 8-week old R6/2 mice. Interneuron markers used are PV (A), SST (B) and CR (C). D - F: Quantification of PV-positive (D), SST-positive (E) and CR-positive (F) neurons in layers 2/3, 5, 6 and all layers taken

together as cells per area in mm². Note a 50% reduction of SST-positive cells in layers 2/3 and 5. Data from three mice per genotype, up to three sections per mouse. Scale bar: A) 150 μm. Unpaired, two-tailed Student's t-test.

2.1.5. Aggregate load and neuronal pathology correlate

2.1.5.1. SST-positive interneurons may be reduced in R6/2 mice

To check whether the decrease in PV-positive terminals was due to a loss of PV-positive interneurons, we performed histological stainings on tissue of 8-week old R6/2 mice and counted PV-positive interneurons in layers 2/3, 5 and 6 of primary motor cortex (Fig. 2-10). Although there was a decrease of 28% in layer 2/3 of R6/2 mice, this was not significant (Unpaired, two-tailed Students' t-test, p-value = 0.12). To test whether other interneuron subtypes might be affected, I also assessed SST- and CR-positive interneurons (Fig. 2-10 B, E and C, F, respectively). These three inhibitory markers label 80 – 90 % of all inhibitory neurons in mouse [186]. For SST-positive cells I saw a decrease of over 50 % in layers 2/3 and 5 of R6/2 mice, whereas there was no difference between wt and R6/2 mice when assessing CR-positive neurons. This decrease could be due to downregulation of SST or due to neuronal loss, both of which can be considered to be pathological.

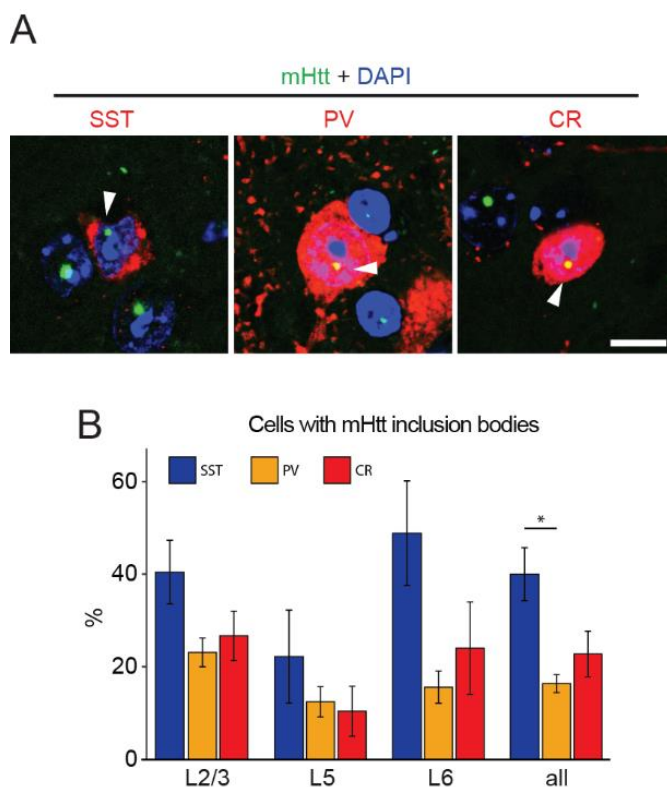


Figure 2-11: mHTT inclusion load correlates with neuronal pathology

A: Example images of different interneuron classes (red), bearing mHTT IB (green, arrowheads) on DAPI staining (blue). B: Quantification of interneurons with mHTT inclusions as percentage of all interneurons of a given population. Data from three (CR) to four (SST, PV) mice, up to three sections per mouse. Scale bar: A) 10 μ m. One-way ANOVA, with a Tukey's HSD posthoc test.

2.1.5.2. Neuronal pathology correlates with aggregate burden

I next assessed whether mHTT inclusion load correlates with loss of particular interneuron populations. For this, neurons with mHTT inclusions were counted per cell population in the primary motor cortex of 8-week-old mice and depicted as percentage of total cell number in this population (Fig. 2-11). Strikingly, in all layers SST-positive neurons had a higher percentage of mHTT inclusion bearing cells. When all layers were taken together the percentage of SST-positive neurons bearing inclusions was significantly higher than for PV-positive neurons (One-way ANOVA with Tukey's honest significance difference (HSD) posthoc test, p -value ≤ 0.05). This suggests that inclusion load might play a role in the cell population specific neurodegeneration observed at 8 weeks of age in R6/2 primary motor cortex.

2.2. Protein homeostasis in R6/2 mice

2.2.1. Data generation

If not stated otherwise, all data was generated and analysed by me. Data from HD94 mice was obtained by Irina Dudanova. Mass-spectrometry data was provided by Fabian Hosp, including statistical t-test analysis comparing R6/2 and wt mice and PCA. Further mass-spectrometry analysis was conducted by me. The transgenic service of the Max Planck Institute of Neurobiology carried out the pronuclear injection for the generation of transgenic mouse lines. Raphaela Götz, Tammo von Knoblauch and André Wilke helped managing the mouse colony.

2.2.2. Fluc functions in primary neurons

2.2.2.1. The HA-epitope does not change reactivity of Fluc in HeLa cells

The Fluc sensor was originally published bearing a myc-epitope. But to enable the possibility of combining it with myc-tagged proteins (for example mHTT(exon1)-constructs), I cloned the Fluc constructs with an HA-tag at the carboxyl-terminus. To investigate whether the change of the tag might influence the sensor's reactivity, I transfected HeLa cells with FlucWT-HA, FlucSM-HA, FlucDM-HA, FlucWT-myc or GFP-HA as a control. I applied heat shock or inhibited the proteasome (Fig. 2-12 A – C). Upon heat shock, Fluc formed a grainy pattern of inclusions throughout the cell. This reaction was evident in almost all cells transfected with either of the four Fluc variants. GFP did not react to either stress condition. After recovery from the heat shock only half of the cells still bore inclusions (Fig. 2-12 A – B). Upon proteasome inhibition Fluc formed single inclusions irrespective of the specific Fluc construct (Fig. 2-12 A, C). The HA-tag therefore did not seem to alter the reactivity of Fluc to proteotoxic stress. Note the increased reaction of Fluc to heat shock compared to MG-132 administration, probably due to the greater stress that is caused by heat shock.

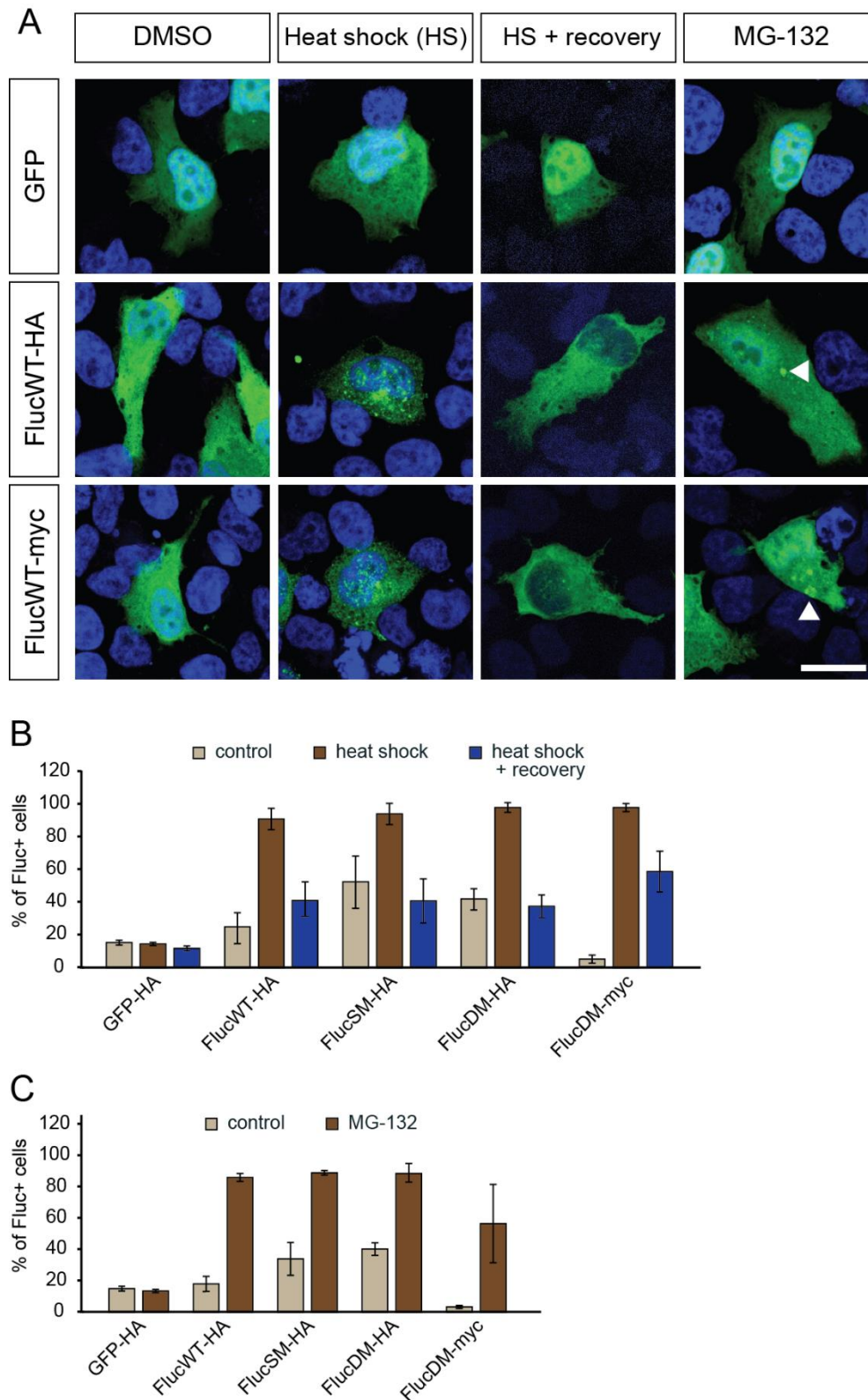


Figure 2-12: The HA-tag does not influence the reaction of Fluc to proteotoxic stress

A - C: HeLa cells were transfected with either FlucWT-HA, FlucSM-HA, FlucDM-HA, FlucWT-myc or GFP-HA as a control. Stress was induced 48 h after transfection. A: FlucWT-HA and FlucWT-myc react to stressors such as heat shock (2h at 43 degrees) and proteasome inhibition (5.0 μ M MG-132 for 8h in DMSO) by forming a grainy pattern of inclusions throughout the cells or by forming distinct inclusions

(arrowheads), respectively. The inclusions formed upon heat shock disappeared after 2 h of recovery. Note that in HeLa cells Fluc is seen in the nucleus and cytoplasm. B - C: The percentage of Fluc or GFP positive cells that showed inclusion formation was quantified from two independent experiments, 20 cells per experiment and condition. Scale bar: A) 20 μ m.

2.2.2.2. Fluc expression is not toxic in primary neurons

To determine whether Fluc expression is toxic in primary neurons, I transfected cortical neurons from embryonic day 15.5 (E15.5) CD1 embryos at 3 days *in vitro* (DIV) with FlucWT-HA, FlucSM-HA, and FlucDM-HA or GFP-HA as a control. Of all transfected cells, less than 20 % were cleaved caspase 3 positive. This was true for all four constructs and there was no significant difference between conditions (Fig. 2-13). These data demonstrate that expression of all three Fluc variants under the conditions used is not toxic in primary cortical neurons.

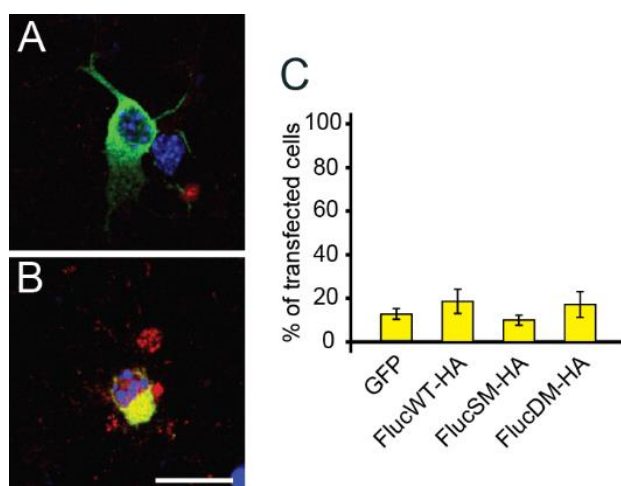


Figure 2-13: Fluc expression in primary neurons is not toxic

A-C: Primary cortical neurons of E15.5 CD1 embryos were transfected with FlucWT-HA, FlucSM-HA, and FlucDM-HA or GFP-HA as a control. At 3+2 DIV neurons were stained for cleaved caspase 3 as a marker for toxicity. A - B: FlucSM-HA transfected cell (green) stained for cleaved caspase 3 (red) and counterstained with DAPI (blue) as an example of a healthy (A) and a dying (B) neuron.

C: Quantification of two FOV per construct from three independent experiments. One-way ANOVA with Tukey's Multiple Comparison post-hoc test. Scale bar: A) 20 μ m.

2.2.2.3. Fluc reacts to different stressors in transfected primary neurons

To investigate, whether Fluc reacts to proteotoxic insults in primary neurons as it does in HeLa cells, I transfected primary cortical neurons with FlucWT-HA, FlucSM-HA, and FlucDM-HA or GFP-HA as a control. At 3+2 DIV I inhibited the proteasome or Hsp90 pharmacologically.

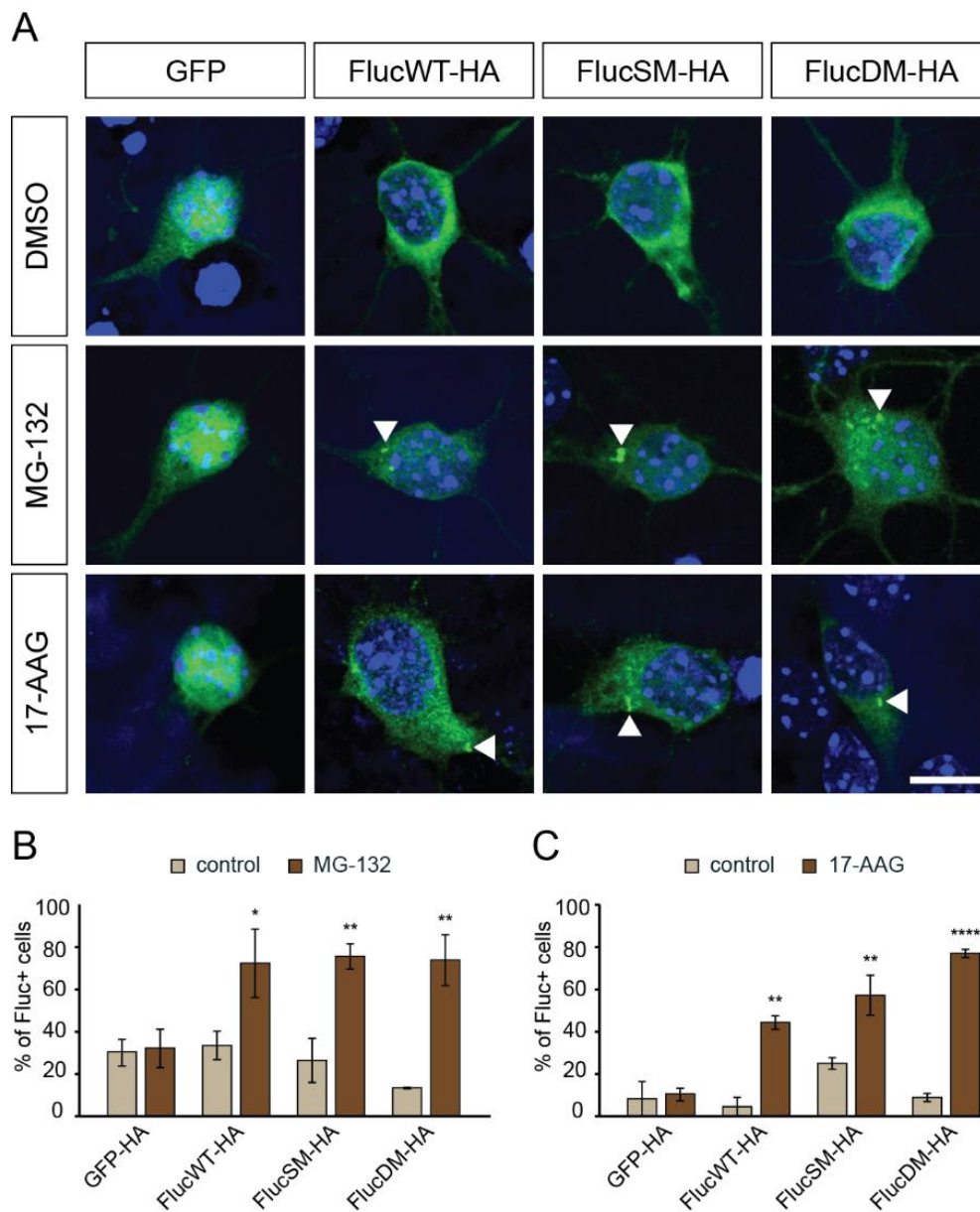


Figure 2-14: Fluc reacts to proteasome and Hsp90 inhibition in primary neurons

A-C: Primary cortical neurons of E15.5 CD1 embryos were transfected with FlucWT-HA, FlucSM-HA, FlucDM-HA and GFP-HA as a control. Stresses were induced at 3+2 DIV: proteasome or Hsp90 inhibition (5.0 μ M MG-132 or 5.0 μ M 17-AAG for 4h in DMSO). A: Primary cortical neurons under stress and control conditions. Fluc forms inclusions upon both stress conditions. B – C: Quantification of transfected cells bearing inclusions shows strong reaction to proteasome and Hsp90 inhibition. Data from three independent experiments, 15 cells per experiment. Scale bar: A) 10 μ m. Two-way ANOVA with Bonferroni multiple comparison posthoc test.

Upon proteasome inhibition, all three Fluc variants reacted to a similar degree: Approximately 80 % of all cells showed formation of distinct inclusions (Fig 2-14 A – B). All three Fluc variants were found to react to a similar degree in transfected HeLa cells challenged

with either heat shock or proteasome inhibition. These results suggest that these stresses are so strong that the different sensitivities of the three Fluc variants are masked. Upon Hsp90 inhibition, reactivity was more diverse between the three Fluc variants. With this stressor, the different sensitivities of the Fluc variants could be distinguished. For the wt, sm and dm types approximately 45 %, 55 % or 75 % of all transfected cells showed inclusion formation (Fig. 2-14 A, C). Interestingly, as compared to transfected HeLa cells, in primary neurons Fluc did not seem to be present in the nucleus, hinting at a different cellular machinery between HeLa cells and primary neurons. In primary neurons, in most of the cases two perinuclear inclusions were visible, which based on location, probably formed at the microtubule-organizing centres (MTOCs). In live cell experiments in transfected primary neurons that were challenged with proteasome inhibitor, I observed the formation of Fluc inclusions in neurites that over time were retrogradely transported to the cell body (Fig. 2-15 A) and fused into bigger inclusions (Fig. 2-15 B). Live cell imaging during a recovery period after proteasome inhibition did not show a re-solubilisation during the first 20 h (Fig. 2-15 A).

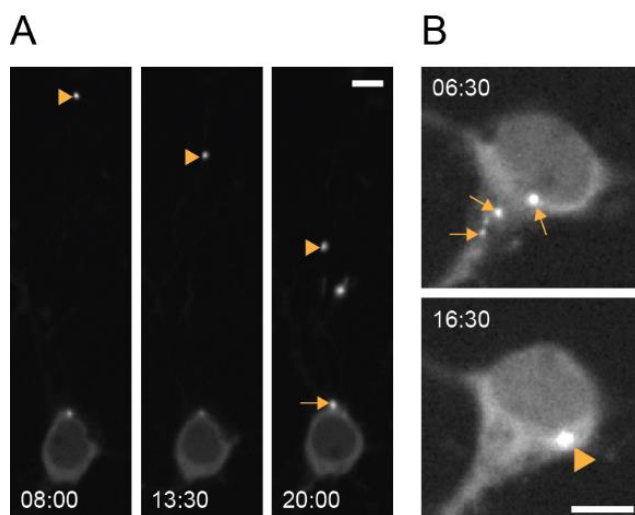


Figure 2-15: Retrograde transport and fusion of Fluc inclusions in neurons

A - B: Primary cortical neurons of E15.5 CD1 embryos were transfected with FlucSM-HA. Proteasome was inhibited at 3+2 DIV (5.0 μ M MG-132 for 4h in DMSO). Medium was then changed to inhibitor-free medium and cells incubated for 3h. Afterwards, neurons were imaged every 30 min. A: An example primary

cortical neuron exhibiting an inclusion in the neurite that over time is transported retrogradely to the soma (arrow head). A representative cell harboring a perinuclear inclusion 20 h after the inhibitor is removed from the medium. B) Somatic inclusions (arrows) fuse over time into one perinuclear inclusion (arrow head). Scale bars: 5 μ m.

To test how Fluc reacts to the stressor heat shock, primary cortical neurons were transfected with FlucSM-HA. Fluc formed inclusions in 80 % of the cases, either distinct inclusions or a grainy pattern of inclusions (Fig. 2-16 B, E), reminiscent of its reaction in HeLa cells (Fig 2-12). Compared to the stress of proteasome and Hsp90 inhibition (Fig. 2-16 C – E), heat shock seemed to be a stronger insult, since in these two conditions the grainy pattern was only seen in dead cells. In opposition to HeLa cells, most of the primary neurons did not survive the recovery phase after heat shock, although the heat shock parameters were carefully titrated.

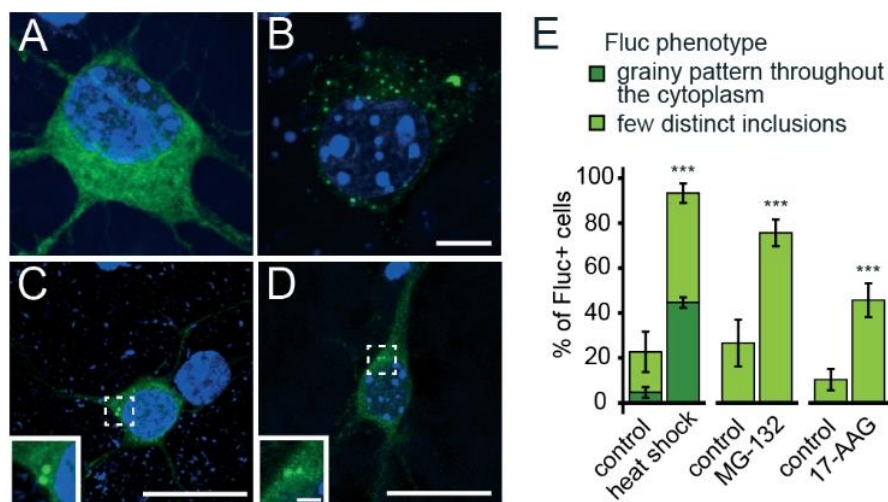


Figure 2-16: FlucSM-HA reacts differently to heat shock as compared to proteasome and Hsp90 inhibition

A-E: Primary cortical neurons of E15.5 CD1 embryos were transfected with FlucSM-HA and stresses were induced at 3+2 DIV: heat shock (30 min at 43 degrees), proteasome or Hsp90 inhibition (5.0 μ M MG-132 or 5.0 μ M 17-AAG for 4h in DMSO). A: A primary cortical neuron under control conditions. B: A primary cortical neuron under heat shock condition, note the grainy pattern of Fluc. C - D: Primary cortical neurons after proteasome (C) or HSP90 (D) inhibition. Note the formation of two distinct inclusions at a perinuclear location. E: Quantification of transfected cells with a grainy pattern (dark green) or inclusion formation (bright green) under stress or control conditions reveals that Fluc reacts stronger (higher percentage and grainy inclusion pattern formation) to heat shock than to proteasome and Hsp90 inhibition. Data from three independent experiments, 15 cells per experiment. Scale bars: A-B) 5 μ m, C-D) 20 μ m, blowups) 2 μ m.

I conclude from these experiments that Fluc reacts clearly to proteotoxic stressors such as proteasome or Hsp90 inhibition or heat shock. The three Fluc variants show different sensitivities to stress, but their reactivities can reach saturation, homogenizing their responses. Its localization

in the cell, exclusion from the nucleus in control conditions, the specific location of its inclusions upon stress (two perinuclear inclusions) and the lack of re-solubilisation, hint at a different biochemistry of this protein in primary neurons compared to HeLa cells.

2.2.2.4. Fluc can measure positive and negative changes of proteostasis capacities in primary neurons

The fluorescence-based readout of Fluc, which is based on the formation of inclusions upon proteotoxic stress, can only measure decreases in proteostasis capacities. Its second readout, which relies on the changed catalytic capacities of Fluc, may be used to measure increases of proteostasis capacities. To test this, I transfected primary cortical neurons with FlucSM-HA and applied the stressors proteasome and

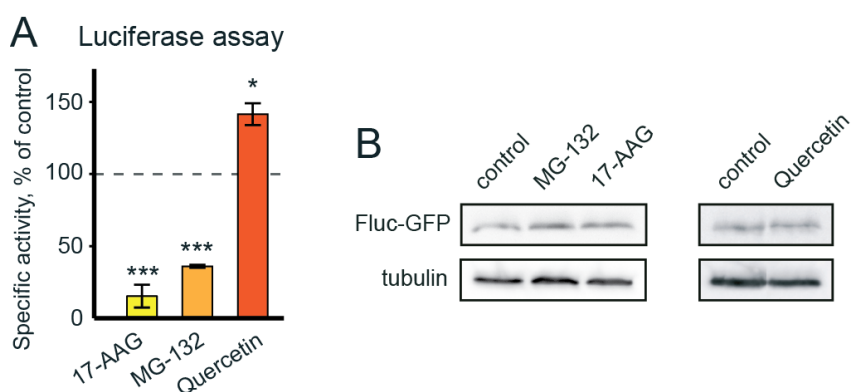


Figure 2-17: Fluc can measure decreased and increased capacities of the PQCS

A - B: Primary cortical neurons of E15.5 CD1 embryos were transfected with FlucSM-HA. At 3+2 DIV Hsp90 or the proteasome were inhibited (5.0 μ M 17-AAG or 5.0 μ M MG-132 for 4h in DMSO) to decrease the capacities of the PQCS. To obtain the opposite effect, Quercetin was added to the medium (20 μ M Quercetin in DMSO for 24h). Every condition was conducted in replicates, one replicate was used for luciferase assay and one for western blotting. A: FlucSM-HA measured a clear decrease in specific activity upon Hsp90 and proteasome inhibition and an increase upon Quercetin administration. Specific activity was calculated as described in materials and methods. Control conditions (DMSO only) were set to 100 % and each stress condition was plotted in relation to control condition. Data from three independent experiments. B: FlucGFP-HA detected by immunodetection after SDS-PAGE and western blotting with an anti-GFP antibody and tubulin as a loading control. Statistical tests: A) One-column t-test compared to a hypothetical value of 100.

Hsp90 inhibitor or boosted the UPS by applying Quercetin [187]. I then measured the luciferase activity, divided it by the protein levels of Fluc quantified by immunodetection after western blotting and normalized it using the normalization formula, as described in Materials and Methods. Three independent experiments were quantified per condition. The specific activity, which I interpret as an approximation of the folding state of Fluc, was drastically and significantly reduced upon proteasome or Hsp90 inhibition (~ 20 and 40 % of DMSO control, respectively, Fig. 2-17). In contrast, upon administration of Quercetin specific activity was significantly increased to 140 % of the control condition. I conclude from these experiments that Fluc can measure positive and negative changes in proteostasis capacities, which is a great advantage of this sensor over others (for example Ub-GFP from [180]).

2.2.3. Fluc senses the presence of an aggregation-prone protein in primary neurons

To determine, whether Fluc can sense changes in proteostasis based on protein aggregates, I co-transfected primary cortical neurons with Fluc and a plasmid coding for mCherry (mCh) tagged exon1 of mHTT bearing either 97 or 25 CAG repeats (mHTT(exon1)-Q97-mCh and control HTT(exon1)-Q25-mCh). As further controls I used two conditions co-expressing either Fluc and mCh or GFP and HTT(exon1)-Q97-mCh. In contrast to the previous experiments, I used FlucWT-HA. The reason for this was its lower reactivity. mCh levels were always much higher than the levels of HTT(exon1)-QX-mCh, and FlucSM-HA with its high sensitivity tended to also react to the high levels of simple mCh expression. In the two control conditions and when Fluc was co-expressed with non-aggregating HTT, HTT(exon1)-Q25-mCh, Fluc formed inclusions in less than 15 % of transfected cells (Fig. 2-18 A, D). Of the cells that contained a mHTT IB, Fluc reacted in almost 70 % of the cells and most of the times by forming a grainy pattern (Fig. 2-18 C, E). This does not only show that Fluc reacts to protein aggregates, but also that the stress induced by them is comparable to heat shock and stronger than the Hsp90 or proteasome inhibition used before. Strikingly though, Fluc also reacted in a subset of cells (~ 30 %) that expressed the aggregation-prone HTT(exon1)-Q97-mCh, but in which mHTT was still diffusely

distributed in the cell (Fig. 2-18 B, E). This shows that Fluc can not only sense the presence of proteotoxic stress caused by the presence of protein inclusions, but also reacts to mere presence of an aggregation-prone protein.

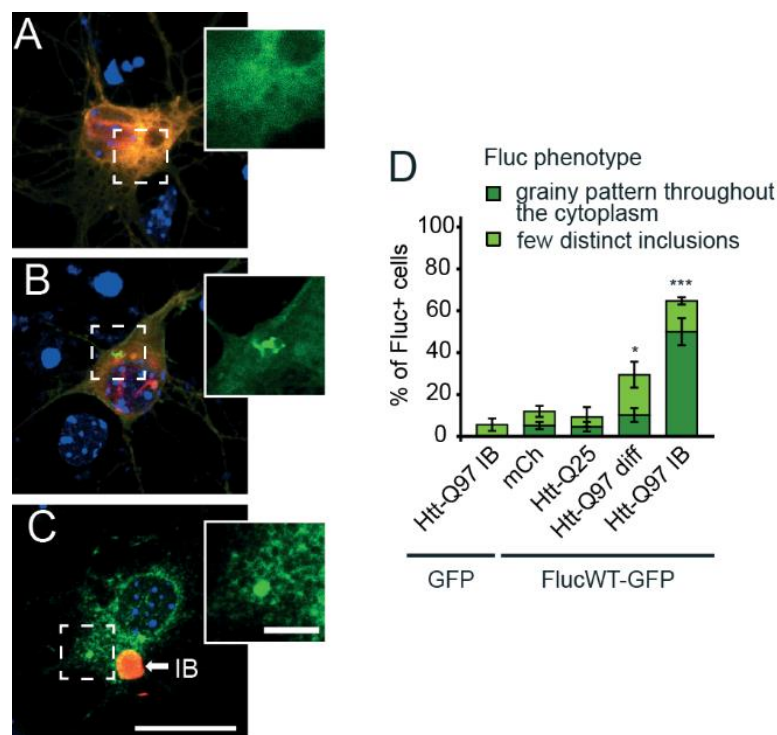


Figure 2-18: Fluc reacts to presence of mHTT inclusion bodies and the presence of soluble aggregation-prone mHTT

A – D) Primary cortical neurons of E15.5 CD1 embryos were transfected with FlucWT-HA and Htt(exon1)-Q97-mCh, Htt(exon1)-Q25-mCh or mCh as a control. GFP was co-transfected with Htt(exon1)-Q97-mCh. Neurons were fixed after 3+1 DIV. A: Representative image of a neuron co-expressing the non-aggregating Htt(exon1)-Q25-mCh and FucWT-HA. Blowup (white box) shows diffuse distribution of Fluc. B: Example of a neuron co-expressing the aggregation-prone Htt(exon1)-Q97-mCh without IB and FucSM-HA. Blowup (white box) shows inclusion formation of Fluc. C: Representative image of a neuron bearing a Htt(exon1)-Q97-mCh IB and co-expressing FucSM-HA. Blowup (white box) shows grainy pattern of Fluc. D: Manual quantification of the percentage of cells showing either a grainy pattern (dark green) or inclusion formation (bright green) of Fluc. Reaction of Fluc to the presence of Htt(exon1)-Q97-mCh either with or without IB formation was significantly increased compared to the condition expressing Htt(exon1)-Q25-mCh. Data from three (GFP / Htt(exon1)-Q97-mCh, FlucSM-HA / Htt(exon1)-Q25-mCh) to four independent experiments (all other conditions), 15 cells per experiment. Statistical test: One-way ANOVA with Dunnett's Multiple Comparison post-hoc test. Scale bars: C) 20 μ m, C blowup) 5 μ m.

2.2.4. Measurements of protein folding in mice

2.2.4.1. Fluc does not measure a decrease in proteostasis capacities in embryonic brains of R6/2

In order to test the ability of Fluc to measure proteostasis in neurons of R6/2 mice, I first electroporated FlucSM-HA under the pCAGG promoter into the cortex of E15.5 mouse embryos. As a proof-of-principle I applied heat shock to electroporated E18.5 wt brains and analysed how many Fluc expressing cells contained inclusions. Upon heat shock almost 90 % of all cells showed inclusions (Fig. 2-19), with one big inclusion per cell. This showed that in intact brains Fluc can measure changes in proteostasis using *in utero* electroporation (IUE) as means of transgene delivery. Nevertheless, there was no significant difference between brains of R6/2 embryos and controls in the percentage of transfected neurons bearing Fluc inclusions. This shows that Fluc does not measure a decrease in proteostasis capacities in E18.5 R6/2 embryos using a means of delivery which does allow for measurement of changes in proteostasis upon heat shock.

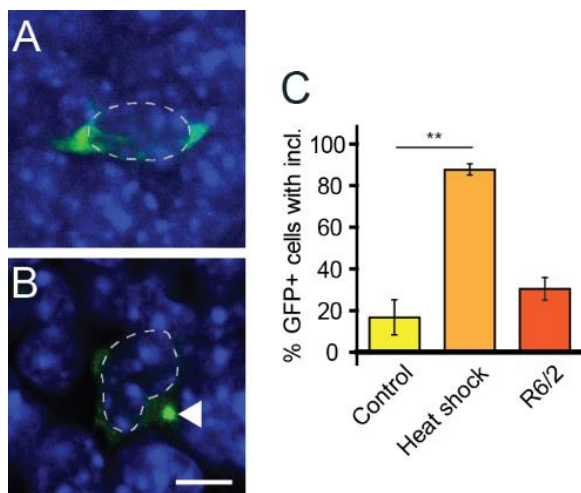


Figure 2-19: Fluc reacts to heat shock in the intact brain but shows no reaction in the R6/2 background

A – C) FlucSM-HA in the pCAGG vector was delivered by *in utero* electroporation into the cortex of E15.5 CD1 or R6/2 mice. A - B: Representative images of cells expressing FlucSM-HA (green) under control condition (A) or after 90 min of heat shock at 43 °C (B), the nucleus stained with DAPI is denoted with a white dotted line. Note the IB forming in the cytosol of this cell marked with an arrowhead. C: Data from two (heat shock) to three independent experiments and two FOV per experiment. Statistical test: One-way ANOVA with Tukey's Multiple Comparison post-hoc test. Scale bar: A) 5 μ m.

Note the IB forming in the cytosol of this cell marked with an arrowhead. C: Data from two (heat shock) to three independent experiments and two FOV per experiment. Statistical test: One-way ANOVA with Tukey's Multiple Comparison post-hoc test. Scale bar: A) 5 μ m.

2.2.4.2. Generation of a transgenic mouse expressing Fluc

Next, we generated several transgenic mouse lines expressing Fluc. For this I cloned FlucSM-HA or FlucWT-HA into the Mo.PrP vector obtained from David R. Borchelt (University of Florida) [188] leading to expression of the transgene under the prion protein (PrP) promoter (Fig. 2-20 A). I chose this promoter because of its strong salt and pepper like expression pattern, which is predominant in the CNS [189], and its expression at embryonic stages [190]. The latter would allow for the usage of primary neurons from these lines. The Mo.PrP vector has been previously used for the generation of neurodegeneration models [190], [189]. Pronuclear injections were conducted by the transgenic service of the Max Planck Institute of Neurobiology.

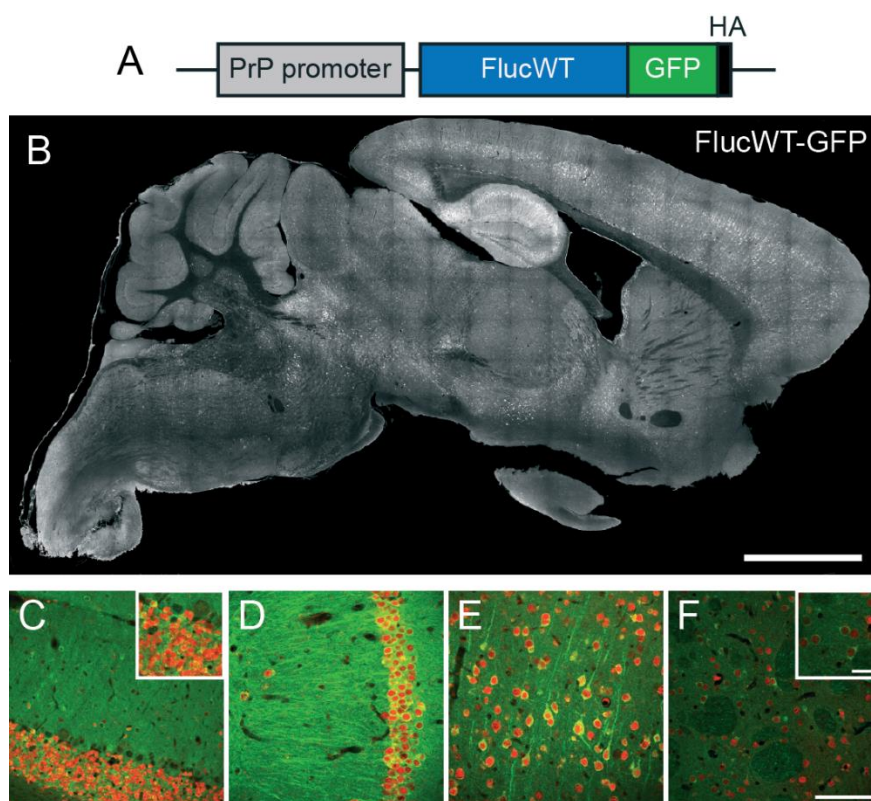


Figure 2-20: Generation of a transgenic mouse expressing Fluc

A: Schematic of the transgene. B: Sagittal section of a 12-week old transgenic mouse from the PrP-FlucWT1214 line, stained for GFP. Note the high expression in the hippocampus and layer 5 of the cortex. C – F: Representative images showing expression of FlucWT-HA in the cerebellum (C), hippocampus (D), cortex (E) and striatum (F) stained for GFP (green). C – E: Counterstained for NeuN (red) to mark neurons. F: Counterstained for DARPP-32 (red) to label MSNs. Scale bars: B) 2 mm, F) 100 μ m (applies to C-F), F inset) 30 μ m.

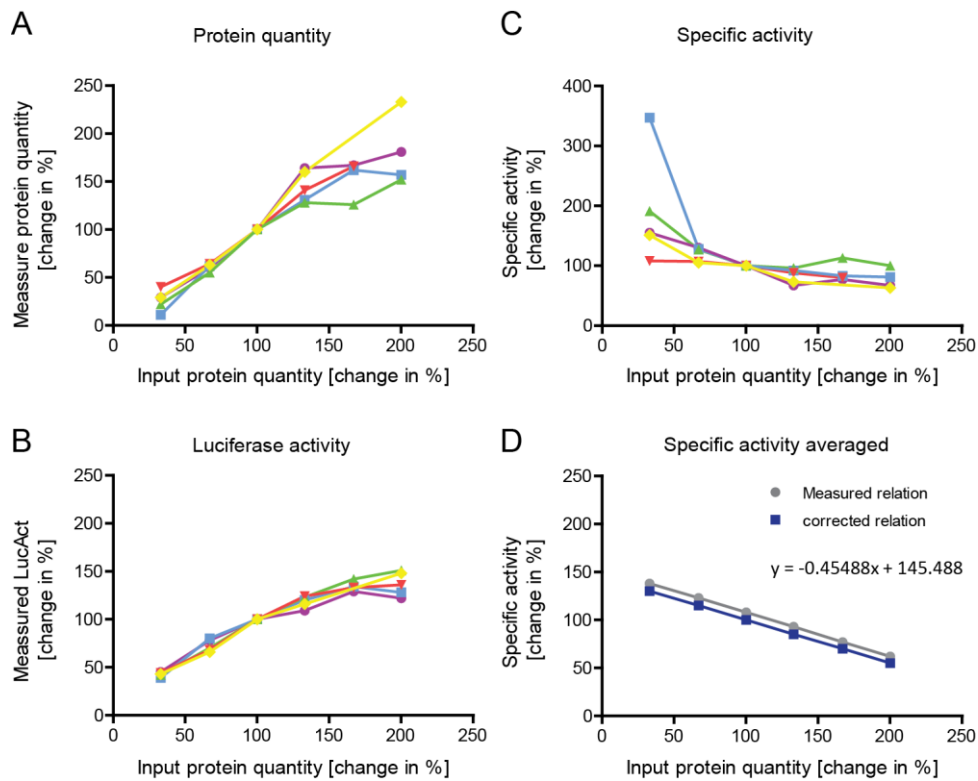


Figure 2-21: Linearity of the bioluminescence assay and normalization

A – D) Six different amounts (25 µg, 50 µg, 75 µg, 100 µg, 125 µg, and 150 µg) of five different cortical tissue samples (five different colours) of PrPWT1214 mice were used for immunodetection and the luciferase assay. 75 µg were set to be 100 %. A – B) Protein quantity and measured luciferase activity is plotted in dependence of the known protein quantity used. C) For each sample and each quantity of sample used the specific activity is measured by dividing luciferase activity by protein quantity. The five different samples are colour-coded. All show a negative slope. D) The average of the five lines in C) is plotted as the “measured relation”. The measured relation is then corrected by a shift on the y-axis, so that 100 % of used protein quantity equals 100 % specific activity. The resulting relation (“corrected relation”) is plotted in blue and the corresponding formula (named “normalization formula”) depicted in the plot.

For the FlucSM-HA construct, seven out of 84 mice were transgenic and two lines showed germline transmission and good expression of the transgene (PrPSM 4977 and PrPSM 4983). For the FlucWT construct, five out of 103 mice were transgenic and two lines showed germline transmission and nice expression of the transgene (PrPWT 1214 and PrPWT 1433). In this thesis the transgenic Fluc expressing mouse refers to the FlucWT 1214 line. The line showed expression in different brain areas, such as the cerebellum (here specifically in the granule cell layer), the hippocampus (mostly in CA1), layer 5 of the cortex and the striatum (in MSNs, but also in interneurons) (Fig. 2-20 B – F). Mice from this line are viable, good breeders and show no evident

phenotype. I also did not observe any difference in expression between female and male mice. I have never seen inclusion formation in tissue of these animals, although I aged them, crossed them to R6/2 mice and challenged slice cultures and primary neurons of this line with proteasome inhibition and heat shock (data not shown). A reason for this could be lower expression levels than needed for visible inclusions to form. Therefore, proteostasis measurements using these animals were restricted to the employment of the specific activity assay.

2.2.4.3. Linearity of the specific activity assay

Using tissue of the Fluc line I tested whether the specific activity assay harbors technical biases. For this I used five cortical samples from different transgenic mice and conducted luciferase assays and protein quantity measurements on six different quantities of protein. First I asked whether both assays were linear for the used ranges of protein quantity (Fig. 2-21 A – B). This was the case for both assays up to 150 µg of protein quantity. Therefore, all experiments were conducted with 150 µg or less of protein quantity. Secondly, I wanted to assess whether the calculated specific activity was the same for one sample, independent of how much protein was used. In line with this hypothesis all six different amounts of protein quantity from the same sample should render the same specific activity. However, this was not the case. Instead, a higher amount of protein lead to a decreased specific activity measured (Fig. 2-21 C - D). The relation between the used protein quantity and the measured specific activity was described by the following normalization formula:

$$y = -0.45488 x + 145.488$$

I conclude from these experiments that both assays are linear for the amounts of protein used in the experiments of this thesis, but that the two assays are not linear to each other. This leads to the technical bias that higher levels of proteins used lead to an artificial decrease in specific activity measured. If not stated differently, all specific activity measurements mentioned are therefore corrected using the normalization formula (refer to Materials and Methods).

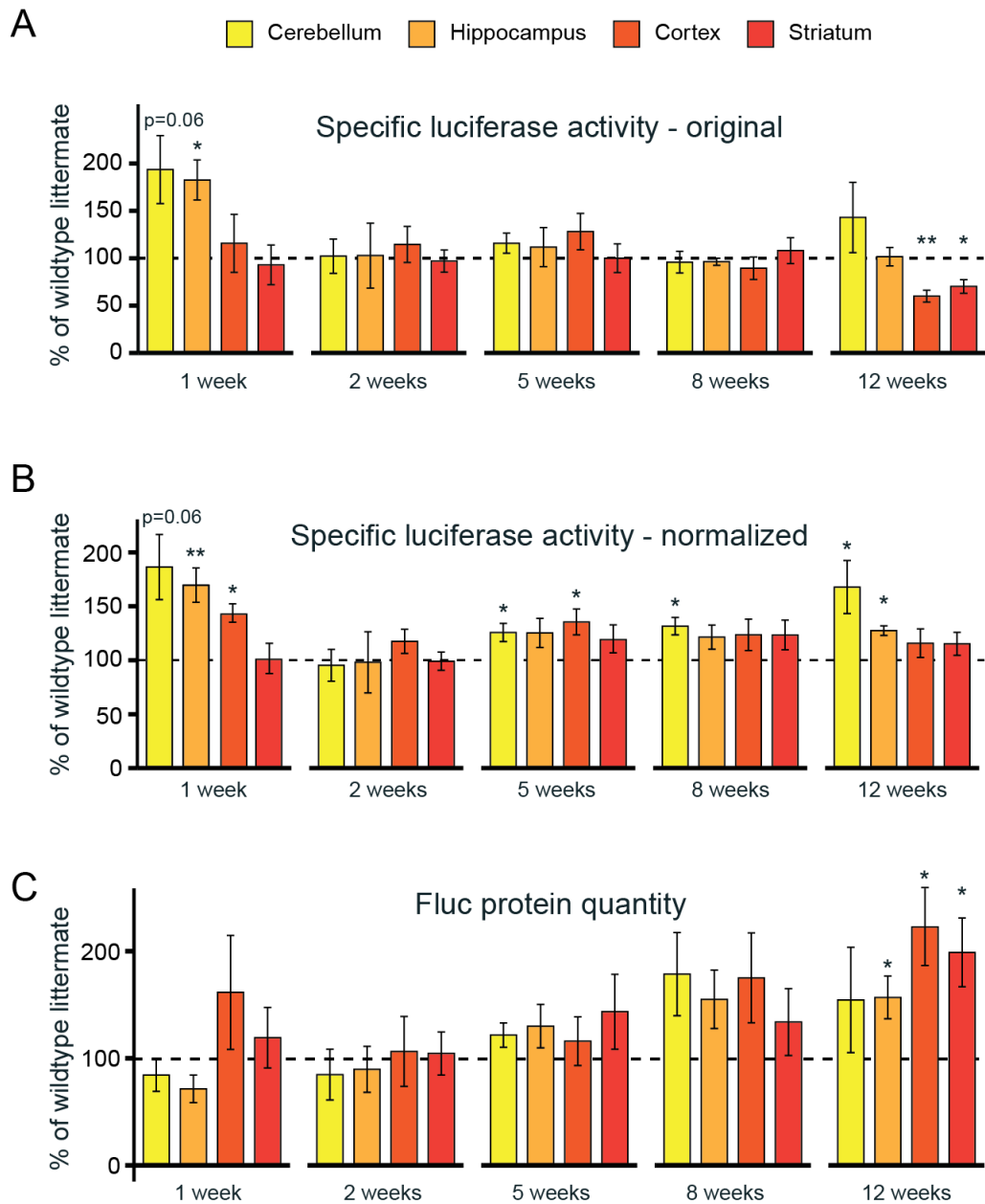


Figure 2-22: Increased folding capacities in specific brain regions of young R6/2 mice

A – B) Specific activity was measured from cerebellar, hippocampal, cortical and striatal tissue (colour-coded) of R6/2 mice and littermate controls at three pre-symptomatic ages (1, 3 and 5 weeks) and two symptomatic ages (8 and 12 weeks). For each tissue and age, wt controls were set to 100 % (dotted line) and R6/2 mouse values plotted accordingly. Data from four to six mice per genotype and age. A: Before normalization, specific activity was increased at 1 week of age in cerebellum and hippocampus and decreased at 12 weeks of age in cortex and striatum. B: After normalization specific activity was increased at 1 week of age in cerebellum, hippocampus and cortex. Slight increases were also seen at 5 and 8 weeks of age in cerebellum and cortex, and in cerebellum only, respectively. Interestingly, the decrease at 12 weeks was no longer observed. C: At 1 week of age Fluc protein levels showed a trend towards a decrease for the cerebellum and hippocampus. Cortex showed an increase in protein quantity, but also a high variability between the samples. Interestingly, at 8 and especially at 12 weeks of age, protein quantity was

increased in R6/2 compared to wt mice. This effect was strongest in cortex and striatum. Statistical test: One-column t-test compared to a hypothetical value of 100.

2.2.5. Fluc is better folded in R6/2 than in wt mice in specific brain regions at 1 week of age

To assess proteostasis in R6/2 mice, I crossed the Fluc line to R6/2 mice and measured the specific activity of Fluc in four different regions (cerebellum, hippocampus, cortex and striatum) at five different time points (1, 2, 5, 8 and 12 weeks of age) from *ex vivo* tissue of R6/2, Fluc-positive and wt, Fluc-positive littermate controls. Before using the normalization formula, I observed two main differences: First, at 12 weeks of age the specific activity in cortex and striatum of R6/2 mice was significantly reduced compared to wt littermate controls. Second, at 1 week of age the specific activity in cerebellum and hippocampus of R6/2 mice was significantly increased compared to wt littermate controls (Fig. 2-22 A). Nevertheless, after using the normalization formula the decrease observed at 12 weeks of age was gone, suggesting that this decrease was due to the technical bias of the assay. The increase at 1 week of age was still present after normalization. Interestingly, the specific activity of the four different brain regions negatively correlated with the vulnerability of these regions to HD (Fig. 2-22 B). This increase came with a trend towards a decrease in protein levels of Fluc in cerebellum and hippocampus of R6/2 mice. At 12 weeks of age, Fluc levels were in general higher in R6/2 mice compared to wt mice, but this increase was less pronounced in hippocampus and cerebellum, exactly the two regions that, at the earliest age assessed, showed an increase in specific activity (Fig. 2-22 B).

Firstly, I conclude from these experiments that the correct normalization of the data is very important when using this assay in order to avoid generation of false positive data. Secondly, proteostasis capacities seem to be upregulated in certain brain regions of very young R6/2 mice compared to wt littermate controls. These are also the regions that show less of an increase in Fluc levels at later stages and are less vulnerable to HD.

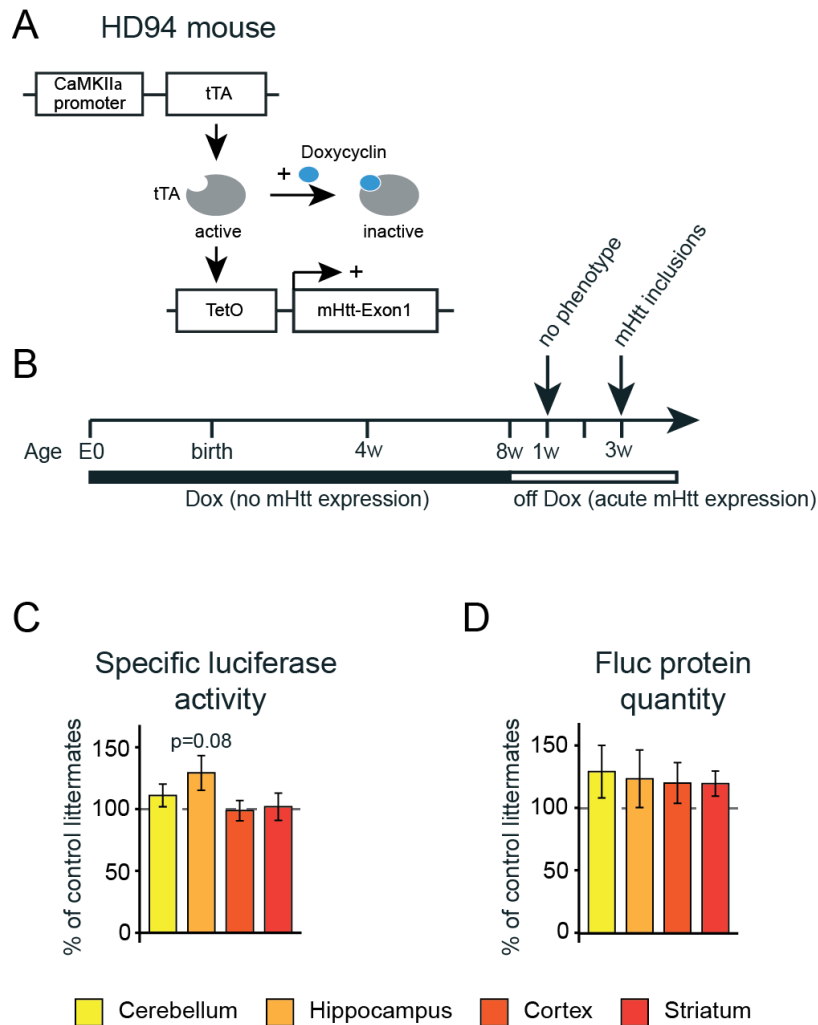


Figure 2-23: Slight increase of folding capacities in hippocampal tissue of HD94 mice

A – D: Specific activity was measured from tissue of HD94 mice crossed to the PrPWT1214 line. A: Schematic of the tet-off system in the HD94 mice. The tTA factor is expressed under the control of the CamKIIa promoter. tTA can bind to the tet-regulated element (TetO) and thereby induce expression of mHTT with 94 glutamines. Doxycycline (blue sphere) inactivates it. Therefore, during administration of doxycycline mHTT is not expressed. B: Timeline of experiment. Mice were given doxycycline from conception until an age of 8 weeks. Then, the transgene was left to express for one week. Subsequently, mice were sacrificed for experiments. C: Specific activity was measured from cerebellar, hippocampal, cortical and striatal tissue (colour-coded) of HD94 mice and littermate controls. For each tissue, controls were set to 100 % (dotted line) and HD94 mouse values plotted accordingly. Data is from 9 mice per genotype. Because the CamkIIa promoter does not express in cerebellum and only expresses at low levels in striatum, the measurements in these regions are not informative. D: Fluc protein levels per region. Statistical test: One-column t-test compared to a hypothetical value of 100. Figure by Irina Dudanova.

2.2.5.1. Confirmation of better folding of Fluc in cultures of R6/2 mice and tissue of HD94 mice

To confirm these results in a different mouse model, Irina Dudanova crossed HD94 mice [191] to Fluc mice and measured specific activity in the same four brain regions (cerebellum, hippocampus, cortex and striatum). The HD94 model is composed of two transgenic lines: the CamkII-tTA and the BiTetO lines [191]. The advantage of this model is that it allows precise temporal control of mHTT expression. Using the tet-off system, exon1 of mHTT with 94 CAG repeats is expressed driven by the CamkIIa promoter. Briefly, the activity of the CamkIIa promoter leads to the expression of the tTA transcription factor which can bind to the tet responsive element (TetO) and thereby induce expression of mHTT. In the presence of doxycycline, tTA is inactivated which inhibits the expression of mHTT (Fig. 2-23 A). In these experiments doxycycline was given during embryonic stages to the mother and after birth to the mice in their drinking water to prevent mHTT expression. At 8 weeks of age doxycycline administration was ceased and mHTT expression allowed for one week, resembling expression in R6/2 at the time point when an increase in specific activity was measured. Then, mice were sacrificed and specific activity measured (Fig. 2-23 B). Due to the CamkIIa promoter, mHTT was not expressed or only expressed at low levels in cerebellum and striatum, respectively. Therefore, measurements in this model are only insightful for hippocampus and cortex. In line with my findings in young R6/2 mice, specific activity was increased in the hippocampus, but not in cortex of HD94 mice compared to controls (single- and non-transgenics).

To confirm the observation made in young R6/2 mice in a different system, I transfected primary cortical and hippocampal cultures from E18.5 R6/2 embryos and wt littermate controls with FlucSM-HA and measured the specific activity 8+2 or 8+5 days after transfection (10 or 13 DIV, respectively). At 13 DIV cortical cultures of R6/2 mice had a small, but not significant reduction of proteostasis capacities, which was not seen at 10 DIV (Fig. 2-24 A). At both ages Fluc protein levels were significantly increased compared to controls (Fig. 2-24 B). In contrast, hippocampal neurons from R6/2 mice had an increased specific activity compared to controls at

10 DIV and no increase in Fluc protein levels (Fig. 2-24). This suggests that hippocampal neurons of R6/2 mice have increased proteostasis capacities compared to controls, whereas cortical neurons lack such capacities and exhibit higher protein levels than controls, either due to more protein synthesis or decreased protein degradation. Cortical and hippocampal neurons seem to have differing capabilities in dealing with the molecular situation in the R6/2 background.

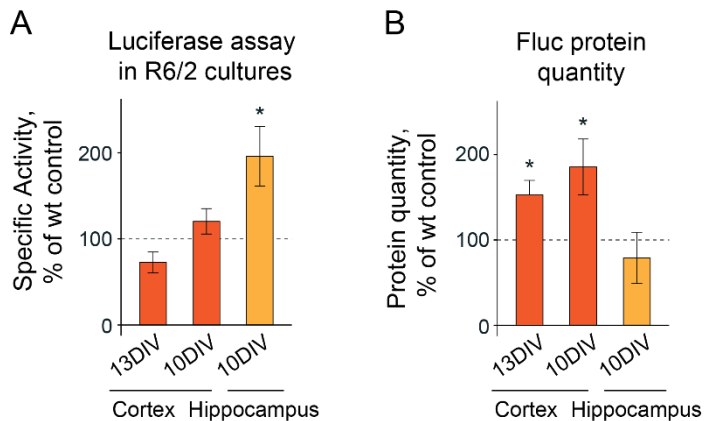


Figure 2-24: Differential folding capacities in cortical and hippocampal R6/2 cultures

A – B: Primary cortical and hippocampal neurons of E18.5 R6/2 and wt littermate control embryos were transfected with FlucSM-HA. At 8+2 or 8+5 DIV (10 and 13 DIV, respectively) specific activity was measured. Data from R6/2 cultures are plotted in relation to wt controls, which are set to 100 % (dashed line). Data from eight cultures per genotype.

A: Specific activity of cortical and hippocampal cultures. B: Fluc protein levels. Statistical tests: A) One-column t-test compared to a hypothetical value of 100.

2.2.6. Mass-spectrometry analyses reveal transient upregulation of specific ubiquitin-related proteins in R6/2 mice at young ages

To understand the mechanism behind the improved proteostasis capacities in young R6/2 mice, we conducted mass-spectrometry analyses from tissue of 1-week old R6/2 mice and wt littermate controls (four mice per genotype). PCA analysis showed that samples from transgenic and non-transgenic mice clustered together and that the biggest inter-sample differences were based on brain region specific protein regulations (Fig. 2-25).

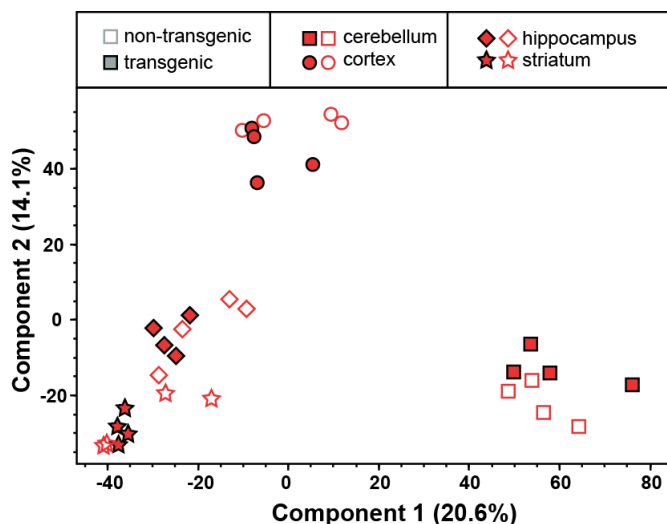


Figure 2-25: PCA of soluble proteome from young mice shows no difference between R6/2 and controls

A: Soluble proteome was analysed by mass-spectrometry of cerebellar, hippocampal, cortical and striatal tissue (encoded by different symbols) of 1-week old R6/2 mice (filled symbols) and wt littermate controls (non-filled symbols). Tissue samples of trans-

genic and non-transgenic mice of the same brain region cluster together suggesting no strong difference in whole proteome based on genotype. Data from 4 mice per genotype. Figure by Fabian Hosp.

Because the biggest changes in proteostasis of young R6/2 mice were seen in cerebellum and hippocampus and no changes seen in striatum, I asked which proteins are significantly up-regulated (p-value under 0.05 and enriched more than two-fold) in cerebellum (Fig. 2-26 A) and hippocampus (Fig. 2-26 B) of R6/2 mice that are not significantly regulated in striatum (Fig. 2-26 C). Out of these proteins I asked which ones could explain in a direct manner the improved proteostasis, that is, which are chaperones, autophagy- or ubiquitin-related. I found in total 11 proteins, of which two were chaperones, one was autophagy-related and eight were ubiquitin-related (Table 2-2). Of the eight ubiquitin-related candidates, four were upregulated in the cerebellum and four in the hippocampus (Fig. 2-26 A – B, Table 2-2). The eight significantly upregulated ubiquitin-related proteins were one ubiquitin-conjugating enzyme (cerebellum: Ube2f), five ubiquitin ligases (cerebellum: Trim32, Ubr2, hippocampus: Peli2, Herc2, Trim23) and two ubiquitin specific peptidases (cerebellum: Usp22, hippocampus: Usp40), as stated also in Table 2-2. As a control I then asked how many of the proteins that were significantly upregulated in the striatum and not regulated in the cortex or hippocampus were chaperones, autophagy- or ubiquitin-related. I only found one chaperone falling into this category (Fig. 2-26 D).

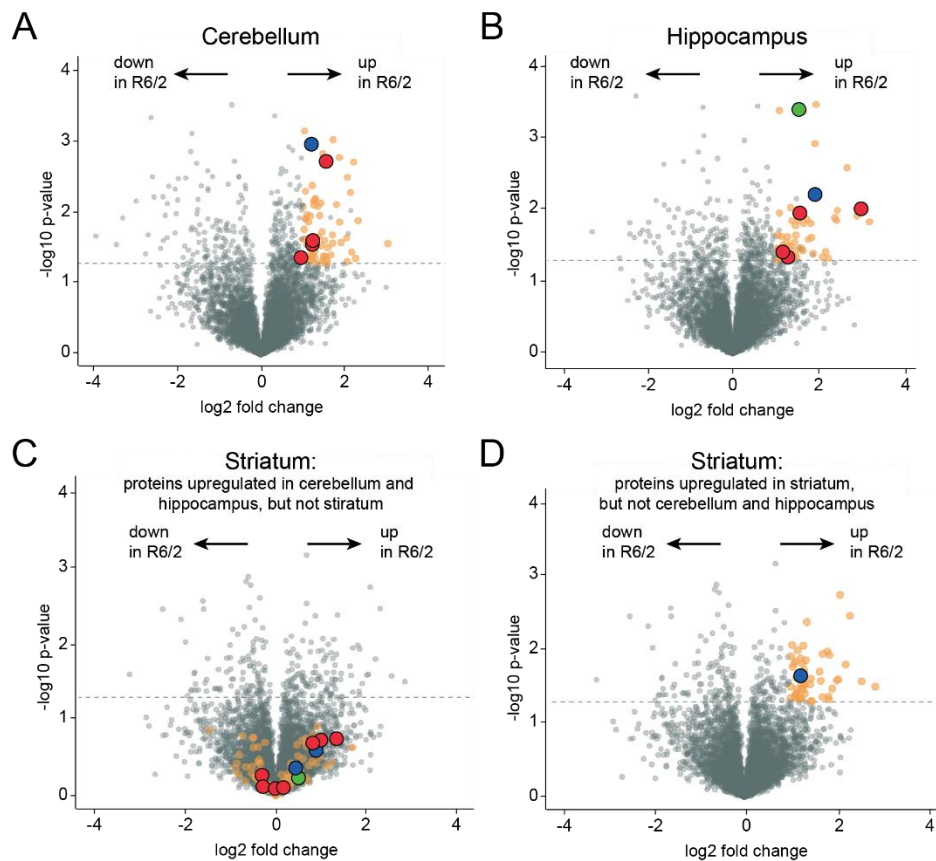


Figure 2-26: Ubiquitin-related proteins are enriched in cerebellar and hippocampal tissue of young R6/2 mice.

A – D: Volcano plots of proteins detected in the soluble proteome of 1-week old R6/2 mice in comparison to wt littermate controls. Proteins are plotted as circles based on fold change between mice of different genotype (x-axis) and p-value between replicates (y-axis). Dotted line indicates p-value of 0.05 on a $-\log_{10}$ scale. Yellow circles represent proteins that are significantly enriched by more than two fold (1 on a \log_2 scale) in cerebellar or hippocampal tissue and not significantly regulated in striatum of R6/2 mice. Proteostasis components among the selected (yellow) proteins are depicted in blue (chaperones), green (autophagy components) and red (ubiquitin-related). Most proteostasis components are ubiquitin-related (8 of 11). A: Volcano plot of proteins regulated in the cerebellum. B: Volcano plot of proteins regulated in the hippocampus. C: Volcano plot of proteins regulated in the striatum. Selected proteins (yellow) are all below the threshold of a p-value of 0.05. D: Proteins significantly upregulated in the striatum of R6/2 mice and not significantly regulated in cerebellum and hippocampus (yellow). Of these, only one protein is a proteostasis component.

The upregulation of the eight candidates was transient, as analysing a mass-spectrometry data set from Fabian Hosp of older R6/2 mice and their littermate controls, showed no upregulation of these candidates at 5 and 8 weeks of age. At 12 weeks of age only Trim32 was upregulated (Fig. 2-27).

Table 2-2: Proteostasis-related candidates, upregulated in the soluble proteome of young R6/2 mice

Protein name	Gene name	Function	Region
Beclin-1	Becn1	autophagy-related	Hc
Heat shock 70 kDa protein 12B	Hspa12b	chaperone	Cb
Protein unc-45 homolog A	Unc45a	chaperone	Hc
NEDD8-conjugating enzyme UBE2F	Ube2f	Ubiquitin-conjugating enzyme	Cb
E3 ubiquitin-protein ligase TRIM32	Trim32	Ubiquitin ligase	Cb
E3 ubiquitin-protein ligase UBR2	Ubr2	Ubiquitin ligase	Cb
E3 ubiquitin-protein ligase HERC2	Herc2	Ubiquitin ligase	Hc
E3 ubiquitin-protein ligase pellino homolog 2	Peli2	Ubiquitin ligase	Hc
E3 ubiquitin-protein ligase TRIM23	Trim23	Ubiquitin ligase	Hc
Ubiquitin carboxyl-terminal hydrolase 22, Ubiquitin carboxyl-terminal hydrolase 27	Usp22, Usp27	Ubiquitin peptidase	Cb
Ubiquitin carboxyl-terminal hydrolase 40	Usp40	Ubiquitin peptidase	Hc

Cb: Cerebellum; Hc: Hippocampus

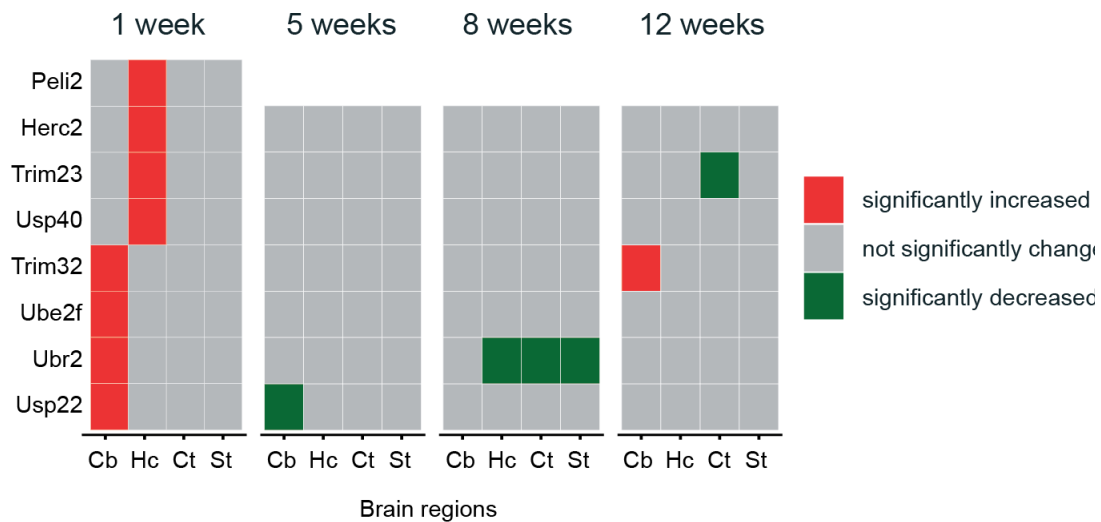


Figure 2-27: Upregulation of candidates is transient

A: Heat map of 8 candidates significantly upregulated in hippocampus or cerebellum and not regulated in striatum of R6/2 mice. Regulation in different brain regions (cerebellum, hippocampus, cortex and striatum) at four different ages (1 week, 5 weeks, 8 weeks and 12 weeks of age). Red indicates significant upregulation (twofold or higher, $p > 0.05$), green significant downregulation (twofold or higher, $p > 0.05$) and grey no significant regulation. These 8 candidates are only transiently upregulated, as at 5 weeks they are not upregulated anymore.

I conclude from these analyses that in the cerebellum and the hippocampus of young R6/2 mice certain ubiquitin-related candidates but no proteasome components are significantly upregulated. In the striatum this upregulation is missing. These candidates could therefore help to explain why the cerebellum and hippocampus have an increased folding capacity in R6/2 animals. These results also support the possibility that the increased folding capacity is not due to an increased overall availability of chaperones, but that an improved protein degradation in these regions increases the ratio between chaperones and their substrates. This improved degradation does not seem to be caused by an upregulation of proteasome components.

2.2.6.1. Normal proteasome activity in young R6/2 mice

To exclude the possibility that protein degradation is increased in R6/2 tissue because of more efficient proteasomes, I conducted a proteasome activity assay on tissue of 1-week old R6/2 mice and wt littermate controls. For this, I incubated the tissue with a Suc-LLVY-AMC, a substrate of the chymotrypsin-like protease activity of the proteasome that becomes fluorogenic after

cleavage. To exclude cleavage products generated by non-proteasome proteases, I incubated part of the reaction with the proteasome inhibitor MG-132 (20 μ M, [192]) and calculated the difference between the measurements (Fig. 2-28). There was no significant difference in chymotrypsin-like proteasome activity between R6/2 and littermate control tissue for any of the four regions analysed. Proteasome activity in R6/2 mice does not seem to be changed compared to controls.

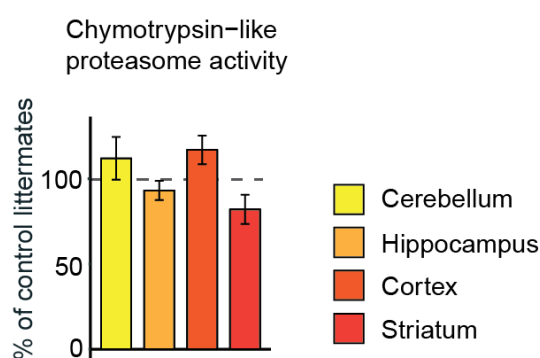


Figure 2-28: Chymotrypsin-like proteasome activity is not altered in tissue of young R6/2 mice

A: Chymotrypsin-like activity was measured in tissue of 1-week old R6/2 mice and wt littermate controls in cerebellum, hippocampus, cortex and striatum (colour-coded) by incubating the tissue with Suc-LLVY-AMC in presence and absence of

proteasome inhibitor MG-132. Data from four mice each. Statistical test: One-column t-test compared to a hypothetical value of 100.

2.2.6.2. Hippocampal neurons might have a faster protein degradation system than cortical neurons

To test whether UPS-related degradation is actually differently efficient between cortical and hippocampal neurons, I transfected neurons of E18.5 wt embryos with mutant carboxypeptidase Y (CPY*-mCh) (Fig. 2-29). At 8+2 DIV I inhibited protein synthesis by administration of cyclohexamide and subsequently analysed protein quantity before and after protein synthesis inhibition. After 30 min, more CPY*-mCh had been degraded in hippocampal neurons compared to cortical neurons, suggesting that hippocampal neurons have a better degradation system than cortical neurons.

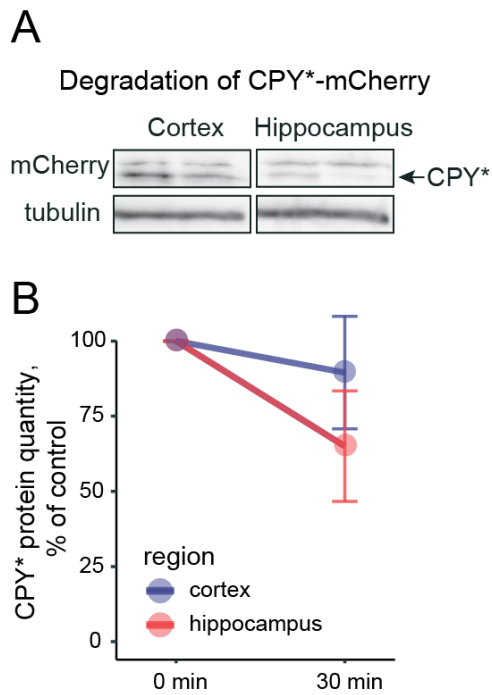


Figure 2-29: Degradation of CPY*-mCh is faster in hippocampal than in cortical cultures

A – B: Primary cortical and hippocampal neurons of E18.5 wt mice transfected with CPY*-mCh. At 8+2 DIV protein synthesis was inhibited for 30 min through incubation with cyclohexamide. Subsequently, mCh was recognized by immunodetection after western blotting. Data from two independent experiments. A: Examples of immunodetected CPY*-mCh in cortical and hippocampal wt cultures before and after inhibition of protein synthesis. B: Quantification of protein levels before and after protein synthesis inhibition. Time point 0 (before protein synthesis) was set at 100 % and protein levels after protein synthesis inhibition plotted as percent change of time point 0.

3. Discussion

3.1. Functional and molecular alterations in motor cortex of R6/2 mice

3.1.1. Summary

Chronic two-photon imaging provides the unique opportunity to image not only from many cells at a given time point in an awake behaving animal, but also to follow the fate of these cells over months. We have shown that at disease onset R6/2 mice exhibit an increase in cellular activity in layer 2/3 of motor cortex. This increase is not due to increased running activity, but seems to be aberrant. This increase is accompanied by a specific decrease of synaptic proteins in cortex of R6/2 mice as shown by mass-spectrometry analyses, which is not due to sequestration by insoluble mHTT. These results suggest an impairment in synaptic function at disease onset. I did not observe a decrease in numbers of excitatory or inhibitory synapses, but I showed that terminals from PV-positive neurons onto excitatory cells were reduced at 8 weeks of age but not yet at 5 weeks of age. This finding therefore correlates with the results from mass-spectrometry analyses and calcium imaging. Also, I observed a decrease in the numbers of SST-positive neurons in the cortex of R6/2 mice. Given that this population bears the highest load of mHTT inclusions, loss of cells in this population could be due to their increased vulnerability to mHTT toxicity.

3.1.2. What does the increase in neuronal activity in R6/2 mice encode?

What could this increase in overall cellular activity encode? The possible answers can be divided into two groups:

1) The increased cellular activity encodes a specific behaviour of the mouse, which happens or whose activity increases at this specific time point. Examples could be pivoting on the ball or shivering, as R6/2 mice do at this age. Running can be excluded, because R6/2 mice did not show an increase in this behaviour at the indicated time point.

2) The increased activity does not code for anything, is therefore aberrant and a consequence of deregulated wiring or impaired molecular regulation.

The first possibility can only be supported by naming the behaviour that is encoded by the activity. Firstly, the behaviour and the activity would have to correlate with one another. Ideally, the behaviour would have to be elicited or modulated by activating or silencing these neurons using pharmacological agents (for example designer receptors exclusively activated by designer drugs, DREADDs) or light-induced regulation of cellular activity (optogenetics). Although this possibility cannot be proven without finding this unknown behaviour, it can also not be refuted completely.

Spine density and turnover have been assessed in R6/2 mice by chronic (6 to 11 weeks of age) structural imaging [193]. R6/2 mice had lower spine densities at all time points. Interestingly, the turnover rate was higher in R6/2 and the fraction of persistent spines lower than in wt controls throughout the imaging period. This goes in line with the decreased and less stable running representation that we observed. It suggests that increased cellular activity could well be aberrant. For the remainder of this thesis I will assume that the second possibility is more likely. In this case, the increase in cellular activity registered at disease onset would be an aberrant activity, based on pathological deregulation of neuronal firing or degeneration of inter-neuronal connectivity. Both would be due to molecular alterations, which we tried to assess through mass-spectrometry and to further support by histology.

3.1.2.1. Which cell type shows increased activity?

The identity of the cells that increase their activity is not clear. This is a shortcoming of this study. Since we used the calcium indicator GCaMP6s under the synapsin I promoter, the measured activity originates from neurons only. Approximately 80 % of all neurons in cortex are

excitatory pyramidal neurons [2], [3]. Assuming that the virus used for delivery of the calcium indicator does not show a preferred transduction of interneurons over pyramidal cells [194], one can assume that 80 % of the activity, and therefore the majority of it, arises from pyramidal neurons. The remaining uncertainty could be removed by imaging from specific cell populations, such as certain interneurons or from excitatory pyramidal neurons. To accomplish this, one could either cross cell population-specific Cre lines with a Cre-dependent reporter line to express a fluorescent marker in these specific cells and thus identify them during imaging, or express GCaMP under a cell type-specific promoter. In our experiments we cannot be absolutely sure, but for the remainder of the discussion I will assume that the increase in activity is attributed to more active pyramidal neurons.

3.1.3. Decrease in synaptic proteins

An increase in cellular activity can come from either increased activation or from decreased inhibition of these cells. Both are received from other cells through synapses. A theoretical third possibility is a change in intrinsic electrical properties, which alters the excitability of a cell in the absence of any change in inputs. Based on the mass-spectrometry analyses, we know that synaptic proteins are significantly downregulated at 8 weeks of age but not yet at 5 weeks of age. Not only does this correlate with the time line of the imaging findings, but the group of regulated synaptic proteins seems to be a major cellular machinery affected at disease onset (compared to other regulated groups such as translation machinery, for example). This hints at a reduced functionality of cortical synaptic transmission.

Nevertheless, it is not clear whether the decrease of synaptic proteins is causative for or a consequence of the increased cell activity or both. I found both excitatory as well as inhibitory synaptic proteins among the strongest downregulated synaptic proteins. Also, I found the GO annotation defining excitatory and inhibitory synaptic proteins not very specific, as many key synaptic markers were missing. Therefore, I cannot conclude that one kind of synapses is specifically impaired. Histological analyses revealed no decrease in the numbers of excitatory or inhibitory synapses. However, I found levels of PSD-95, a scaffolding protein in the PSD of

excitatory synapses, to be reduced by 50 % in all layers of the motor cortex. PSD-95 has also been reported to be reduced in striatum of models of HD [195]. Although PSD-95 is known to interact with HTT [53], its reduction does not seem to be caused by sequestration by mHTT inclusions, as the protein was not enriched in the insoluble fraction of R6/2 mice. Its reduction suggests that excitatory synapses are at least impaired in their function if not in their number. Another finding supporting this, is that CamKII α and SAPAP3, components of excitatory synapses, were not only among the proteins strongest downregulated in the soluble proteome of 8 week old mice, but were even downregulated in the insoluble fraction of transgenic mice. This suggests that levels of CamKII α and SAPAP3 were so low, that even the amount normally found in the insoluble fraction was reduced in R6/2 mice. Also significantly reduced in the insoluble fraction of R6/2 mice at 8 weeks of age were the proteins SAPAP2, Synaptopodin and NMDA subunit 2A, all proteins found in excitatory synapses. Again, such an impairment could be a cause or a consequence of the measured increased activity in R6/2 mice. Indeed, Jarabek et al. [195] propose that the downregulation of PSD-95 and other synaptic proteins is a protective mechanism against excitotoxicity arising in HD.

Decreased inhibitory input could lead to an increase in activity of excitatory cells. Indeed, decreased inhibition of pyramidal neurons has been observed in 11.5 week old R6/2 mice [109]. Although I did not observe a decrease when measuring the number of inhibitory synapses, I did observe a decrease in synapses from PV-positive neurons onto pyramidal excitatory cells at 8 weeks of age but not yet at 5 weeks of age. Because this was a 20 % decrease and PV-positive neurons make up 40 % of all inhibitory (GAD67-positive) cells [3] [196] it could well be possible that this decrease (it would be 8 % of all inhibitory synapses) was not detectable when assessing all inhibitory synapses. Our mass-spectrometry analysis supports this finding, since I found Synaptotagmin-2 to be downregulated in the insoluble proteome of 5- and 8-week old R6/2 mice. Synaptotagmin-2 has been proposed to be a marker for synapses from PV-positive neurons onto pyramidal cells [197]. I analysed these synapses firstly, because they are reliably detectable by staining, contrary to, for example, synapses from SST-positive neurons in which the marker is exclusively nuclear in location and therefore does not fill and identify synapses. Secondly,

synapses from PV-positive neurons innervate their targets by contacting the soma instead of distant dendritic areas, thereby inducing fast and strong inhibition on their target cells. Indeed, PV-positive interneurons exert the strongest inhibition on pyramidal cells of all major interneurons classes [127]. This decrease in inhibition of excitatory neurons could explain the increase in measured cellular activity (Fig. 3-1).

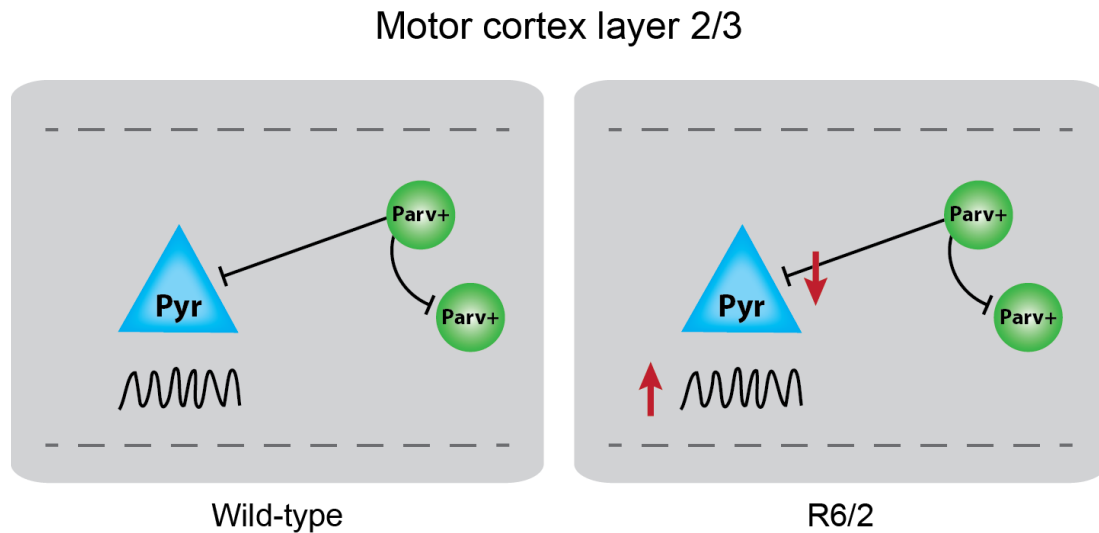


Figure 3-1: Proposed model explaining increased cellular activity

In layer 2/3 of primary motor cortex of wt animals, PV-positive interneurons (green circle) inhibit excitatory pyramidal cells (blue triangle), which in turn fire at a given rate (black schematic of an activity trace). In R6/2 mice we observed a decrease of PV-positive terminals on pyramidal neurons, which could explain the measured increase in cellular activity observed using two-photon calcium imaging.

Indeed, it has been shown that pharmacogenetic inhibition of PV-positive neurons can lead to an increase in overall cellular activity measured by calcium imaging [198]. Additionally, it has been shown in an HD mouse model that excitatory neurons of layer 2/3 of the motor cortex receive less inhibitory input, whereas PV-positive neurons receive less excitatory input [148]. Cortical hyperactivity is also induced by selective expression of mHTT in PV-positive neurons using the Cre/loxP system [199]. Interestingly, in this experiment PV-positive neurons did not die upon expression of mHTT, suggesting that these neurons might be especially resistant to toxicity of mHTT. This also fits with our findings that at 8 weeks of age R6/2 mice do not exhibit a loss of PV-positive neurons. When assessing the numbers of specific interneuron populations,

I found that in R6/2 mice the number of SST-positive neurons was reduced by half. This decrease in inhibitory cells that synapse onto excitatory cells could also explain the increase in cellular activity. However, SST-positive neurons also inhibit PV-positive neurons [127]. This would lead to more activity of PV-positive neurons and therefore more inhibition of excitatory cells, contrary to our finding. This discussion displays the complexity of the system studied and the need for further thorough investigation of the circuitry in HD model mice to understand the underlying mechanisms of the disease.

3.1.4. Link between aggregate load and neuronal pathology

I observed that cell population-specific degeneration correlated with aggregate load in interneurons. It is appealing to think that cells from certain cell populations die because they bear higher mHTT levels which is followed by more aggregate formation. This does not necessarily mean a higher level of mHTT expression, but could also be a decreased rate of degradation or other, cell type-specific, protective mechanisms to deal with the mHTT load. Further cell population-specific transcriptomic and proteomic studies will be required to gain insights into these mechanisms.

Interestingly, only very few of the synaptic proteins that were downregulated at 8 weeks of age in the soluble proteome of R6/2 mice were also found in the insoluble proteome and most of these were actually also downregulated in the insoluble proteome. First of all, this allows us to conclude that the reason for the downregulation of synaptic proteins in the soluble proteome is not sequestration by mHTT aggregates. A regulation on the transcriptional level seems likely. Transcriptome analysis of human iPSC and mouse model tissue revealed that genes most significantly downregulated in HD belonged to the GO term “synaptic transmission” [132]. Secondly, the proteins that are both downregulated in the soluble and in the insoluble proteome seem to be so drastically decreased in levels that even the amount normally found in the insoluble pool is decreased. This finding shows, that toxicity of mHTT comprises more than mere inclusion formation and sequestration of important players in the cell.

3.1.5. Hyperactivity in HD

Cellular hyperactivity and excitotoxicity are common findings in HD mouse models. In one study [109], electrophysiological recordings were conducted from pyramidal neurons in cortical layer 2/3 in slices of three different HD mouse models, the full-length transgenic HD model YAC128, the knock-in model CAG140 KI and the R6/2 model. Pyramidal neurons in all three models showed an increase in input resistance. This finding could be a consequence of spine loss and therefore decreased synaptic input. Spine loss has been described in cortex of R6/2 [193]. The loss of synaptic proteins that we observed at 8 weeks of age fits with these findings. Also, these findings go in line with the increased activity in cortical layer 2/3 neurons which we observed through calcium imaging. Cummings et al. also described increased inhibitory postsynaptic currents (IPSCs) in pyramidal neurons of R6/2 mice, and therefore more inhibition, until an age of 6 weeks followed by decreased IPSCs at 11.5 weeks of age [109]. This change in inhibition could explain the increase in cellular activity observed at disease onset.

3.1.5.1. Excitotoxicity in HD

Increased activity of pyramidal neurons in layer 2/3 leads to increased excitation of layer 5 pyramidal neurons, since their main excitatory inputs are pyramidal neurons of layer 2/3. Thus, I would also expect to observe increased activity in layer 5 of motor cortex. However, this would have to be shown by calcium imaging of pyramidal neurons from this layer. Layer 5 neurons are the main input from cortex to striatum, although some input also arises from layer 2/3, especially in the motor cortex [5]. Increased activity in layers 2/3 and 5 could then lead to excitotoxicity in striatum. Indeed, it has been shown using magnetic resonance tomography that HD patients exhibit higher levels of glutamate in the striatum than healthy individuals [200]. Also, increased firing of MSNs in R6/2 mice of 6 to 9 weeks of age has been reported [201]. Treatment of R6/2 mice with the glutamate release inhibitor riluzole led to an increase in body weight, life span and reduction of mHTT inclusion ubiquitination [202], suggesting the negative influence of glutamate mediated hyper-excitation in this mouse model.

3.1.6. Outlook

In the future, calcium imaging from specific cell populations would be very revealing. For this, specific Cre lines would have to be crossed with a Cre-dependent reporter line that expresses a fluorescent marker in a Cre-dependent fashion. Alternatively, one could use a Cre-dependent virus to express GCaMP selectively. First of all, imaging should be conducted from interneurons and excitatory neurons separately using specific Cre lines such as GAD67-Cre and CamkIIa-Cre. This would clearly demonstrate that the increased activity observed arises from excitatory neurons only. To dissect the activity pattern of different interneuron populations, one could use the lines PV-Cre, SST-Cre and CR-Cre. This approach should be complemented by cell specific mass-spectrometry and transcriptome analyses of the different cell populations. For this, the same intersectional genetic approach described above could be used. It would be of great interest to compare layers 2/3 and layer 5 for both proteomic and transcriptomic as well as for imaging analyses.

In order to then suggest causality between the cellular activity and the R6/2 phenotype one could use pharmacological and light-induced activation and silencing of cells to replicate the observed cellular activity pattern, but also to influence the phenotype of the R6/2 mice. For example, increased activation of PV-positive neurons and thereby increased inhibition of excitatory cells could ameliorate the R6/2 phenotype. Last but not least, the main findings would have to be replicated in other mouse models, preferentially in a full-length HD model to exclude artefacts of the R6/2 model specifically and of exon1 models in general.

3.2. Alterations of protein homeostasis in R6/2 mice

3.2.1. Summary

In summary, I have shown that the Fluc sensor can be used in primary neurons to measure proteotoxic stress either induced by pharmacological agents or by the presence of aggregating proteins. I have demonstrated that there is no decrease of folding capacities measured with this sensor in older R6/2 mice, contrary to current models in the field. Instead, I have measured an increase in folding capacities in cerebellum and hippocampus of young R6/2 mice compared to controls and reproduced this finding partly in another mouse model and primary neurons. An increase in folding capacities at young ages in certain regions could give these regions an advantage and explain why they are less vulnerable to the disease at symptomatic stages (Fig. 3-2).

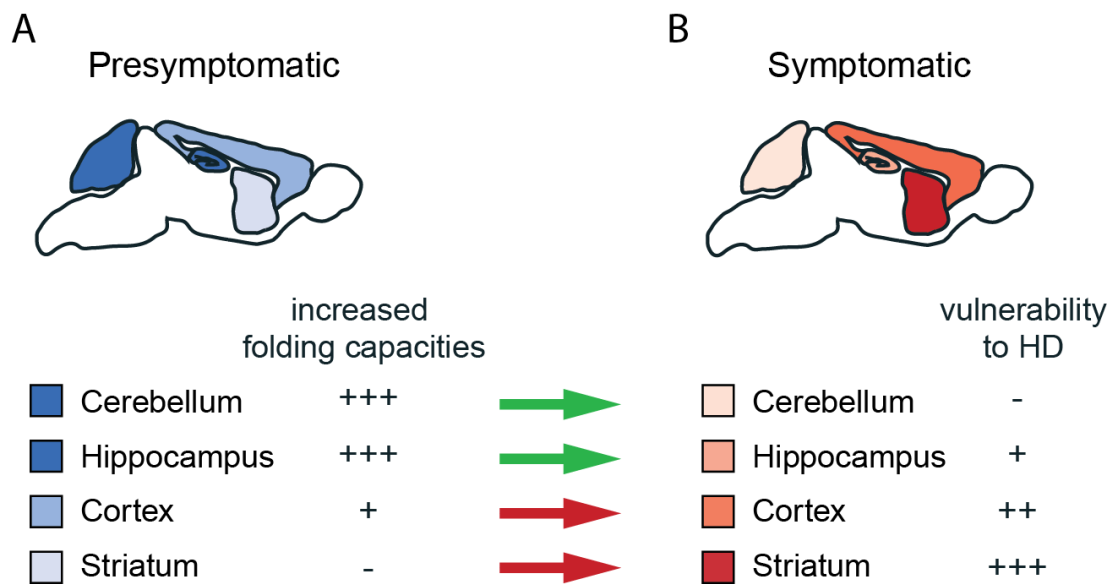


Figure 3-2: Proposed model explaining how increased folding capacities could influence vulnerability of different brain regions to the HD phenotype in R6/2 mice

In young presymptomatic R6/2 mice (left) folding capacity is increased and specific ubiquitin-related proteins components are upregulated in cerebellum and hippocampus compared to wt controls. This finding could in part explain why cerebellum and hippocampus are less susceptible to the disease at later stages than cortex and striatum, which lack such an increase in folding capacities at young ages.

I have found specific UPS-related candidates to be upregulated at this specific age in these regions. The increased folding capacities could therefore be due to an increase in degradation of proteins, perhaps induced by the need of the cell to degrade high amounts of mHTT.

3.2.2. Fluc as a proteostasis sensor in primary neurons

I tested the reactivity of Fluc to external stressors such as heat shock, proteasome and Hsp90 inhibition. Fluc reacted by forming distinct inclusions or a grainy pattern throughout the cell, which I interpreted as a stronger reaction to greater stress. From this I concluded that heat shock was a stronger stressor than HSP90 or proteasome inhibition for 4 h. The fact that Fluc formed distinct perinuclear inclusions, could indicate that it is stored into aggresomes [203]. This could also explain why Fluc did not dissolve after MG-132 administration and subsequent washout for 24 h, because aggresomes have been described to be “refractory to intracellular proteolysis” [203]. Whether Fluc forms aggresomes could be analysed by staining against vimentin, which should surround the aggresome and by staining against gamma-tubulin to visualise the MTOC.

In general, FlucDM-HA expression was very low in primary neurons, which is why for subsequent experiments I used either FlucSM-HA or FlucWT-HA. Although I did not test this experimentally, the low levels of FlucDM-HA could be due to the high levels of degradation of this very metastable and mutated protein. Using the second readout of Fluc, its enzymatic activity, I could show that Fluc can measure both decreases as well as increases of proteostasis capacities (Hsp90 and proteasome inhibition and UPS boosting by Quercetin administration, respectively). This is a clear advantage of this readout over the inclusion formation readout. The assumption underlying this readout is that not all Fluc molecules are ever perfectly folded. Of course, it stands to reason that a state of 100 % folding of Fluc could be reached in theory, and at this time point increases in proteostasis capacities could no longer be measured. Whether such a state can actually be reached is unknown and I assume that during all experiments conducted such a state was not attained.

3.2.2.1. Fluc senses the presence of mHTT in primary neurons

By co-transfecting mCh tagged mHTT and Fluc I assessed proteotoxic stress induced by aggregation-prone proteins and protein aggregates in primary cortical neurons. I could quantify that in the majority of cells Fluc reacted to the presence of IB formed in cells expressing mHTT with elongated (Q97) poly-glutamine stretches, whereas Fluc almost never reacted to the non-aggregating HTT with 25 Qs. I would like to emphasize, that Fluc often formed a grainy pattern similar to its reaction to heat shock, suggesting that the presence of mHTT inclusions is a strong stressor. The formation of distinct inclusions was mostly at a different location than the mHTT aggregate and therefore Fluc did not solely form inclusions due to sequestration by mHTT. Interestingly, Fluc also reacted significantly more often to the mere presence of aggregation-prone mHTT with 97 glutamines, which had not yet aggregated, than to the presence of HTT with 25 glutamines. This suggests that also other forms of aggregation-prone mHTT other than only IB can induce a stress onto the cell. This is in line with the many reports that state that oligomers of mHTT are actually the more toxic form and not necessarily only the big, insoluble aggregates (reviewed [204]). For example, Ortega et al. reported that the proteasome is clogged by mHTT only shortly after the start of mHTT expression or if mHTT is not allowed to aggregate [106].

3.2.3. No decrease in proteostasis capacities in R6/2 mice at advanced disease stage

Contrary to our expectations, I did not observe a decrease of specific activity of Fluc in R6/2 mice when I crossed R6/2 mice to Fluc sensor mice. A lack of UPS impairment in HD mice has been reported in earlier studies, in which R6/2 and HD94 mice were crossed to a sensor mouse line that expresses the Ub-GFP sensor to measure UPS capacities [205], [206], [106]. The authors reported that there was no reaction of the sensor in aged HD mice, suggesting that there is no defect in proteasomal degradation in aged animals of these models that can be measured with this sensor. Regarding chaperone dependent folding, studies have measured decreased levels of chaperons in HD models [170] or showed amelioration of HD phenotype by upregulation of specific chaperones [172], [173]. This is however very different from actually measuring how

well the complex cellular system folds a certain metastable protein. Our results provide evidence that proteostasis capacities are not reduced in a model of HD.

3.2.4. Region-specific improvement of proteostasis in young R6/2 mice

When I electroporated Fluc into brains of R6/2 embryos, it did not form inclusions, although it did when wt brains were challenged with heat shock. I concluded that at this very young age, the cortex of R6/2 mice did not exhibit a decrease in proteostasis capacities. Indeed, when crossing the transgenic mice expressing Fluc with R6/2 mice and measuring proteostasis capacities in different brain regions at different time points, I observed an increase in specific activity of Fluc in the cerebellum, hippocampus and cortex of 1-week old R6/2 mice compared to the wt controls. This was not the case in the striatum. In the cerebellum and hippocampus, the protein levels of Fluc were slightly reduced compared to controls, suggestive of a stronger degradation or reduced expression in these regions in R6/2 mice. This was not the case in cortex. Here, the levels were even increased, suggesting that the mechanism in cerebellum and hippocampus is different from the one in cortex. To determine whether the PrP promoter is influenced by the R6/2 background, I searched in the mass-spectrometry data set of R6/2 mice from Fabian Hosp for PrP. It was not significantly regulated in any region of R6/2 mice at the time point of 1 and 5 weeks of age, but was significantly downregulated at 8 weeks of age in striatum and at 12 weeks of age in hippocampus. This suggests that altered expression due to the PrP promoter in the R6/2 background is not the reason for the increased specific activity at 1 week of age. However, this should be further investigated, for example by performing quantitative PCR analysis. The increase in specific activity in hippocampus was in part reproduced by crossing the Fluc mice with HD94 mice, in which we induced expression of mHTT for 1 week at 8 weeks of age, resembling the expression in 1-week old R6/2 mice. The increased specific activity in tissue of R6/2 mice was also reproduced in cultures of hippocampal neurons of R6/2 mice. Also here a slight decrease of protein quantity suggested stronger degradation.

Cortical neurons in contrast showed no increase in Fluc folding but an increase in Fluc protein levels as seen in the *ex vivo* tissue analyses.

At 12 weeks of age all four regions showed increased levels of Fluc protein in R6/2 mice, but this increase was clearly higher in cortex and striatum than in cerebellum and hippocampus. It is appealing to think that the higher degradation rate in early life provides these regions a head-start, which in turn causes them to experience less of an increase in Fluc levels, and presumably in levels of other metastable proteins, compared to cortex and striatum. The idea, that different tissues use different mechanisms to deal with proteotoxic stress is not new. For example, in *C. elegans*, intestine and muscle use different ways of inducing the HSR [207]. To investigate this, it would first of all be important to measure mHTT levels at 12 weeks of age comparing these different regions. Secondly, assessing causality would be the next big step in this project (refer to point 3.2.8).

3.2.4.1. Upregulation of ubiquitin-related proteins in young R6/2 mice

Mass-spectrometry analyses confirmed that from the PQCS proteins upregulated in the regions which showed improved proteostasis, the majority were ubiquitin-related proteins and not chaperones, in contrast to what was expected. In total, I identified 8 proteins related to ubiquitination in cerebellum and hippocampus of young R6/2 mice compared to wt controls that were not regulated in striatum. I identified no ubiquitin-related protein that was upregulated in the striatum. Therefore, the better folding of Fluc could be due to a higher degradation rate because of an upregulation of these candidates. That the upregulation of these 8 candidates was transient and not visible anymore at 5 weeks of age, matched the transient increase of specific activity of Fluc, which was not observed anymore at 3 weeks of age. That the UPS system is very important for the degradation of mHTT aggregates has been shown by using the reversible HD94 model, in which synthesis of mHTT was stopped. Aggregates were then cleared over time by the system unless proteasome inhibitor was administered [208]. The fact that the chymotrypsin-like activity of the proteasome is not changed in R6/2 animals compared to wt controls is in accordance with the lack of upregulated proteasome subunits found in the proteomic analysis.

Also, it goes in line with the report by Zhuo et al. who saw no change in proteasome activity between HD model mice and wt controls [88].

To my knowledge there are no studies on R6/2 mice that looked at protein changes and proteostasis alterations at such an early time point, with the exception of a proteomic analysis conducted on tissue of 2-week old R6/2 mice [209]. This study, contrary to ours, found many changes on whole proteome occurring at this young age, whereas we did not see this at either 1 week of age nor in the data set of Fabian Hosp at 5 weeks of age. This disparity could be due to technical differences or the number of proteins identified. Interestingly though, the authors of this study also propose that early changes in protein levels could have a lasting impact on the brain in late disease stages.

3.2.5. Aspects to consider

3.2.5.1. The transgenic models

Aspects to consider regarding this study are first of all the use of rodent models to understand HD. No model can reproduce all aspects of the HD phenotype, which makes the translation of findings in mice to human disease difficult. Experiments in post-mortem human tissue add to the current generation of HD-related data. In the future, better non-invasive imaging techniques in human patients, proteomics from human post-mortem samples and biomarker development would be ideal avenues to explore. Nevertheless, until that point, the use of animal models and specifically mouse models is irreplaceable to understand diseases of such complicated systems as the brain.

Secondly, the HD models used in this study are both models that express exon1 of HTT. Although spliced forms including mainly exon1 of HTT have been found in patients [210], the findings made in this thesis should be reproduced in full-length HD models to assess their accuracy beyond exon1-expressing mice.

Last but not least, the sensor mouse is also a transgenic mouse, which may influence the findings of experiments conducted using this tool. Apart from the issue of whether the R6/2 background influences the activity of the PrP promoter, we do not know where the transgene

integrated and therefore how the sensor is specifically influenced by mHTT expression. To our advantage, expression was highest in hippocampus and cortex and much lower in cerebellum and striatum. However, cerebellum and hippocampus were similar in their proteostasis capacities, as were cortex and striatum, suggesting that overall expression levels did not dictate the observed result. Nevertheless, differential expression levels in different neurons could therefore influence the sensor's sensitivity. This could be determined by single-cell quantitative PCR. Also, the data should be reproduced using a second Fluc line to ensure that the results are independent of the specific mouse line used.

3.2.5.2. Proteostasis, Fluc and autophagy

A second aspect that should be considered is the lack of data on autophagy. Autophagy has been shown to play a big role in HD (reviewed by Nixon [211]). For example, Bauer et al. [212] used a construct made of QBP1, which binds elongated but not normal HTT and an Hsc70-binding motif to target mHTT for chaperone-mediated autophagy. Treatment of R6/2 mice with a virus that expresses this construct leads to an amelioration of the phenotype and elongation of the life span [212], showing the usefulness of autophagy in dealing with mHTT toxicity. Fluc is not degraded by autophagy in cell lines (Dr. Frédéric Frottin, laboratory of Prof. Ulrich Hartl, personal communication), however, I have not shown this in neurons. Even without the sensor being degraded by autophagy, alterations in this degradation pathway do influence the proteostasis network and the sensor should be able to measure this. Cell culture experiments could answer these questions. In our mass-spectrometry analyses we only found one autophagy-related protein, consistent with a model that this part of the proteostasis machinery might not play a big role in the increased folding capacities observed in young R6/2 mice.

3.2.6. Outlook

3.2.6.1. Proving causality and elucidating the mechanism

Future work should first of all determine causality between better folding capacities in cerebellum and hippocampus of young wt mice and upregulation of specific ubiquitin-related

proteins at this time point in these regions. Current data only shows that both observations are correlative to one another. The data of hippocampal neurons degrading CPY*-mCh faster than cortical neurons is already a good step in the direction of elucidating the mechanism. It would be interesting to see, if this difference is specific to neurons from wt mice or is also seen in R6/2 neurons. But to assess causality, the best approach would be to improve the proteostasis capacities by overexpression of the specific UPS components in cortex and striatum of young R6/2 mice and thereby reduce neuropathology in these regions and ultimately ameliorate the disease phenotype and increase life span. This improvement however, is not easy to achieve. I observed that different UPS-related proteins were upregulated in cerebellum and hippocampus. It could be that the specific cocktail of proteins needed is again different in striatum. Also, overexpression of four proteins at the same time *in vivo* is a technical challenge. One could first conduct the overexpression in cultured primary neurons, although the appropriate combination of proteins to use is not clear. Use of pharmacological methods to increase UPS-related degradation could be a solution. Another possibility would be to decrease proteostasis capacities in hippocampal neurons of R6/2 mice, by administering a proteasome inhibitor or using RNA interference to knock-down certain UPS components and thereby induce a neuropathology comparable to the one found in cortex or striatum. Although perhaps easier to perform, this would only provide an indirect support of this hypothesis and would be less relevant in terms of therapeutic approach development.

3.2.6.2. Measuring proteostasis in other mouse models and in aging

First of all, it would be interesting to measure proteostasis capacities in mouse models of other neurodegenerative disease such as AD or PD, since these diseases also have been linked to impairments in the PQCS (reviewed by McKinnon and Tabrizi [213]). Proteostasis measurements would entail crossing the Fluc mouse to mouse models of AD and PD and measuring specific activity of Fluc in different brain regions at different time points. Mass-spectrometry and transcriptome analyses would shed light onto the possible changes in protein expression that

underlie alterations in Fluc folding. Subsequently, studies in primary neurons and immortalized cell lines could help elucidate the mechanisms.

Secondly, it would be of great interest to measure proteostasis with this transgenic model in aging wt mice. It is a long standing belief that proteostasis capacities decrease with aging and this has been shown to be the case in *C. elegans* [176]. In line with this, the proteasome activity has been reported to decrease with aging in several brain regions of the mouse [88]. That a good proteostasis capacity is indispensable for health in aging was also shown by a study where life span and proteostasis were compared between different rodent strains. The authors found that the maximum life span potential of different rodents correlates with proteasome activity, HSF1 upregulation, and autophagy and UPS markers [214]. A recent study compared expression of HSPs in old (22 months) and young (3 months) mouse brains and found no significant difference [215], suggesting that chaperones are not necessarily the most important players. In the longest-lived rodent, the naked mole rat, proteomics identified nine proteostasis components, whose expression correlated with aging [216]. Among these nine proteins were three autophagy-related proteins, two chaperones, one proteasome subunit and four UPS-components, resembling our findings in young R6/2 mice. This suggests that components of the proteostasis network, but specifically of the UPS are important for a long life. This prompts the question whether the UPS system would still be as functional in old as in young animals. Our transgenic model would provide the opportunity to measure alterations in proteostasis in a brain region specific way during aging of mice.

4. Materials and Methods

4.1. Materials

4.1.1. Chemicals, reagents and kits

Chemicals, reagents, enzymes, and kits were purchased at the following companies: Merck, Sigma-Aldrich, Roth, VWR, New England Biolabs, Roche, Qiagen and Machery-Nagel.

4.1.2. Solutions and buffers

Phosphate-buffered saline (PBS) pH 7.3

137 mM NaCl

2.7 mM KCL

4.3 mM Na₂HPO₄*7H₂O

1.4 mM KH₂PO₄

4.1.2.1. Solutions and buffers for molecular biology

Master mix for genotyping, 48 µl

H₂O (distilled)

0.5 µl of each primer (50 pmol)

5.0 µl 10x Thermo Pol Reaction buffer (New England Biolabs)

0.4 µl dNTPS-mix (25 mM each, Fermentas)

0.5 µl Taq Polymerase (New England Biolabs)

50x TRIS-acetate buffer (TAE)

2 M Tris acetate

50 mM EDTA

Gel loading buffer, 50 ml

24 ml H₂O

25 ml Glycerol

1 ml 50x TAE

0.1 g Orange G

24 ml H₂O

4.1.2.2. Solutions and buffers for biochemistry

Lysis buffer

H₂O (distilled)

50 mM Tris pH 7.5

150 mM NaCl

1 % Triton

Stored at 4 °C. One tablet protease inhibitor was added to 25 ml of buffer prior to use.

Buffer A (for proteasome activity buffer)

H₂O (distilled)

50 mM Tris-HCl pH 7.4

5 mM MgCl₂

10 % glycerol

Stored at 4 °C.

Proteasome activity buffer, 15 ml

Buffer A

200 mM ATP (Sigma-Aldrich, freshly dissolved in ultrapure H₂O)

200 mM DTT (Roth, freshly dissolved in ultrapure H₂O)

SDS PAGE separating gel (10 %), 10 ml for one gel

4.05 ml H₂O

2.6 ml 1.5M Tris pH 8.8 0.4 % SDS

3.3 ml Acryl-bis

50 µl APS

5 µl TEMED (Sigma)

SDS PAGE stacking gel (4 %), 5ml for one gel

3.05 ml H₂O

1.3 ml 1.5 M Tris pH 8.8 0.4 % SDS

0.65 ml Acryl-bis

50 µl APS

5 µl TEMED

6x Sample buffer

0.125 M Tris-HCl pH 6.8

20 % glycerol

4 % SDS

2 % beta-mercaptoethanol

0.02 % bromphenolblue

5x Electrophoresis buffer (10L)

154.5 g Tris base

721 g Glycine

50 g SDS

H₂O up to 10 L

Protein transfer buffer, 1 L

3.03 g Tris base

14.4 g Sodium dodecyl sulfate (SDS)

200 ml Methanol

H₂O up to 1 L

Protein running buffer (5x, 10 L)

154.5 g Tris base

721 g Glycine

50 g SDS

H₂O up to 10 L

Tris-buffered saline with Tween20 (TBS-T)

20 mM Tris, pH 7.5

120 mM NaCl

0.1 % Tween20

4.1.2.3. Buffers for immunocytochemistry and immunohistochemistry

Blocking solution (Immunocytochemistry, ICC)

PBS

2 % bovine serum albumin (BSA)

4 % normal donkey serum (DS, Jackson Immuno Research)

Blocking solution (Immunohistochemistry, IHC)

PBS

5 % DS

0.2 % BSA

0.2 % Lysine

0.2 % Glycine

Primary antibody solution (IHC)

PBS

0.3 % Triton X-100

2 % BSA

0.02 % sodium azide (SA)

Secondary antibody solution (IHC)

PBS

0.3 % Triton X-100

3 % DS

4.1.3. Media

Luria-Bertani (LB) medium (1 L, pH 7.5)

10 g Bacto-Tryptone

5 g Bacto-Yeast extract

5 g NaCl

H₂O to 1 L, adjust pH

0.05 M Borate buffer pH 8.5

50 mM Boric acid

12.5 mM Sodium tetraborate (borax)

Medium for cell lines

DMEM (+ D-Glucose, - Pyruvate, Gibco)

1 % Penicillin-Streptomycin (Invitrogen)

1 % L-Glutamine (Invitrogen)

10 % FBS (HyClone)

Dissection medium

HBSS (+ CaCl₂, +MgCl₂, Gibco)

1 % Penicillin-Streptomycin (Invitrogen)

7 mM Hepes (Biomol)

2 mM L-Glutamine (Gibco)

Plating medium (primary neurons)

Neurobasal medium (- L-Glutamine, Gibco)

1x B27 supplement (Invitrogen)

2 mM L-Glutamine (Gibco)

1 % Penicillin-Streptomycin (Invitrogen)

4.1.4. Oligonucleotides and plasmids

Oligonucleotides were purchased at Metabion, in dried and desalted form, and subsequently solubilized in H₂O.

Table 4-1: Oligonucleotides for cloning

Name	Sequence	Purpose
GFP 5'	AAAGCTAGCATGGTGAGCAAGGGCGAG	GFP-HA from FlucGFP-myc
Fluc 5'	ATCTCTTTTCCGTCATCGTCTTTCCG	FlucGFP-HA from FlucGFP-myc
FlucWT-HA 3' myc	AAAGCGGCCGCCTAAGCGTAATCTGGAACA	FlucGFP-HA from FlucGFP-myc
FlucWT-HA 5' PrP	AAAGTCGACATGGAAGACGCCAAAAACATA AAG	FlucGFP-HA into PrP.Mo.Xho
FlucWT-HA 3' PrP	AAAGTCGACCTAAGCGTAATCTGGAACATC GTATGGGTATGCTGCTGCTTTCTTGTACAGC TCGTCC	FlucGFP-HA into PrP.Mo.Xho
FlucWT-HA 5' pCAGG	CGCCTGGGCCGGATCCATGGAAGACGCCAA AAACATAAAG	FlucGFP-HA into pCAGG
FlucWT-HA 3' pCAGG	GTTGCACTTAACGCGTCTAAGCGTAATCTGG AACATCG	FlucGFP-HA into pCAGG

Table 4-2: Oligonucleotides for genotyping

Name	Sequence	Mouse line
FlucGeno 5'	GTG TCG CTC TGC CTC ATA GAA CTG CCT GCG TG	PrPWT1214, PrPWT1433, PrPSM4983, PrPSM4978
FlucGeno 3'	CAT CCT TGT CAA TCA AGG CGT TGG TCG CTT CCG	PrPWT1214, PrPWT1433, PrPSM4983, PrPSM4978
R62 forward	CCG CTC AGG TTC TGC TTT TA	R6/2
R62 reverse	TGG AAG GAC TTG AGG GAC TC	R6/2
CamK Tg forward	CGC TGT GGG GCA TTT TAC TTT AG	Camk-tTA
CamK Tg reverse	CAT GTC CAG ATC GAA ATC GTC	Camk-tTA
CamK Control forward	CAA ATG TTG CTT GTC TGG TG	Camk-tTA wt allele
CamK Control reverse	GTC AGT CGA GTG CAC AGT TT	Camk-tTA wt allele
LacZ forward	CCA GCT GGC GTA ATA GCG	BiTetO
LacZ reverse	CGC CCG TTG CAC CAC AGA TG	BiTetO

Table 4-3: Oligonucleotides for sequencing

Name	Sequence	Construct
firefly	CCG GCG CCA TTC TAT CC	FlucGFP
FG4f	GTT AAT CAA AGA GGC GAA CTG TG	FlucGFP
FG3f	GAC AAT TGC ACT GAT CAT GAA C	FlucGFP
FG4.2f	TCT TAC CGG AAA ACT CGA CGC	FlucGFP
FG1r	GCA ATA GCA TCA CAA ATT TCA C	FlucGFP
FG2f	CCA AAA TGT CGT AAC AAC TGC G	FlucGFP

Table 4-4: Plasmids

ID	name	backbone	resistance	source
ID10	FlucGFP(wt)-myc	pCI-neo	Amp	Frédéric Frottin, Hartl lab
ID13	FlucGFP(wt)-HA	pCI-neo	Amp	cloned from ID10
ID14	FlucGFP(dm)-HA	pCI-neo	Amp	cloned from ID12
ID15	FlucGFP(sm)-HA	Mo.PrP.Xho	Amp	cloned from ID9
ID77	GFP-HA	pCI-neo	Amp	Cloned
ID51	Htt-Q25-mCh	pcDNA	Amp	Lisa Vincenz, Hartl lab
ID52	Htt-Q97-mCh	pcDNA	Amp	Lisa Vincenz, Hartl lab
ID9	NaN	Mo.PrP.Xho	Amp	David R. Borchelt, University of Florida
NaN	pCAGG	pCAGG	Amp	Daniel del Toro Ruiz
NaN	FlucGFP(sm)-HA	pCAGGs	Amp	Cloned

4.1.5. Antibodies

Table 4-5: Primary antibodies

Target	Species	Dilution	Application	Source	Catalogue number
Htt (EM48)	mouse	1:1000, 1:200	ICC, IHC	Millipore	MAB5374
GFP	rabbit	1:1000, 1:200	ICC, IHC	Life technologies	A11122
GFP (JL-8)	mouse	1:1000	WB	Clontech	632381
Tubulin	mouse	1:1000	WB	Covance	MMS-435P
NeuN	mouse	1:1000, 1:500	ICC, IHC	Millipore	MAB377
NeuN	rabbit	1:500, 1:300	ICC, IHC	Cell Signaling	12943
Cleaved Caspase 3	rabbit	1:500	ICC	abcam	ab13847
Darpp-32	goat	1:300	IHC	Lifespan Biosciences	LS-C150127
Neurogranin	rabbit	1:500	IHC	abcam	ab235870
SST	rabbit	1:500	IHC	Peninsula Laboratories International	T4103.0050
CR	rabbit	1:500	IHC	Swant	CR-7697
PV	rabbit	1:500	IHC	abcam	ab11427
PSD95	mouse	1:500	IHC	Sigma	P246

VGLUT1	guinea-pig	1:500	IHC	Millipore	ab5905
VGLUT2	guinea-pig	1:500	IHC	Millipore	ab2251
VGAT	rabbit	1:500	IHC	Synaptic Systems	131002
Gephyrin	mouse	1:500	IHC	Synaptic Systems	147111

All secondary antibodies for immunohisto- or immunocytochemical detection were purchased at Jackson Immunoresearch and those for immunodetection after western blotting were purchased at GE Healthcare.

Table 4-6: Secondary antibodies

Conjugated	Target	Species	Application	Dilution
HRP	mouse / rabbit	goat	WB	1:5000
Cy2 / Cy3 / Cy5	mouse / rabbit / guinea-pig	donkey	IH	1:300
Cy2 / Cy3 / Cy5	mouse / rabbit	donkey	ICC	1:500

4.1.6. Mouse lines

PrP-FlucSM and PrP-FlucWT mice were generated as described under Point 4.2.7. R6/2 mice were obtained from Jackson Laboratory, generated in the lab of Gillian Bates and published originally by Mangiarini et al. [107]. CAG repeat length was determined from tail biopsies using the services of Laragen, Inc., and only males with CAG repeats under 180 were used for breedings. BiTetO mice were generated in the lab of René Hen and published originally by Yamamoto et al. [191]. Mice were kindly given to us by Lucas Hen and colleagues. Camk-tTA

were obtained by the Jackson Laboratory, generated in the lab of Eric Kandel and originally published by Mayford et al. [217]. Mice were housed under SPF conditions with *ad libitum* access to food and water. R6/2, BitetO and CamK-tTA mice were kept in CBAxB16 background. Fluc mice were kept in a B16 background. Mice of either sex were used for the experiments.

4.2. Methods

4.2.1. Molecular biology and immortalized cell culture

4.2.1.1. Preparation of plasmid DNA

Cultures of single colonies were grown overnight at 37 °C and 220 rpm in LB medium supplemented with 100 µg/ml ampicillin or kanamycin as required. Plasmid DNA was isolated using kits by Qiagen (mini-preparation) or Machery-Nagel (maxi-preparation) following company protocols. DNA concentration was measured using a nanodrop (peqlab, Nanodrop 1000) and the software NanoDrop 1000 3.7.1 (Thermo Scientific).

4.2.1.2. Transformation of competent E.coli by electroporation

For the transformation 1-4 µl of DNA of maximum 50 ng/ µl concentration was added to 50 µl of electro-competent cells (Top10 from Thermo Fisher Scientific for transformation after ligation or custom-made DH5α for regular transformations) on ice and subsequently transferred to a pre-chilled cuvette (Bio-Rad, Gene Pulser Cuvettes, 0.2 cm electrodes). In the electroporation chamber (Bio-Rad, Puls Controller) the cuvettes were treated with two pulses of 25 µF. Cells were suspended in 200 µl LB medium, transferred to a 14 ml Falcon tube and incubated for 1h at 37 °C and 220 rpm rotation. Subsequently, they were plated on LB medium plates containing ampicillin or kanamycin and left to grow overnight at 37 °C.

4.2.1.3. Cloning of expression plasmids

For cloning of DNA into vector backbones, vectors were digested with an appropriate enzyme (New England Laboratories) overnight at the temperature indicated by the manufacturer and in

the corresponding buffers at a concentration of at least 4 units per microgram DNA. The next morning, an additional 50 % of the enzyme was added and DNA left for digestion for another 2 h. Correct digestion was checked on an agarose gel after electrophoresis. For amplification of DNA fragments intended for cloning, Pfu polymerase from Promega was used with the corresponding buffers. Vector and insert DNA were purified from agarose gels after electrophoresis using a gel extraction kit (Qiagen) and subsequent column purification (Qiagen) following the manufacturer's protocols. Ligation was conducted using T4 DNA ligase (New England Biolabs) overnight at 16 °C. For this, 50 ng of vector DNA and the corresponding amount of insert was used, based on the ratio of vector to insert length to obtain a stoichiometric ratio of 1:1, 1:3, 1:10 and 1:0 as a negative control in a total volume of 20 µl. Subsequently, 2 µl of ligase reaction were used for transformation of Top10 electro-competent cells (Thermo Fisher Scientific). Alternatively, DNA inserts were cloned into digested vector backbones using the In-Fusion HD Cloning Kit (Clontech) following manufacturer protocols.

4.2.1.4. Agarose gel electrophoresis

Agarose gels were prepared by dissolving agarose in TAE buffer (1 to 2 %, depending on the size of DNA fragments to separate) by boiling the suspension for 5 min, cooling it to approximately 60 °C and adding Ethidium bromide (Roth) to a concentration of 0.5 µg/ml. Subsequently, the solution was poured into a plastic tray and left to cool for polymerization. Gels were stored in plastic wrap at 4 °C. DNA was separated based on size by gel electrophoresis, at a voltage of 100 – 230 Volts. DNA was visualised by UV light using a Gel Doc XR+ machine (Biorad).

4.2.1.5. Propagation, thawing and transfection of mammalian cells

HeLa cells were grown at 37 °C with 5 % CO₂ in medium for cell lines. Confluent cells were washed with pre-warmed PBS and incubated with Trypsin-EDTA (Sigma) for 3 min. Subsequently, cells were taken up in the medium by pipette and newly seeded as needed. HeLa cells were transfected at 70 % confluency with Lipofectamine LTX and PLUS reagent (Life

technologies) according to the manufacturer protocol. Transfection medium was replaced by new medium for cell lines 3 - 6 h after transfection.

4.2.2. Mouse work

4.2.2.1. Generating FlucGFP transgenic mice

For generation of transgenic mice expressing FlucGFP under the prion promoter, Mo.PrP plasmid was obtained from David Borchelt (University of Florida). Mo.PrP plasmid was cleaved with Sall. The insert coding for FlucGFP was amplified by PCR adding an HA tag to the sequence. The insert was cloned into the linearized vector. DNA was verified for correctness by sequencing (Eurofins). The final vector was then amplified by maxi preparation and cleaved with NotI, excising the pBluescript vector bone. The linearized vector was extracted from an agarose gel using JetSorb gel extraction kit (Genomed) and subsequently filtered using PVDF 0.45 μm Ultrafree MC GV filters (Millipore). Purity of the DNA was checked by gel electrophoresis. The purified, linearized vector was then given to the transgenic service at a concentration of 50 - 100 ng/ μl . The transgenic service conducted the pronuclear injection and provided us with several transgenic mouse lines. Animals obtained from this procedure were validated for transgene integration by PCR against FlucGFP of tail biopsies. For the sm construct, seven out of 84 mice were transgenic. Out of these transgenic lines, two lines showed germline transmission and good expression of the transgene (PrPSM4977 and PrPSM 4983). For the WT construct, five out of 103 mice mice were transgenic. Out of these transgenic lines, two lines showed germline transmission and expression of the transgene (PrPWT1214 and PrPWT 1433). For this thesis, all work with the Fluc transgenic mouse was conducted on the PrPWT1214 line.

4.2.2.2. Doxycycline administration

HD94 mice and their single-transgenic and non-transgenic littermates were administered doxycycline from embryonic day 0 until 8 weeks of age. For this, the mice or, before birth, the mother, were given 2 mg/ml doxycycline in the drinking water. To mask the bitter taste of the

antibiotic, it was diluted in 5 % sucrose. Doxycycline solution was kept in dark bottles to prevent light exposure and renewed once every week [191].

4.2.2.3. *In utero* electroporation

IUE was performed as previously described [218], [219]. Briefly, pregnant Bl6 or R6/2 mice carrying E15.5 embryos were anesthetized with Buprenorphin, Lidocaine (0.05 mg per kg body weight, intraperitoneal injection, 4 mg per kg body weight, subcutaneous injection, respectively) and constant administration of isoflurane. The abdomen was opened and the uterus extracted carefully. Embryos were injected into the ventricle of the brain with 4 $\mu\text{g}/\mu\text{l}$ DNA in a total volume of 1 μl TE buffer. For better visualization 0.02 % FastGreen was added to the DNA mix. For the injection, a glass capillary (1.5 x 0.86 x 80 mm, Science Products) was used, which was pulled on a micropipette puller (Sutter Instruments, settings: 680 °C, pull = 30, velocity = 125, time = 210). Injection was achieved with a Picospritzer III (Intracel) injecting with 30 V, five currents of 50 msec duration at 1 sec intervals. The positively charged electrode of an ECM830 electroporator (Harvard Apparatus) was held to one side of the skull so that the DNA was directed to that side. After the procedure, the peritoneal wall and skin were sewed (Mersilk 6-0, Ethicon) and the mouse left to recover on a heated pad. The mouse was sacrificed three days later, the embryonic brains extracted and fixed in 4 % PFA overnight either directly or after a heat shock of 2 h at 43 °C.

4.2.2.4. Tail DNA preparation and genotyping using PCR

From each mouse 1 mm of tail was lysed in 100 μl of 50 mM NaOH for 45 min at 95 °C, with vortexing every 15 min, and subsequently neutralized by adding 100 μl of 1.5 M Tris-HCl pH 8.8. Tail lysates were stored at 4 °C. For genotyping by PCR, DNA solution obtained from lysed tails was used. A PCR master mix was prepared on ice (48 μl per sample) and mixed with the respective DNA samples (2 μl per sample).

Table 4-7: PCR protocols

Program	Mouse lines	Denaturing	Denaturing repeated	Annealing indicated	Extension no. of times	Extension	No. of cycles
FlucGeno	PrPWT-1214	95 °C 3:00	95 °C 0:30	69 °C 0:30	72 °C 1:00	72 °C 5:00	35
LacZ	BiTetO, HD94	95 °C 5:00	95 °C 0:30	58 °C 0:30	72 °C 0:30	72 °C 5:00	35
CamK	CamK-tTA	95 °C 3:00	95 °C 0:30	57 °C 1:00	72 °C 1:00	72 °C, 2:00	35
R6.2 part I	R6/2	95 °C 2:00	95 °C 0:20	72 °C 0:15 (-Δ 0.5 °C /cycle)	72 °C 0:15	NaN	10
R6.2 part II	R6/2	NaN	94 °C, 0:15	60 °C, 0:15	72 °C, 0:15	72 °C, 1:00	35

4.2.2.5. Transcardial perfusion

Animals were narcotized with isoflurane (cp-pharma) and subsequently with Ketamine/Xylazine (1.6 % ketamine, 0.08 % xylazine in saline, medistar, Bernburg, respectively) and transcardially perfused for 6 min at a speed of 1 ml/min with cold PBS and for additional 8 min with cold 4 % PFA. Subsequently, brains were removed and post-fixed in 4 % PFA for 48 h. For future use, brains were stored in PBS at 4 °C.

4.2.2.6. Dissection of mouse tissue

Animals were narcotized with isoflurane and subsequently killed by cervical dislocation. Brains were removed and cerebellum, hippocampus, cortex and striatum dissected on ice. Tissue was snap-frozen in liquid nitrogen and stored for future use at -80 °C.

4.2.3. Primary neuronal culture and biochemistry

4.2.3.1. Primary culture of dissociated mouse cortical and hippocampal neurons

Culture plates or coverslips were coated with 0.1 or 1.0 $\mu\text{g/ml}$ poly-D-lysine (Sigma, respectively) for a minimum of 2 h. Plates or coverslips were subsequently washed three times for 5 min with PBS and then coated with 5 $\mu\text{g/ml}$ laminin for a minimum of 2 h. Cultures of wildtype neurons were performed using E15.5 CD1 embryos. Cultures of R6/2 animals were conducted at E18.5. Females were checked for vaginal plugs the morning after mating and counted as 0.5 days after pregnancy. Embryos at E15.5 or E18.5 were dissected in dissection medium. First, the head was removed and the brain dissected out of the skull. Hemispheres were cut off the rest of the brain and the meninges removed with forceps. The cortex and/or hippocampus was then dissected. The obtained tissue was washed three times in 2 ml dissection medium and then trypsinized in 2 ml Trypsin at 37 °C for the number of min that corresponded to the age of the dissected embryo. Trypsin activity was quenched with 5 % FBS in plating medium. FBS was removed and the tissue washed three times with 2 ml plating medium. Cells were mechanically dissociated in 0.5 ml plating medium by pipetting with a cut 1 ml pipette 30 times and subsequently with a normal tip 15 times. Dissociated cells were centrifuged in 2.5 ml plating medium at 129 g for 5 min and the supernatant discarded. Cells were re-suspended in 0.5 ml plating medium by pipetting 15 times with a 1 ml pipette and then diluted in 10 ml plating medium for counting, which was conducted on 10 μl volume in a Neubauer counting chamber (Blaubrand, Brand). Cells were seeded at a density of 100 000 to 120 000 cells per well in a 24-well plate (0.5 ml volume per well). Half of the medium was changed after 7 days in culture.

4.2.3.2. Transfection of primary neurons using calcium phosphate

Transfection of primary neurons was conducted as described by Jiang and Chen [220]. Briefly, a transfection mix was prepared by adding DNA into H_2O . After mixing by flicking the tube, calcium chloride solution was added dropwise and the solution mixed again. Last, HBS 2x solution was layered on top of the solution. The solution was then mixed well by flicking and

inverting the tube. The transfection mix was left incubating for 45 min at room temperature (RT). Neurons were transferred into fresh plating medium and 30 μ l of the transfection mix was added per 24 well plate well in a dropwise manner. Cells were incubated at 37 °C for 3 h and then transferred into plating medium, which had been acidified for at least 30 min at 10 % CO₂. After 30 min neurons were transferred back into their original medium.

4.2.3.3. Semi-automated quantification of inclusions

Quantification of proteasome and Hsp90 inhibition was conducted semi-automatically using self-written macros in ImageJ (by Daniel del Toro Ruiz). Inclusions were only assessed in the cytosol of the cell body excluding nucleus and neurites. An inclusion was counted if its size was bigger than 200 x 300 μ m, the circularity was between 0.6 and 1.0 and the brightness was higher than the mean fluorescence of the whole cell plus four standard deviations. Quantification of heat shock was assessed manually.

4.2.3.4. Luciferase assay

For the luciferase assay on transfected immortalized cells, cells were grown in 24 well plates and transfected upon 70 % confluency. 24 h after transfection cells were split and seeded into 12 well and 96 well plates (1 ml and 200 μ l volume per well, respectively). 48 h after transfection 30 μ l per well of luciferin (Promega E1500) was added into the medium of the 96 well plate. Cells grown in 12 well plates were used for protein quantification by western blotting. For the luciferase assay on transfected primary neurons, neurons were grown in 6 well plates (2.5 ml volume per well). 2 to 5 days after transfection, the medium was removed and 200 μ l of fresh medium added to the well. Subsequently, 100 μ l of luciferin (Promega E1500) was added per well. For luciferase assay on frozen tissue 50 – 100 μ g of protein from tissue lysates were mixed with 100 μ l of luciferin (Promega 1501). Luciferase activity was measured for 2 sec in a luminometer (Lumat LB 9507, Berthold) 15 min after administration of the substrate in technical duplicates.

4.2.3.5. Cell and tissue lysis

Primary neurons and cultured cell lines were lysed by application of 1.5x SDS-containing sample buffer, followed by 3 min incubation on ice. DNA was fragmented by repeated pipetting. For tissue lysis, tissue was thawed on ice and weighted. 10 µl/mg pre-chilled lysis buffer was added and the tissue homogenized for 1 min at maximum speed using a VOS14 (VWR) homogenizer. Tissue homogenates were placed on ice for 20 min for protein solubilization and the solution subsequently centrifuged at 13000 g for 12 min to remove cell debris. The supernatant was transferred to a new pre-chilled Eppendorf tube. Protein concentration was measured by Bradford assay following the manufacturer's protocol (Bio-Rad). Lysates were stored at -20 or -80 °C.

4.2.3.6. Western blotting and immunodetection

Tissue lysates were mixed with loading buffer to obtain a 1x solution. Cell or tissue lysates were boiled at 95 °C for 5 min and subsequently centrifuged for 15 min at 13 000 g. Proteins were separated based on size by SDS-PAGE on 10 % gels running at 80 V for approximately 2 h. After electrophoresis, gels were incubated for 10 min in transfer buffer. PVDF membranes (Immobilon-P) were activated for 10 sec in Methanol, washed for 5 min in H₂O and incubated for 10 min in transfer buffer. Subsequently, proteins were transferred by semi-dry blotting (Trans-Blot Turbo Transfer System, Biorad) at maximum 25 V and 2.5 A for 35 min. Transferred protein was visualised on the membrane by Ponceau staining through incubation in Ponceau solution for 5 min and subsequent washing in H₂O. Membranes were then blocked with 5 % milk and 5 % BSA in TBS-T for at least 30 min, then washed once in TBS-T. Membranes were incubated overnight with the primary antibody in 3 % BSA, 0.02 % SA in TBS-T. The next day, membranes were washed three times in TBS-T for 10 min per wash and incubated for at least 2 h with secondary HRP-conjugated antibody in 3 % milk in TBS-T. After three washes with TBS-T for 10 min per wash, immunodetection was conducted by incubating the membrane for 1 min in ECL solution and detecting the substrate reaction with a peqlab Fusion Fx7.

4.2.3.7. Calculation of specific activity

Values obtained from the luciferase assay were divided by protein quantity measured by immunodetection after western blotting. Fold change of protein quantity was introduced as the x-value in the normalization formula. Therefore the expected fold change of specific activity solely based on the protein level difference was calculated. Expected specific activity was subtracted from measured specific activity and plotted as the fold change as a percentage.

4.2.3.8. Proteasome activity assay

Tissue was lysed in proteasome activity buffer as described under Point 4.2.2.1. 50 µg of protein from tissue lysates were incubated with Suc-LLVY-AMC (20 mM, Bachem) for 30 min at 37 °C either with or without proteasome inhibitor (20 µM MG-132, AG Scientific) as described in Myeku et al. [192]. Samples were excited at 340 nm emission wavelength and measured at 465 nm in a Tecan plate reader (software RdrOle4). Values of samples incubated with proteasome inhibitor were subtracted from values without proteasome inhibition.

4.2.4. Histology and Immunofluorescence

4.2.4.1. Embedding and sectioning of tissue

Fixed tissue was either embedded in albumin or cryo-preserved. For embedding in albumin, glutaraldehyde was added 20:1 and the solution was mixed vigorously. The tissue was then covered with the solution. Subsequently brains were stored in PBS with 0.02 % SA at 4 °C. For cryo-preservation, brains were dehydrated overnight in 30 % sucrose in PBS, embedded in Tissue-Tek O.C.T. Compound (Sakura) on dry ice and subsequently stored at -80 °C. Not embedded and albumin-embedded tissue was sectioned at a vibratome VT1000S (Leica) into 70 µm thick sections. Sections were stored in PBS at 4 °C for future use. Cryo-fixed tissue was sectioned at a cryostat CM3050S (Leica) into 30 - 40 µm thick sections. Sections were mounted onto Superfrost Plus glass-slides (Thermo Scientific) and stored at - 20 °C for future use.

4.2.4.2. Immunofluorescence on cells

Cells were grown on 13 mm coverslips in 24-well plates. After transfection and experimentation (specified in the figure legends), cells were washed once with PBS and fixed for 15 min with 4 % PFA at RT. Subsequently, cells were washed 3 times with PBS and stored in PBS at 4 °C. Cells on coverslips were washed once with PBS and then permeabilised in 0.1 % Triton X-100 in PBS for 10 min at RT. Triton residues were removed by a wash with PBS for 5 min. Cells were blocked for 30 min in blocking solution, subsequently transferred to a wet and dark plastic chamber and incubated for 1 h with primary antibody in blocking solution. After three washes of 5 min with PBS, cells were incubated for 30 min with fluorescently labelled secondary antibodies in blocking solution. Coverslips were mounted with DAKO mounting medium, dried overnight at RT and stored at 4 °C.

4.2.4.3. Immunofluorescence on tissue sections

Sections were washed once with PBS and then permeabilised in 0.5 % Triton X-100 in PBS for 30 min at RT. Triton residues were removed by a wash with PBS for 5 min. Sections were then blocked for 30 min in blocking solution, subsequently incubated overnight with primary antibody in primary antibody solution. After three washes of 10 min with PBS, sections were incubated for at least 2 h with fluorescently labelled secondary antibodies in secondary antibody solution. Sections were mounted with DAKO mounting medium, dried overnight at RT and stored at 4 °C.

4.2.4.4. Microscopy and image analysis

All images were acquired using a Leica TCS SP8 scanning confocal microscope equipped with a 10 x air objective, a 20 x immersion objective, a 40 x oil objective and a 63 x oil objective. Images were processed and analysed using the open-access image analysis software ImageJ (<https://imagej.net>). The use of custom-written macros is stated in the Results section.

4.2.5. Data analysis

If not differently indicated, data was processed, analysed and plotted using R in RStudio.

4.2.5.1. Analysis of mass-spectrometry data

All mass-spectrometry analyses were conducted by Fabian Hosp in a label-free manner. I was given the mass-spectrometry data from Fabian Hosp including statistical analyses using Student's t-test on LFQ intensities [221]. LFQ intensities are globally normalized using a population of proteins that are marginally altered between experiments and therefore renders the use of housekeeping genes obsolete [221]. This analysis delivers a p-value and expression difference (fold change) for every protein at a given age and in given brain region.

4.2.5.2. Statistical analysis

Statistical analyses were carried out using R in RStudio, GraphPad Prism and MatLab (MathWorks). Two-photon imaging data was statistically analysed by Sabine Liebscher. If not stated differently in the figure legends, all data was compared by one-sample or two-sample unpaired, two-tailed Student's T-test. Differences were considered statistically significant when the p-value was lower than 0.05, denoted by an asterisk (*). Two or three asterisk denoted a p-value lower than 0.01 or 0.001, respectively. If not stated differently, data was presented as mean \pm standard error of the mean (SEM).

4.2.6. Calcium imaging

4.2.6.1. Virus injection, window preparation and two-photon imaging

Virus injection, window preparation and two-photon imaging was performed by Johanna Neuner. Further information is stated in the figure legends.

4.2.6.2. Two-photon image data processing

Images were saved as tagged image file format files and image processing was conducted using ImageJ. Briefly, all images of one imaging session and FOV were saved using ImageJ as stacked files. Stacks were motion corrected using the "moco" plugin [222]. On average z-

projections ROIs were manually drawn around cells for one time point and saved as a ROIS mask. This ROI mask was moved in x- and y-dimension to fit projections of other time points using the plugin “Roi Manager Move Selections” (<https://imagej.nih.gov/ij/macros/>) and ROIs added based on visibility of the cell until all cells visible at at least one time point were included in the ROI mask. Cell-specific imaging traces were extracted using the ROI Manager Multi Measure function. Overfilled cells were excluded from future analyses.

4.2.6.3. Running data analysis

Running analyses were conducted on the camera-acquired images using the software EthoVision XT 11 (Noldus Information Technology). Briefly, an area was drawn around the paws of the mouse excluding the nose and the Styrofoam ball. Then, mean activity was quantified by measuring pixel change in that area. Frame-rate of video-acquisition of calcium imaging and imaging of running differed. Therefore, the length of the data vector containing the running activity per time was adjusted using the resample function from the scipy.signal library.

4.2.6.4. Two-photon image data analysis with Matlab

Two-photon imaging data analysis was conducted by Sabine Liebscher using MatLab from MathWorks. Further information is stated in the figure legends.

Bibliography

1. Kandel, E.R. and S. Mack, *Principles of neural science*. 2014.
2. Hendry, S.H., et al., *Numbers and proportions of GABA-immunoreactive neurons in different areas of monkey cerebral cortex*. *J Neurosci*, 1987. **7**(5): p. 1503-19.
3. Tamamaki, N., et al., *Green fluorescent protein expression and colocalization with calretinin, parvalbumin, and somatostatin in the GAD67-GFP knock-in mouse*. *J Comp Neurol*, 2003. **467**(1): p. 60-79.
4. Shipp, S., *Structure and function of the cerebral cortex*. *Curr Biol*, 2007. **17**(12): p. R443-9.
5. McGeorge, A.J. and R.L. Faull, *The organization of the projection from the cerebral cortex to the striatum in the rat*. *Neuroscience*, 1989. **29**(3): p. 503-37.
6. Levesque, M., et al., *Corticostriatal projections from layer V cells in rat are collaterals of long-range corticofugal axons*. *Brain Res*, 1996. **709**(2): p. 311-5.
7. Parent, M. and A. Parent, *Single-axon tracing study of corticostriatal projections arising from primary motor cortex in primates*. *J Comp Neurol*, 2006. **496**(2): p. 202-13.
8. Kemp, J.M. and T.P. Powell, *The structure of the caudate nucleus of the cat: light and electron microscopy*. *Philos Trans R Soc Lond B Biol Sci*, 1971. **262**(845): p. 383-401.
9. Nieoullon, A. and L. Kerkerian-Le Goff, *Cellular interactions in the striatum involving neuronal systems using "classical" neurotransmitters: possible functional implications*. *Mov Disord*, 1992. **7**(4): p. 311-25.
10. Galvan, L., et al., *Functional Differences Between Direct and Indirect Striatal Output Pathways in Huntington's Disease*. *J Huntingtons Dis*, 2012. **1**(1): p. 17-25.
11. Soto, C., *Unfolding the role of protein misfolding in neurodegenerative diseases*. *Nat Rev Neurosci*, 2003. **4**(1): p. 49-60.
12. Glenner, G.G. and C.W. Wong, *Alzheimer's disease: initial report of the purification and characterization of a novel cerebrovascular amyloid protein*. *Biochem Biophys Res Commun*, 1984. **120**(3): p. 885-90.
13. Grundke-Iqbal, I., et al., *Microtubule-associated protein tau. A component of Alzheimer paired helical filaments*. *J Biol Chem*, 1986. **261**(13): p. 6084-9.
14. Forno, L.S., *Neuropathology of Parkinson's disease*. *J Neuropathol Exp Neurol*, 1996. **55**(3): p. 259-72.
15. Conneally, P.M., *Huntington disease: genetics and epidemiology*. *Am J Hum Genet*, 1984. **36**(3): p. 506-26.
16. Huntington, G., *On chorea. George Huntington, M.D.* *J Neuropsychiatry Clin Neurosci*, 2003. **15**(1): p. 109-12.
17. Gusella, J.F., et al., *A polymorphic DNA marker genetically linked to Huntington's disease*. *Nature*, 1983. **306**(5940): p. 234-8.
18. Group, T.H.s.D.C.R., *A novel gene containing a trinucleotide repeat that is expanded and unstable on Huntington's disease chromosomes. The Huntington's Disease Collaborative Research Group*. *Cell*, 1993. **72**(6): p. 971-83.
19. Andrew, S.E., et al., *The relationship between trinucleotide (CAG) repeat length and clinical features of Huntington's disease*. *Nat Genet*, 1993. **4**(4): p. 398-403.
20. Snell, R.G., et al., *Relationship between trinucleotide repeat expansion and phenotypic variation in Huntington's disease*. *Nat Genet*, 1993. **4**(4): p. 393-7.

21. Josiassen, R.C., et al., *Patterns of intellectual deficit in Huntington's disease*. J Clin Neuropsychol, 1982. **4**(2): p. 173-83.
22. Gómez-Tortosa, E., et al., *Severity of Cognitive Impairment in Juvenile and Late-Onset Huntington Disease*. Archives of Neurology, 1998. **55**(6): p. 835.
23. Paulsen, J.S., et al., *Neuropsychiatric aspects of Huntington's disease*. J Neurol Neurosurg Psychiatry, 2001. **71**(3): p. 310-4.
24. Novak, M.J. and S.J. Tabrizi, *Huntington's disease*. BMJ, 2010. **340**: p. c3109.
25. Rawlins, M.D., et al., *The Prevalence of Huntington's Disease*. Neuroepidemiology, 2016. **46**(2): p. 144-53.
26. Rosenblatt, A., et al., *Predictors of neuropathological severity in 100 patients with Huntington's disease*. Ann Neurol, 2003. **54**(4): p. 488-93.
27. Di Maio, L., et al., *Suicide risk in Huntington's disease*. J Med Genet, 1993. **30**(4): p. 293-5.
28. Robins Wahlin, T.B., et al., *High suicidal ideation in persons testing for Huntington's disease*. Acta Neurol Scand, 2000. **102**(3): p. 150-61.
29. Zoghbi, H.Y. and H.T. Orr, *Glutamine repeats and neurodegeneration*. Annu Rev Neurosci, 2000. **23**: p. 217-47.
30. Nakamura, K., et al., *SCA17, a novel autosomal dominant cerebellar ataxia caused by an expanded polyglutamine in TATA-binding protein*. Hum Mol Genet, 2001. **10**(14): p. 1441-8.
31. Rolfs, A., et al., *Clinical features and neuropathology of autosomal dominant spinocerebellar ataxia (SCA17)*. Ann Neurol, 2003. **54**(3): p. 367-75.
32. MacDonald, M.E., et al., *Gametic but not somatic instability of CAG repeat length in Huntington's disease*. J Med Genet, 1993. **30**(12): p. 982-6.
33. Anca, M.H., et al., *Different phenotypic expression in monozygotic twins with Huntington disease*. Am J Med Genet A, 2004. **124A**(1): p. 89-91.
34. Trottier, Y., V. Biancalana, and J.L. Mandel, *Instability of CAG repeats in Huntington's disease: relation to parental transmission and age of onset*. J Med Genet, 1994. **31**(5): p. 377-82.
35. Kennedy, L. and P.F. Shelbourne, *Dramatic mutation instability in HD mouse striatum: does polyglutamine load contribute to cell-specific vulnerability in Huntington's disease?* Hum Mol Genet, 2000. **9**(17): p. 2539-44.
36. Swami, M., et al., *Somatic expansion of the Huntington's disease CAG repeat in the brain is associated with an earlier age of disease onset*. Hum Mol Genet, 2009. **18**(16): p. 3039-47.
37. Kuhl, D.E., et al., *Cerebral metabolism and atrophy in Huntington's disease determined by 18FDG and computed tomographic scan*. Ann Neurol, 1982. **12**(5): p. 425-34.
38. de la Monte, S.M., J.P. Vonsattel, and E.P. Richardson, Jr., *Morphometric demonstration of atrophic changes in the cerebral cortex, white matter, and neostriatum in Huntington's disease*. J Neuropathol Exp Neurol, 1988. **47**(5): p. 516-25.
39. Heinsen, H., et al., *Cortical and striatal neurone number in Huntington's disease*. Acta Neuropathol, 1994. **88**(4): p. 320-33.
40. Mann, D.M., R. Oliver, and J.S. Snowden, *The topographic distribution of brain atrophy in Huntington's disease and progressive supranuclear palsy*. Acta Neuropathol, 1993. **85**(5): p. 553-9.
41. Jackson, M., et al., *The cortical neuritic pathology of Huntington's disease*. Neuropathol Appl Neurobiol, 1995. **21**(1): p. 18-26.
42. Tabrizi, S.J., et al., *Biochemical abnormalities and excitotoxicity in Huntington's disease brain*. Ann Neurol, 1999. **45**(1): p. 25-32.
43. Dawbarn, D., M.E. De Quidt, and P.C. Emson, *Survival of basal ganglia neuropeptide Y-somatostatin neurones in Huntington's disease*. Brain Res, 1985. **340**(2): p. 251-60.

44. Petryszyn, S., A. Parent, and M. Parent, *The calretinin interneurons of the striatum: comparisons between rodents and primates under normal and pathological conditions*. J Neural Transm (Vienna), 2017.
45. Richfield, E.K., et al., *Preferential loss of preproenkephalin versus preprotachykinin neurons from the striatum of Huntington's disease patients*. Ann Neurol, 1995. **38**(6): p. 852-61.
46. Kanazawa, I., et al., *Studies on neurotransmitter markers and striatal neuronal cell density in Huntington's disease and dentatorubropallidolusian atrophy*. J Neurol Sci, 1985. **70**(2): p. 151-65.
47. Morton, A.J., R.L. Faull, and J.M. Edwardson, *Abnormalities in the synaptic vesicle fusion machinery in Huntington's disease*. Brain Res Bull, 2001. **56**(2): p. 111-7.
48. Grafton, S.T., et al., *A comparison of neurological, metabolic, structural, and genetic evaluations in persons at risk for Huntington's disease*. Ann Neurol, 1990. **28**(5): p. 614-21.
49. Hedreen, J.C., et al., *Neuronal loss in layers V and VI of cerebral cortex in Huntington's disease*. Neurosci Lett, 1991. **133**(2): p. 257-61.
50. Thu, D.C., et al., *Cell loss in the motor and cingulate cortex correlates with symptomatology in Huntington's disease*. Brain, 2010. **133**(Pt 4): p. 1094-110.
51. Goto, S. and A. Hirano, *Synaptophysin expression in the striatum in Huntington's disease*. Acta Neuropathol, 1990. **80**(1): p. 88-91.
52. Ginovart, N., et al., *PET study of the pre- and post-synaptic dopaminergic markers for the neurodegenerative process in Huntington's disease*. Brain, 1997. **120** (Pt 3): p. 503-14.
53. Sun, Y., et al., *Polyglutamine-expanded huntingtin promotes sensitization of N-methyl-D-aspartate receptors via post-synaptic density 95*. J Biol Chem, 2001. **276**(27): p. 24713-8.
54. Modregger, J., et al., *PACSIN 1 interacts with huntingtin and is absent from synaptic varicosities in presymptomatic Huntington's disease brains*. Hum Mol Genet, 2002. **11**(21): p. 2547-58.
55. Hassel, B., et al., *Glutamate uptake is reduced in prefrontal cortex in Huntington's disease*. Neurochem Res, 2008. **33**(2): p. 232-7.
56. Twelvetrees, A.E., et al., *Delivery of GABAARs to synapses is mediated by HAP1-KIF5 and disrupted by mutant huntingtin*. Neuron, 2010. **65**(1): p. 53-65.
57. Scherzinger, E., et al., *Huntingtin-encoded polyglutamine expansions form amyloid-like protein aggregates in vitro and in vivo*. Cell, 1997. **90**(3): p. 549-58.
58. Davies, S.W., et al., *Formation of neuronal intranuclear inclusions underlies the neurological dysfunction in mice transgenic for the HD mutation*. Cell, 1997. **90**(3): p. 537-48.
59. DiFiglia, M., et al., *Aggregation of huntingtin in neuronal intranuclear inclusions and dystrophic neurites in brain*. Science, 1997. **277**(5334): p. 1990-3.
60. Becher, M.W., et al., *Intranuclear neuronal inclusions in Huntington's disease and dentatorubral and pallidolusian atrophy: correlation between the density of inclusions and IT15 CAG triplet repeat length*. Neurobiol Dis, 1998. **4**(6): p. 387-97.
61. Sieradzan, K.A., et al., *Huntington's disease intranuclear inclusions contain truncated, ubiquitinated huntingtin protein*. Exp Neurol, 1999. **156**(1): p. 92-9.
62. Gutekunst, C.A., et al., *Nuclear and neuropil aggregates in Huntington's disease: relationship to neuropathology*. J Neurosci, 1999. **19**(7): p. 2522-34.
63. Jansen, A.H., et al., *Frequency of nuclear mutant huntingtin inclusion formation in neurons and glia is cell-type-specific*. Glia, 2017. **65**(1): p. 50-61.
64. Strong, T.V., et al., *Widespread expression of the human and rat Huntington's disease gene in brain and nonneural tissues*. Nat Genet, 1993. **5**(3): p. 259-65.

65. Gutekunst, C.A., et al., *Identification and localization of huntingtin in brain and human lymphoblastoid cell lines with anti-fusion protein antibodies*. Proc Natl Acad Sci U S A, 1995. **92**(19): p. 8710-4.
66. Sharp, A.H., et al., *Widespread expression of Huntington's disease gene (IT15) protein product*. Neuron, 1995. **14**(5): p. 1065-74.
67. DiFiglia, M., et al., *Huntingtin is a cytoplasmic protein associated with vesicles in human and rat brain neurons*. Neuron, 1995. **14**(5): p. 1075-81.
68. Cattaneo, E., C. Zuccato, and M. Tartari, *Normal huntingtin function: an alternative approach to Huntington's disease*. Nat Rev Neurosci, 2005. **6**(12): p. 919-30.
69. Gerber, H.P., et al., *Transcriptional activation modulated by homopolymeric glutamine and proline stretches*. Science, 1994. **263**(5148): p. 808-11.
70. Perutz, M.F., et al., *Glutamine repeats as polar zippers: their possible role in inherited neurodegenerative diseases*. Proc Natl Acad Sci U S A, 1994. **91**(12): p. 5355-8.
71. Saudou, F. and S. Humbert, *The Biology of Huntingtin*. Neuron, 2016. **89**(5): p. 910-26.
72. Hilditch-Maguire, P., et al., *Huntingtin: an iron-regulated protein essential for normal nuclear and perinuclear organelles*. Hum Mol Genet, 2000. **9**(19): p. 2789-97.
73. Elias, S., et al., *Huntingtin regulates mammary stem cell division and differentiation*. Stem Cell Reports, 2014. **2**(4): p. 491-506.
74. Gauthier, L.R., et al., *Huntingtin controls neurotrophic support and survival of neurons by enhancing BDNF vesicular transport along microtubules*. Cell, 2004. **118**(1): p. 127-38.
75. Rigamonti, D., et al., *Wild-type huntingtin protects from apoptosis upstream of caspase-3*. J Neurosci, 2000. **20**(10): p. 3705-13.
76. Leavitt, B.R., et al., *Wild-type huntingtin protects neurons from excitotoxicity*. J Neurochem, 2006. **96**(4): p. 1121-9.
77. Nasir, J., et al., *Targeted disruption of the Huntington's disease gene results in embryonic lethality and behavioral and morphological changes in heterozygotes*. Cell, 1995. **81**(5): p. 811-23.
78. Duyao, M.P., et al., *Inactivation of the mouse Huntington's disease gene homolog Hdh*. Science, 1995. **269**(5222): p. 407-10.
79. Zeitlin, S., et al., *Increased apoptosis and early embryonic lethality in mice nullizygous for the Huntington's disease gene homologue*. Nat Genet, 1995. **11**(2): p. 155-63.
80. Leavitt, B.R., et al., *Wild-type huntingtin reduces the cellular toxicity of mutant huntingtin in vivo*. Am J Hum Genet, 2001. **68**(2): p. 313-24.
81. Dragatsis, I., M.S. Levine, and S. Zeitlin, *Inactivation of Hdh in the brain and testis results in progressive neurodegeneration and sterility in mice*. Nat Genet, 2000. **26**(3): p. 300-6.
82. Ambrose, C.M., et al., *Structure and expression of the Huntington's disease gene: evidence against simple inactivation due to an expanded CAG repeat*. Somat Cell Mol Genet, 1994. **20**(1): p. 27-38.
83. Wexler, N.S., et al., *Homozygotes for Huntington's disease*. Nature, 1987. **326**(6109): p. 194-7.
84. Lee, J.M., et al., *CAG repeat expansion in Huntington disease determines age at onset in a fully dominant fashion*. Neurology, 2012. **78**(10): p. 690-5.
85. Hoffner, G., M.L. Island, and P. Djian, *Purification of neuronal inclusions of patients with Huntington's disease reveals a broad range of N-terminal fragments of expanded huntingtin and insoluble polymers*. J Neurochem, 2005. **95**(1): p. 125-36.
86. Preisinger, E., et al., *Evidence for a recruitment and sequestration mechanism in Huntington's disease*. Philos Trans R Soc Lond B Biol Sci, 1999. **354**(1386): p. 1029-34.
87. Goldberg, Y.P., et al., *Cleavage of huntingtin by apopain, a proapoptotic cysteine protease, is modulated by the polyglutamine tract*. Nat Genet, 1996. **13**(4): p. 442-9.

88. Zhou, H., et al., *Huntingtin forms toxic NH2-terminal fragment complexes that are promoted by the age-dependent decrease in proteasome activity*. J Cell Biol, 2003. **163**(1): p. 109-18.
89. Li, S.H. and X.J. Li, *Aggregation of N-terminal huntingtin is dependent on the length of its glutamine repeats*. Hum Mol Genet, 1998. **7**(5): p. 777-82.
90. Martindale, D., et al., *Length of huntingtin and its polyglutamine tract influences localization and frequency of intracellular aggregates*. Nat Genet, 1998. **18**(2): p. 150-4.
91. Hackam, A.S., et al., *The influence of huntingtin protein size on nuclear localization and cellular toxicity*. J Cell Biol, 1998. **141**(5): p. 1097-105.
92. Cooper, J.K., et al., *Truncated N-terminal fragments of huntingtin with expanded glutamine repeats form nuclear and cytoplasmic aggregates in cell culture*. Hum Mol Genet, 1998. **7**(5): p. 783-90.
93. Peters, M.F., et al., *Nuclear targeting of mutant Huntingtin increases toxicity*. Mol Cell Neurosci, 1999. **14**(2): p. 121-8.
94. Gu, X., et al., *N17 Modifies mutant Huntingtin nuclear pathogenesis and severity of disease in HD BAC transgenic mice*. Neuron, 2015. **85**(4): p. 726-41.
95. Maiuri, T., et al., *The huntingtin N17 domain is a multifunctional CRM1 and Ran-dependent nuclear and cilia export signal*. Hum Mol Genet, 2013. **22**(7): p. 1383-94.
96. Woerner, A.C., et al., *Cytoplasmic protein aggregates interfere with nucleocytoplasmic transport of protein and RNA*. Science, 2016. **351**(6269): p. 173-6.
97. Hosp, F., et al., *Quantitative interaction proteomics of neurodegenerative disease proteins*. Cell Rep, 2015. **11**(7): p. 1134-46.
98. Kim, Y.E., et al., *Soluble Oligomers of PolyQ-Expanded Huntingtin Target a Multiplicity of Key Cellular Factors*. Mol Cell, 2016. **63**(6): p. 951-64.
99. F. Hosp, S.G.-Á., M. H. Schaefer, J. Cox, F. Meissner, M. S. Hipp, F.-U. Hartl, R. Klein, I. Dudanova, and M. Mann, *Spatiotemporal proteomic profiling of Huntington's disease inclusions reveals widespread loss of protein function*. Cell Reports, 2017(in press).
100. Grima, J.C., et al., *Mutant Huntingtin Disrupts the Nuclear Pore Complex*. Neuron, 2017. **94**(1): p. 93-107 e6.
101. Gasset-Rosa, F., et al., *Polyglutamine-Expanded Huntingtin Exacerbates Age-Related Disruption of Nuclear Integrity and Nucleocytoplasmic Transport*. Neuron, 2017. **94**(1): p. 48-57 e4.
102. Bauerlein, F.J.B., et al., *In Situ Architecture and Cellular Interactions of PolyQ Inclusions*. Cell, 2017.
103. Arrasate, M., et al., *Inclusion body formation reduces levels of mutant huntingtin and the risk of neuronal death*. Nature, 2004. **431**(7010): p. 805-10.
104. Kuemmerle, S., et al., *Huntington aggregates may not predict neuronal death in Huntington's disease*. Ann Neurol, 1999. **46**(6): p. 842-9.
105. van Roon-Mom, W.M., et al., *Aggregate distribution in frontal and motor cortex in Huntington's disease brain*. Neuroreport, 2006. **17**(6): p. 667-70.
106. Ortega, Z., et al., *Acute polyglutamine expression in inducible mouse model unravels ubiquitin/proteasome system impairment and permanent recovery attributable to aggregate formation*. J Neurosci, 2010. **30**(10): p. 3675-88.
107. Mangiarini, L., et al., *Exon 1 of the HD gene with an expanded CAG repeat is sufficient to cause a progressive neurological phenotype in transgenic mice*. Cell, 1996. **87**(3): p. 493-506.
108. Woodman, B., et al., *The Hdh(Q150/Q150) knock-in mouse model of HD and the R6/2 exon 1 model develop comparable and widespread molecular phenotypes*. Brain Res Bull, 2007. **72**(2-3): p. 83-97.
109. Cummings, D.M., et al., *Alterations in cortical excitation and inhibition in genetic mouse models of Huntington's disease*. J Neurosci, 2009. **29**(33): p. 10371-86.

110. Langfelder, P., et al., *Integrated genomics and proteomics define huntingtin CAG length-dependent networks in mice*. Nat Neurosci, 2016. **19**(4): p. 623-33.
111. Carter, R.J., et al., *Characterization of progressive motor deficits in mice transgenic for the human Huntington's disease mutation*. J Neurosci, 1999. **19**(8): p. 3248-57.
112. Lione, L.A., et al., *Selective discrimination learning impairments in mice expressing the human Huntington's disease mutation*. J Neurosci, 1999. **19**(23): p. 10428-37.
113. Murphy, K.P., et al., *Abnormal synaptic plasticity and impaired spatial cognition in mice transgenic for exon 1 of the human Huntington's disease mutation*. J Neurosci, 2000. **20**(13): p. 5115-23.
114. McGowan, D.P., et al., *Amyloid-like inclusions in Huntington's disease*. Neuroscience, 2000. **100**(4): p. 677-80.
115. Meade, C.A., et al., *Cellular localization and development of neuronal intranuclear inclusions in striatal and cortical neurons in R6/2 transgenic mice*. J Comp Neurol, 2002. **449**(3): p. 241-69.
116. Klapstein, G.J., et al., *Electrophysiological and morphological changes in striatal spiny neurons in R6/2 Huntington's disease transgenic mice*. J Neurophysiol, 2001. **86**(6): p. 2667-77.
117. Kiehn, O., *Development and functional organization of spinal locomotor circuits*. Curr Opin Neurobiol, 2011. **21**(1): p. 100-9.
118. Grillner, S., et al., *Mechanisms for selection of basic motor programs--roles for the striatum and pallidum*. Trends Neurosci, 2005. **28**(7): p. 364-70.
119. Schieber, M.H. and L.S. Hibbard, *How somatotopic is the motor cortex hand area?* Science, 1993. **261**(5120): p. 489-92.
120. Vucic, S. and M.C. Kiernan, *Pathophysiology of neurodegeneration in familial amyotrophic lateral sclerosis*. Curr Mol Med, 2009. **9**(3): p. 255-72.
121. Caviness, J.N., et al., *Parkinson's disease, cortical dysfunction, and alpha-synuclein*. Mov Disord, 2011. **26**(8): p. 1436-42.
122. Abbruzzese, G., et al., *Intracortical inhibition and facilitation are abnormal in Huntington's disease: a paired magnetic stimulation study*. Neurosci Lett, 1997. **228**(2): p. 87-90.
123. Schippling, S., et al., *Abnormal motor cortex excitability in preclinical and very early Huntington's disease*. Biol Psychiatry, 2009. **65**(11): p. 959-65.
124. Philpott, A.L., et al., *Cortical inhibitory deficits in premanifest and early Huntington's disease*. Behav Brain Res, 2016. **296**: p. 311-7.
125. Isaacson, J.S. and M. Scanziani, *How inhibition shapes cortical activity*. Neuron, 2011. **72**(2): p. 231-43.
126. Lee, S., et al., *The largest group of superficial neocortical GABAergic interneurons expresses ionotropic serotonin receptors*. J Neurosci, 2010. **30**(50): p. 16796-808.
127. Pfeffer, C.K., et al., *Inhibition of inhibition in visual cortex: the logic of connections between molecularly distinct interneurons*. Nat Neurosci, 2013. **16**(8): p. 1068-76.
128. Kawaguchi, Y. and Y. Kubota, *GABAergic cell subtypes and their synaptic connections in rat frontal cortex*. Cereb Cortex, 1997. **7**(6): p. 476-86.
129. Miyoshi, G., et al., *Genetic fate mapping reveals that the caudal ganglionic eminence produces a large and diverse population of superficial cortical interneurons*. J Neurosci, 2010. **30**(5): p. 1582-94.
130. Xu, X., K.D. Roby, and E.M. Callaway, *Mouse cortical inhibitory neuron type that coexpresses somatostatin and calretinin*. J Comp Neurol, 2006. **499**(1): p. 144-60.
131. Tang, B., et al., *Gene expression profiling of R6/2 transgenic mice with different CAG repeat lengths reveals genes associated with disease onset and progression in Huntington's disease*. Neurobiol Dis, 2011. **42**(3): p. 459-67.

132. Consortium, H.D.i., *Developmental alterations in Huntington's disease neural cells and pharmacological rescue in cells and mice*. Nat Neurosci, 2017. **20**(5): p. 648-660.
133. Cha, J.H., et al., *Altered brain neurotransmitter receptors in transgenic mice expressing a portion of an abnormal human huntington disease gene*. Proc Natl Acad Sci U S A, 1998. **95**(11): p. 6480-5.
134. Cepeda, C., et al., *Transient and progressive electrophysiological alterations in the corticostriatal pathway in a mouse model of Huntington's disease*. J Neurosci, 2003. **23**(3): p. 961-9.
135. Levine, M.S., et al., *Enhanced sensitivity to N-methyl-D-aspartate receptor activation in transgenic and knockin mouse models of Huntington's disease*. J Neurosci Res, 1999. **58**(4): p. 515-32.
136. Gourfinkel-An, I., et al., *Changes in GAD67 mRNA expression evidenced by in situ hybridization in the brain of R6/2 transgenic mice*. Journal of Neurochemistry, 2003. **86**(6): p. 1369-1378.
137. Ferris, C.F., et al., *Studies on the Q175 Knock-in Model of Huntington's Disease Using Functional Imaging in Awake Mice: Evidence of Olfactory Dysfunction*. Front Neurol, 2014. **5**: p. 94.
138. Murphy-Nakhnikian, A., et al., *Abnormal burst patterns of single neurons recorded in the substantia nigra reticulata of behaving 140 CAG Huntington's disease mice*. Neurosci Lett, 2012. **512**(1): p. 1-5.
139. Brini, M., et al., *Neuronal calcium signaling: function and dysfunction*. Cell Mol Life Sci, 2014. **71**(15): p. 2787-814.
140. Nakai, J., M. Ohkura, and K. Imoto, *A high signal-to-noise Ca(2+) probe composed of a single green fluorescent protein*. Nat Biotechnol, 2001. **19**(2): p. 137-41.
141. Wang, J.W., et al., *Two-photon calcium imaging reveals an odor-evoked map of activity in the fly brain*. Cell, 2003. **112**(2): p. 271-82.
142. Pologruto, T.A., R. Yasuda, and K. Svoboda, *Monitoring neural activity and [Ca2+] with genetically encoded Ca2+ indicators*. J Neurosci, 2004. **24**(43): p. 9572-9.
143. Chen, T.W., et al., *Ultrasensitive fluorescent proteins for imaging neuronal activity*. Nature, 2013. **499**(7458): p. 295-300.
144. Holtmaat, A., et al., *Long-term, high-resolution imaging in the mouse neocortex through a chronic cranial window*. Nat Protoc, 2009. **4**(8): p. 1128-44.
145. Denk, W., J.H. Strickler, and W.W. Webb, *Two-photon laser scanning fluorescence microscopy*. Science, 1990. **248**(4951): p. 73-6.
146. Busche, M.A., et al., *Clusters of hyperactive neurons near amyloid plaques in a mouse model of Alzheimer's disease*. Science, 2008. **321**(5896): p. 1686-9.
147. Liebscher, S., et al., *Selective Persistence of Sensorimotor Mismatch Signals in Visual Cortex of Behaving Alzheimer's Disease Mice*. Curr Biol, 2016. **26**(7): p. 956-64.
148. Spampanato, J., et al., *Progressive synaptic pathology of motor cortical neurons in a BAC transgenic mouse model of Huntington's disease*. Neuroscience, 2008. **157**(3): p. 606-20.
149. Gu, X., et al., *Pathological cell-cell interactions elicited by a neuropathogenic form of mutant Huntingtin contribute to cortical pathogenesis in HD mice*. Neuron, 2005. **46**(3): p. 433-44.
150. Balch, W.E., et al., *Adapting proteostasis for disease intervention*. Science, 2008. **319**(5865): p. 916-9.
151. Parsell, D.A. and S. Lindquist, *The function of heat-shock proteins in stress tolerance: degradation and reactivation of damaged proteins*. Annu Rev Genet, 1993. **27**: p. 437-96.
152. Richter, K., M. Haslbeck, and J. Buchner, *The heat shock response: life on the verge of death*. Mol Cell, 2010. **40**(2): p. 253-66.

153. Saibil, H., *Chaperone machines for protein folding, unfolding and disaggregation*. Nat Rev Mol Cell Biol, 2013. **14**(10): p. 630-42.
154. Sharma, S.K., et al., *The kinetic parameters and energy cost of the Hsp70 chaperone as a polypeptide unfoldase*. Nat Chem Biol, 2010. **6**(12): p. 914-20.
155. Ali, A., et al., *HSP90 interacts with and regulates the activity of heat shock factor 1 in Xenopus oocytes*. Mol Cell Biol, 1998. **18**(9): p. 4949-60.
156. Zou, J., et al., *Repression of heat shock transcription factor HSF1 activation by HSP90 (HSP90 complex) that forms a stress-sensitive complex with HSF1*. Cell, 1998. **94**(4): p. 471-80.
157. Voellmy, R., *On mechanisms that control heat shock transcription factor activity in metazoan cells*. Cell Stress Chaperones, 2004. **9**(2): p. 122-33.
158. Guo, Y., et al., *Evidence for a mechanism of repression of heat shock factor 1 transcriptional activity by a multichaperone complex*. J Biol Chem, 2001. **276**(49): p. 45791-9.
159. Ciechanover, A. and P. Brundin, *The ubiquitin proteasome system in neurodegenerative diseases: sometimes the chicken, sometimes the egg*. Neuron, 2003. **40**(2): p. 427-46.
160. Bedford, L., et al., *Assembly, structure, and function of the 26S proteasome*. Trends Cell Biol, 2010. **20**(7): p. 391-401.
161. Kitada, T., et al., *Mutations in the parkin gene cause autosomal recessive juvenile parkinsonism*. Nature, 1998. **392**(6676): p. 605-8.
162. Todde, V., M. Veenhuis, and I.J. van der Klei, *Autophagy: principles and significance in health and disease*. Biochim Biophys Acta, 2009. **1792**(1): p. 3-13.
163. Hara, T., et al., *Suppression of basal autophagy in neural cells causes neurodegenerative disease in mice*. Nature, 2006. **441**(7095): p. 885-9.
164. Komatsu, M., et al., *Loss of autophagy in the central nervous system causes neurodegeneration in mice*. Nature, 2006. **441**(7095): p. 880-4.
165. Marcuccilli, C.J., et al., *Regulatory differences in the stress response of hippocampal neurons and glial cells after heat shock*. J Neurosci, 1996. **16**(2): p. 478-85.
166. Carnemolla, A., et al., *In Vivo Profiling Reveals a Competent Heat Shock Response in Adult Neurons: Implications for Neurodegenerative Disorders*. PLoS One, 2015. **10**(7): p. e0131985.
167. Cummings, C.J., et al., *Chaperone suppression of aggregation and altered subcellular proteasome localization imply protein misfolding in SCA1*. Nat Genet, 1998. **19**(2): p. 148-54.
168. Smith, H.L., W. Li, and M.E. Cheetham, *Molecular chaperones and neuronal proteostasis*. Semin Cell Dev Biol, 2015. **40**: p. 142-52.
169. Hayashida, N., et al., *Heat shock factor 1 ameliorates proteotoxicity in cooperation with the transcription factor NFAT*. EMBO J, 2010. **29**(20): p. 3459-69.
170. Labbadia, J., et al., *Altered chromatin architecture underlies progressive impairment of the heat shock response in mouse models of Huntington disease*. J Clin Invest, 2011. **121**(8): p. 3306-19.
171. Zourlidou, A., et al., *Hsp27 overexpression in the R6/2 mouse model of Huntington's disease: chronic neurodegeneration does not induce Hsp27 activation*. Hum Mol Genet, 2007. **16**(9): p. 1078-90.
172. Popiel, H.A., et al., *Hsp40 gene therapy exerts therapeutic effects on polyglutamine disease mice via a non-cell autonomous mechanism*. PLoS One, 2012. **7**(11): p. e51069.
173. Labbadia, J., et al., *Suppression of protein aggregation by chaperone modification of high molecular weight complexes*. Brain, 2012. **135**(Pt 4): p. 1180-96.
174. Dragatsis, I., et al., *CAG repeat lengths > or =335 attenuate the phenotype in the R6/2 Huntington's disease transgenic mouse*. Neurobiol Dis, 2009. **33**(3): p. 315-30.

175. Morton, A.J., et al., *Paradoxical delay in the onset of disease caused by super-long CAG repeat expansions in R6/2 mice*. *Neurobiol Dis*, 2009. **33**(3): p. 331-41.
176. Ben-Zvi, A., E.A. Miller, and R.I. Morimoto, *Collapse of proteostasis represents an early molecular event in *Caenorhabditis elegans* aging*. *Proc Natl Acad Sci U S A*, 2009. **106**(35): p. 14914-9.
177. Yang, S., et al., *Age-dependent decrease in chaperone activity impairs MANF expression, leading to Purkinje cell degeneration in inducible SCA17 mice*. *Neuron*, 2014. **81**(2): p. 349-65.
178. Gupta, R., et al., *Firefly luciferase mutants as sensors of proteome stress*. *Nat Methods*, 2011. **8**(10): p. 879-84.
179. Dooley, C.T., et al., *Imaging dynamic redox changes in mammalian cells with green fluorescent protein indicators*. *J Biol Chem*, 2004. **279**(21): p. 22284-93.
180. Dantuma, N.P., et al., *Short-lived green fluorescent proteins for quantifying ubiquitin/proteasome-dependent proteolysis in living cells*. *Nat Biotechnol*, 2000. **18**(5): p. 538-43.
181. Lindsten, K., et al., *A transgenic mouse model of the ubiquitin/proteasome system*. *Nat Biotechnol*, 2003. **21**(8): p. 897-902.
182. Myeku, N., et al., *Tau-driven 26S proteasome impairment and cognitive dysfunction can be prevented early in disease by activating cAMP-PKA signaling*. *Nat Med*, 2016. **22**(1): p. 46-53.
183. Gidalevitz, T., et al., *Progressive disruption of cellular protein folding in models of polyglutamine diseases*. *Science*, 2006. **311**(5766): p. 1471-4.
184. Schroder, H., et al., *DnaK, DnaJ and GrpE form a cellular chaperone machinery capable of repairing heat-induced protein damage*. *EMBO J*, 1993. **12**(11): p. 4137-44.
185. Frydman, J., et al., *Folding of nascent polypeptide chains in a high molecular mass assembly with molecular chaperones*. *Nature*, 1994. **370**(6485): p. 111-7.
186. Yavorska, I. and M. Wehr, *Somatostatin-Expressing Inhibitory Interneurons in Cortical Circuits*. *Front Neural Circuits*, 2016. **10**: p. 76.
187. Chakraborty, J., et al., *Quercetin improves the activity of the ubiquitin-proteasomal system in 150Q mutated huntingtin-expressing cells but exerts detrimental effects on neuronal survivability*. *J Neurosci Res*, 2015. **93**(10): p. 1581-91.
188. Borchelt, D.R., et al., *A vector for expressing foreign genes in the brains and hearts of transgenic mice*. *Genet Anal*, 1996. **13**(6): p. 159-63.
189. Arnold, E.S., et al., *ALS-linked TDP-43 mutations produce aberrant RNA splicing and adult-onset motor neuron disease without aggregation or loss of nuclear TDP-43*. *Proc Natl Acad Sci U S A*, 2013. **110**(8): p. E736-45.
190. Gavrulina, T.O., et al., *Neuronal SMN expression corrects spinal muscular atrophy in severe SMA mice while muscle-specific SMN expression has no phenotypic effect*. *Hum Mol Genet*, 2008. **17**(8): p. 1063-75.
191. Yamamoto, A., J.J. Lucas, and R. Hen, *Reversal of Neuropathology and Motor Dysfunction in a Conditional Model of Huntington's Disease*. *Cell*, 2000. **101**(1): p. 57-66.
192. Myeku, N., et al., *Assessment of proteasome impairment and accumulation/aggregation of ubiquitinated proteins in neuronal cultures*. *Methods Mol Biol*, 2011. **793**: p. 273-96.
193. Murmu, R.P., et al., *Dendritic spine instability leads to progressive neocortical spine loss in a mouse model of Huntington's disease*. *J Neurosci*, 2013. **33**(32): p. 12997-3009.
194. Nathanson, J.L., et al., *Preferential labeling of inhibitory and excitatory cortical neurons by endogenous tropism of adeno-associated virus and lentivirus vectors*. *Neuroscience*, 2009. **161**(2): p. 441-50.

195. Jarabek, B.R., R.P. Yasuda, and B.B. Wolfe, *Regulation of proteins affecting NMDA receptor-induced excitotoxicity in a Huntington's mouse model*. Brain, 2004. **127**(Pt 3): p. 505-16.
196. Rudy, B., et al., *Three groups of interneurons account for nearly 100% of neocortical GABAergic neurons*. Dev Neurobiol, 2011. **71**(1): p. 45-61.
197. Sommeijer, J.P. and C.N. Levelt, *Synaptotagmin-2 is a reliable marker for parvalbumin positive inhibitory boutons in the mouse visual cortex*. PLoS One, 2012. **7**(4): p. e35323.
198. Hamm, J.P., et al., *Altered Cortical Ensembles in Mouse Models of Schizophrenia*. Neuron, 2017. **94**(1): p. 153-167 e8.
199. Dougherty, S.E., et al., *Hyperactivity and cortical disinhibition in mice with restricted expression of mutant huntingtin to parvalbumin-positive cells*. Neurobiol Dis, 2014. **62**: p. 160-71.
200. Taylor-Robinson, S.D., et al., *Evidence for glutamate excitotoxicity in Huntington's disease with proton magnetic resonance spectroscopy*. Lancet, 1994. **343**(8906): p. 1170.
201. Rebec, G.V., S.K. Conroy, and S.J. Barton, *Hyperactive striatal neurons in symptomatic Huntington R6/2 mice: variations with behavioral state and repeated ascorbate treatment*. Neuroscience, 2006. **137**(1): p. 327-36.
202. Schiefer, J., et al., *Riluzole prolongs survival time and alters nuclear inclusion formation in a transgenic mouse model of Huntington's disease*. Mov Disord, 2002. **17**(4): p. 748-57.
203. Johnston, J.A., C.L. Ward, and R.R. Kopito, *Aggresomes: a cellular response to misfolded proteins*. J Cell Biol, 1998. **143**(7): p. 1883-98.
204. Hoffner, G. and P. Djian, *Monomeric, oligomeric and polymeric proteins in huntington disease and other diseases of polyglutamine expansion*. Brain Sci, 2014. **4**(1): p. 91-122.
205. Bett, J.S., et al., *The ubiquitin-proteasome reporter GFPu does not accumulate in neurons of the R6/2 transgenic mouse model of Huntington's disease*. PLoS One, 2009. **4**(4): p. e5128.
206. Maynard, C.J., et al., *Accumulation of ubiquitin conjugates in a polyglutamine disease model occurs without global ubiquitin/proteasome system impairment*. Proc Natl Acad Sci U S A, 2009. **106**(33): p. 13986-91.
207. Ma, J., et al., *Cellular Proteomes Drive Tissue-Specific Regulation of the Heat Shock Response*. G3 (Bethesda), 2017. **7**(3): p. 1011-1018.
208. Martin-Aparicio, E., et al., *Proteasomal-dependent aggregate reversal and absence of cell death in a conditional mouse model of Huntington's disease*. J Neurosci, 2001. **21**(22): p. 8772-81.
209. Zabel, C., et al., *A large number of protein expression changes occur early in life and precede phenotype onset in a mouse model for huntington disease*. Mol Cell Proteomics, 2009. **8**(4): p. 720-34.
210. Neueder, A., et al., *The pathogenic exon 1 HTT protein is produced by incomplete splicing in Huntington's disease patients*. Sci Rep, 2017. **7**(1): p. 1307.
211. Nixon, R.A., *The role of autophagy in neurodegenerative disease*. Nat Med, 2013. **19**(8): p. 983-97.
212. Bauer, P.O., et al., *Harnessing chaperone-mediated autophagy for the selective degradation of mutant huntingtin protein*. Nat Biotechnol, 2010. **28**(3): p. 256-63.
213. McKinnon, C. and S.J. Tabrizi, *The ubiquitin-proteasome system in neurodegeneration*. Antioxid Redox Signal, 2014. **21**(17): p. 2302-21.
214. Rodriguez, K.A., et al., *Determinants of rodent longevity in the chaperone-protein degradation network*. Cell Stress Chaperones, 2016. **21**(3): p. 453-66.

215. Carnemolla, A., et al., *Contesting the dogma of an age-related heat shock response impairment: implications for cardiac-specific age-related disorders*. Hum Mol Genet, 2014. **23**(14): p. 3641-56.
216. Triplett, J.C., et al., *Age-related changes in the proteostasis network in the brain of the naked mole-rat: Implications promoting healthy longevity*. Biochim Biophys Acta, 2015. **1852**(10 Pt A): p. 2213-24.
217. Mayford, M., et al., *Control of memory formation through regulated expression of a CaMKII transgene*. Science, 1996. **274**(5293): p. 1678-83.
218. Tabata, H. and K. Nakajima, *Efficient in utero gene transfer system to the developing mouse brain using electroporation: visualization of neuronal migration in the developing cortex*. Neuroscience, 2001. **103**(4): p. 865-72.
219. Saito, T. and N. Nakatsuji, *Efficient gene transfer into the embryonic mouse brain using in vivo electroporation*. Dev Biol, 2001. **240**(1): p. 237-46.
220. Jiang, M. and G. Chen, *High Ca²⁺-phosphate transfection efficiency in low-density neuronal cultures*. Nat Protoc, 2006. **1**(2): p. 695-700.
221. Cox, J., et al., *Accurate proteome-wide label-free quantification by delayed normalization and maximal peptide ratio extraction, termed MaxLFQ*. Mol Cell Proteomics, 2014. **13**(9): p. 2513-26.
222. Dubbs, A., J. Guevara, and R. Yuste, *moco: Fast Motion Correction for Calcium Imaging*. Front Neuroinform, 2016. **10**: p. 6.

Appendix

Appendix I: Supplementary tables

Table A- 1: PCA drivers, downregulated in old R6/2 mice

Protein name	Gene name	Annotation original	Annotation figure	Down- regulation
Voltage-dependent calcium channel gamma-3 subunit	Cacng3	synaptic	synaptic	8w
Complexin-1	Cplx1	synaptic	synaptic	8w, 12w
Neuromodulin	Gap43	synaptic	synaptic	8w
Proline-rich transmembrane protein 2	Prpt2	synaptic	synaptic	8w
Syntaxin-1A	Stx1a	synaptic	synaptic	8w, 12w
Synaptogyrin-1	Syngr1	synaptic	synaptic	8w
Vesicle-associated membrane protein 1	Vamp1	synaptic	synaptic	8w, 12w
Vesicle-associated membrane protein 2	Vamp2	synaptic	synaptic	8w, 12w
	A830010			
	M20Rik	other	other	8w
Alpha-actinin-1	Actn1	cytoskeleton	cytoskeleton	12w
ADP-ribosylation factor 5	Arf5	ribosomes	ribosomes	8w, 12w

Appendix

ATP synthase subunit delta, mitochondrial	Atp5d	mitochondria	mitochondria	8w
Brain acid soluble protein 1	Basp1	trans- membranal	other	8w
CD81 antigen	Cd81	immune system	other	8w
Coiled-coil-helix-coiled-coil- helix domain-containing protein 3, mitochondrial	Chchd3	mitochondria	mitochondria	8w
Cytochrome c oxidase subunit 7C, mitochondrial	Cox7c	mitochondria	mitochondria	8w, 12w
Cytochrome b5 type B	Cyb5b	mitochondria	mitochondria	8w
Acyl-CoA-binding protein	Dbi	signalling	signaling	8w
ETS-related transcription factor Elf-3	Elf3	transcription	histone	5w
Histone H3.3,Histone H3.3C,Histone H3	H3f3a, H3f3c	histone	histone	5w, 8w
Heat shock factor-binding protein 1	Hsbp1	protein homeostasis	protein homeostasis	8w, 12w
Mitochondrial fission factor	Mff	mitochondria	mitochondria	5w, 8w
Protein phosphatase 1 regulatory subunit 11	Ppp1r11	phosphatase inhibitor	signaling	12w
Parathymsin	Ptms	other	other	8w, 12w ^{##}
Putative RNA-binding protein 3	Rbm3	translation	ribosomes	8w
60S ribosomal protein L22	Rpl22	ribosomes	ribosomes	5w, 8w

Serine incorporator 1	Serinc1	serine transporter	other	12w
14-3-3 protein sigma	Sfn	class-switch recombination	other	not
Small ubiquitin-related modifier 2	Sumo2	protein homeostasis	protein homeostasis	8w
Thymosin beta-4,Hematopoietic system regulatory peptide	Tmsb4x	cytoskeleton	cytoskeleton	8w
	Tpm1	cytoskeleton	cytoskeleton	8w, 12w
Ubiquitin-conjugating enzyme E2 D3	Ube2d3	protein homeostasis	protein homeostasis	8w
Cytochrome b-c 1 complex subunit 6, mitochondrial	Uqcrh	mitochondria	mitochondria	8w, 12w
14-3-3 protein eta	Ywhah	class-switch recombination	other	8w, 12w

Downregulated in the insoluble fraction at 5 weeks of age.

Table A- 2: PCA drivers, upregulated in old R6/2 mice

Protein names	Gene names	Annotation	Upregulation
Brain-specific angiogenesis inhibitor 1-associated protein 2	Baiap2	cytoskeleton	5w, 8w, 12w
Chromobox protein homolog 3	Cbx3	hetero-chromatin	8w
CREB-regulated transcription coactivator 3	Crtc3	transcription	8w
H-2 class I histocompatibility antigen, D-B alpha chain	H2-D1	immune system	8w
Mannose-P-dolichol utilization defect 1 protein	Mpdu1	saccharides	5w, 8w
Negative elongation factor D	Nelfcd	translation	8w
Origin recognition complex subunit 3	Orc3	histone	8w
SH3 domain-binding glutamic acid-rich-like protein 2	Sh3bgrl2	others	8w
tRNA dimethylallyltransferase, mitochondrial	Trit1	mitochondria	8w
Cytochrome b-c1 complex subunit 10	Uqcr11	mitochondria	8w ^{##}

^{##} Downregulated in the soluble fraction at 5 weeks of age.

All proteins highly regulated (≥ 8 -fold enriched, p -value ≤ 0.001), were downregulated in R6/2 mice.

Table A- 3: Synaptic proteins most significantly regulated in the soluble proteome of R6/2 mice

Protein name	Gene name	P-value / fold-change	
		0.001 / 8-fold	0.05 / 2-fold
Neuronal-specific septin-3	3-Sep	8w, 12w	8w, 12w
V-type proton ATPase subunit G 2	Atp6v1g2	8w, 12w	8w, 12w
Voltage-dependent L-type calcium channel subunit alpha-1C	Cacna1c	12w	12w
Voltage-dependent calcium channel gamma-8 subunit	Cacng8	8w	8w
Calbindin	Calb1	8w	8w, 12w
Calcium/calmodulin-dependent protein kinase II inhibitor 1	Camk2n1	12w	12w
Cholecystokinin,Cholecystokinin-33,Cholecystokinin-12,Cholecystokinin-8	Cck	12w	5w, 8w, 12w
Drebrin-like protein	Dbnl	8w	8w
Dynamin-1-like protein	Dnm1l	8w	8w
DOMON domain-containing protein FRRS1L	Frrs1l	8w	8w
Potassium/sodium hyperpolarization-activated cyclic nucleotide-gated channel 4	Hcn4	12w	12w
Protein lin-7 homolog B	Lin7b	8w	8w
Pro-neuropeptide Y,Neuropeptide Y,C-flanking peptide of NPY	Npy	12w	12w
BDNF/NT-3 growth factors receptor	Ntrk2	8w	5w, 8w

Appendix

Paralemmin-1	Palm	12w	5w, 12w
Phosphatidylethanolamine-binding protein 1, Hippocampal cholinergic neurostimulating peptide	Pebp1	8w	8w
Neurabin-2	Ppp1r9b	8w	8w
Ras-related protein Rab-3D	Rab3d	12w	12w
Synaptosomal-associated protein 25	Snap25	8w, 12w	8w, 12w
Syntaxin-1A	Stx1a	8w, 12w	8w, 12w

Table A- 4: Synaptic proteins significantly upregulated in the insoluble proteome of R6/2 mice

Protein name	Gene name	Upregulation
Synaptogyrin-3	Syngn3 *	8w
AP2-associated protein kinase 1	Aak1	12w
A-kinase anchor protein 9	Akap9	12w
Sodium/potassium-transporting ATPase subunit alpha-2	Atp1a2 **	12w
Serine/threonine-protein kinase BRSK1	Brsk1	12w
Voltage-dependent calcium channel gamma-8 subunit, Voltage-dependent calcium channel gamma subunit	Cacng8	12w
Tyrosine-protein kinase Fyn	Fyn	12w
Glutaminase kidney isoform, mitochondrial	Gls	12w
Kinesin-like protein KIF1A	Kif1a	12w
Kinesin-like protein KIF3A	Kif3a	12w

Protein kinase C and casein kinase substrate in neurons protein 1	Pacsin1	12w
Profilin-2, Profilin	Pfn2	12w
Ras-related C3 botulinum toxin substrate 1	Rac1	12w
SLIT-ROBO Rho GTPase-activating protein 2	Srgap2	12w
Synapsin-2	Syn2	12w
Synaptopodin	Synpo	12w ^{##}
Vimentin	Vim	12w
14-3-3 protein zeta/delta	Ywhaz	12w

^{##} Downregulated in the insoluble fraction at 8 weeks of age.

* Downregulated in the soluble fraction at 8 weeks of age.

** Downregulated in the soluble fraction at 12 weeks of age.

Table A- 5: Synaptic proteins significantly downregulated in the insoluble proteome of R6/2 mice

Protein name	Gene name	Downregulation
Synaptotagmin-2	Syt2	5w, 8w
Inositol 1,4,5-trisphosphate receptor type 1	Itpr1	5w
Septin-5	5-Sep	8w
Calcium/calmodulin-dependent protein kinase type II subunit alpha	Camk2a *	8w
Disks large-associated protein 2	Dlgap2	8w
Disks large-associated protein 3	Dlgap3 *	8w
Gamma-aminobutyric acid type B receptor subunit 2	Gabbr2 *	8w
Glutamate receptor ionotropic, NMDA 2A	Grin2a	8w
BTB/POZ domain-containing protein KCTD16	Kctd16 *	8w
Myelin basic protein	Mbp	8w
Phosphatase and actin regulator 1, Phosphatase and actin regulator	Phactr1 *	8w
Myelin proteolipid protein	Plp1	8w
Synaptopodin	Synpo	8w ##
Synaptotagmin-7	Syt7 *	8w
Ras-related protein Rab-3A	Rab3a	12w

Upregulated in the insoluble fraction at 12 weeks of age.

* Downregulated in the soluble fraction at 8 weeks of age.

** Downregulated in the soluble fraction at 12 weeks of age.

Appendix II: Curriculum Vitae

Personal information

Name Elena Katharina Schulz-Trieglaff

University Education

- 2012 - 2017 Doctoral studies at the Max Planck Institute of Neurobiology, Munich
Thesis with Prof. Dr. Ruediger Klein
“Alterations of neuronal activity and protein homeostasis in a mouse model of Huntington’s disease”
- 2012 – 2017 International Max Planck Research School of Molecular and Cellular Life Science
- 2010 - 2011 Master of Science in Integrative Neuroscience at Imperial College London;
Thesis with Prof. Dr. Richard Reynolds
“Cerebellar pathology in multiple sclerosis is associated with meningeal inflammation”
- 2007 - 2010 Bachelor of Science in Molecular Life Sciences at University of Hamburg;
Thesis with PD Dr. Stefan Kindler
“The significance of Inositol-1,4,5-trisphosphate 3-kinase A in neurons”

Appendix III: List of publications

Paper

O. Howell *, E. K. Schulz-Trieglaff *, D. Carassiti, S. M. Gentleman, R. Nicholas, F. Roncaroli and R. Reynolds *joint first authors (2015) “*Extensive grey matter pathology in the cerebellum in multiple sclerosis is linked to inflammation in the subarachnoid space*” *Neuropathology and Applied Neurobiology* 41: 798–813

Conference abstracts

E. K. Schulz-Trieglaff*, J. Neuner*, F. Hosp, M. Mann, R. Klein[#], S. Liebscher[#] and I. Dudanova[#], *joint first authors, [#]joint last authors, “*Chronic two-photon imaging in primary motor cortex of behaving Huntington’s disease mice*” Eibsee meeting, Grainau, October 25 – 27, 2017 (Poster and Flash talk)

E. K. Schulz-Trieglaff, F. Hosp, M. Mann, R. Klein, I. Dudanova “*Luciferase-based sensor reveals proteostasis changes in cellular and mouse models of Huntington’s disease*” Embo Conference Mechanisms of Neurodegeneration, Heidelberg, June 14 – 17, 2017 (Poster and Flash talk)

E. K. Schulz-Trieglaff, R. Klein, I. Dudanova “*Assessing the protein quality control system in the Huntington disease model R6/2 using a luciferase-based sensor*” Society for Neuroscience meeting Annual meeting, San Diego, United States, Nov 12 - 16, 2016 (Talk)

E. K. Schulz-Trieglaff, R. Klein, I. Dudanova “*A transgenic mouse model expressing a luciferase-based sensor to study proteostasis in vivo*” Society for Neuroscience Annual meeting, Washington, D.C., United States, Nov 15 - 19, 2014 (Poster)

Appendix IV: Contributions and Affidavit

Author contributions

All author contributions to data generation have been stated for both projects in the specific Results section – Data generation.

Additionally, Dr. Irina Dudanova generated the data for and made the Figure 2-23.

Dr. Johanna Neuner generated the data for and made the Figures 2-2 and 2-3.

Dr. Sabine Liebscher generated the data for and made the Figure 2-4.

Dr. Fabian Hosp generated the data for and made the Figure 2-25.

Eidesstattliche Erklärung

Ich versichere hiermit an Eides statt, dass die vorgelegte Dissertation von mir selbständig und ohne unerlaubte Hilfe angefertigt ist.

München, den 12. Oktober 2017

Elena Katharina Schulz-Trieglaff

Erklärung

Hiermit erkläre ich, dass die Dissertation nicht ganz oder in wesentlichen Teilen einer anderen Prüfungskommission vorgelegt worden ist und dass ich mich anderweitig einer Doktorprüfung ohne Erfolg nicht unterzogen habe.

München, den 12. Oktober 2017

Elena Katharina Schulz-Trieglaff

Appendix V: Acknowledgements

My thanks go to Irina Dudanova, Rüdiger Klein, Amelia Douglass, Svenja Hüser and Tobias Ruff for critically reading this manuscript.

I would like to thank Rüdiger Klein for the opportunity to work in this great international atmosphere, for supervising me throughout my PhD and for never pressurizing me too much to lose motivation. I am grateful to my supervisor Irina Dudanova for her attentive supervision, her endless patience and her constant helpful input to the projects. I want to thank my thesis advisory committee for supporting me throughout this PhD with scientific input and career advice. I am thankful to Johanna Neuner, Fabian Hosp, Frédéric Frottin and Sabine Liebscher for fruitful collaborations and to Johanna Neuner for trusting me with her project and teaching me a bit of calcium imaging. I would like to thank the IMPRS coordination office for organizing great retreats and for creating an environment in which PhD students can interact confidentially. I am indebted to my HiWis Raphaela Goetz, Tammo von Knoblauch, André Wilke and Julia Boshart for excellent technical support in the lab. I would like to thank my students Ritu Roy Chowdhury and Anna Salerno-Kochan for teaching me how to supervise.

I thank former and present lab mates for making the working atmosphere such a pleasant one. Special thanks go to Archana Mishra, Daniel del Toro and Augusto Escalante for giving me much postdoctoral advice in scientific questions, but also in personal and career development matters. Also, big thanks to my lab mates Irene Riera Tur and Sara Gutiérrez Ángel for sharing lab, office and cookies with me for many, many years, during fun and stressful times and for having made it a more fun experience. I thank Amelia Douglass, Hakan Kucukdereli and Tobias Ruff for many discussions about how science should and should not be, what the future holds and for struggling through this PhD with me.

Finally, I am grateful to my parents Beate Schulz-Trieglaff and David Mora for their unconditional love and endless support. I wish to thank my wife Svenja Hüser for her love, for discussing my project with me, even on weekends, for keeping me sane and for sharing her life with me.